PROFORMA FOR SUBMISSION OF INFORMATION AT THE TIME OF SENDING THE FINAL REPORT OF THE WORK DONE ON THE PROJECT

1. Title of the Project	Investigations into Phytoliths for Identification and Taxonomic Analysis of Grasses of North Western Himalayan Region.
2. Name and Address of thePrincipal Investigator	Dr. Amarjit Singh Soodan Department of Botanical & Environmental Sciences, Guru Nanak Dev University, Amritsar.143005. Residential: B-5 Guru Nanak Dev University campus, Amritsar-143005.
3. UGC Approval No. & Date	43-131/2014(SR)
4. **Date of Implementation**	July 01, 2015
5. Tenure of the Project	3 Years (from July 01, 2015 to 30-06-2018)
6. Total Grant Allocated	Rs. 11,25,000/-
7. Total Grant Received	Rs. 6,75,000/-
8. Final Expenditure	Rs. 8,54,155

Grant of Rs. 1,79,155/- (Rs. 1,26,568/- + HRA of Rs.52,587/-) has to be reimbursed by the UGC

Principal Investigator
(Signature with Seal)

Registrar/Principal
(Signature with Seal)

(ANNEXURE-I)

S. No.	Particulars	Amount Approved (Rs.)	Grant Received (Rs.)	Expenditure (Rs.)
A.	**Non-Recurring**			
1.	Equipment	1,00,000/-	1,00,000/-	79,893/-
2.	Books & Journals	50,000/-	50,000/-	19,376/-
	Total	**1,50,000/-**	**1,50,000/-**	**99,269/-**
B.	**Recurring**			
1.	Project Fellow HRA to be Paid	6,00,000/-	3,00,000/-	4,73,290/- +52,587/- 5,25,877/-
2.	Chemicals	1,00,000/-	50,000/-	82,380/-
3.	Contingency	50,000/-	25,000/-	44,888/-
4.	Travel/Field work	1,50,000/-	75,000/-	26,741/-
5.	Overhead Charges	75,000/-	75,000/-	75,000/-
	Total	**9,03,000/-**	**5,75,000/-**	**7,54,886/-**
	Grand Total (A+B)	**11,25,000/-**	**6,75,000/-**	**8,54,155/-**

Grant of Rs. 1,79,155/- (Rs. 1,26,568/- + HRA of Rs. 52, 587/-) has to be reimbursed by the UGC.

UTILIZATION CERTIFICATE

Certified that out of the grant of Rs.**11,25,000** (Rupees **Eleven lakh twenty five thousand** only) approved by University Grant Commission, out of which only Rs. **6,75,000** ((Rupees **Six lakh seventy five thousand** only) received from the University Grant Commission under the scheme of support for Major Research Project entitled **Investigations into Phytoliths for Identification and Taxonomic Analysis of Grasses of North Western Himalayan Region** vide UGC letter No. F. **43-131/2014(SR)** dated **01 July, 2015.** An amount of **Rs. 8,54,155 (Rupees Eight lakh fifty four thousand one hundred fifty five)** utilized for the purpose for which it was sanctioned and in accordance with the terms and conditions laid down by the University Grants Commission. The amount of **Rs. 1,79,155/- (Rupees One lakh seventy nine thousand one hundred fifty five)** has to be reimbursed by the University Grant Commission.

(Dr. A. S. Soodan)
Principal Investigator

ANNEXURE-II

OBJECTIVES

1. **Inventorization:** The territories of North Western Himalayan region shall be surveyed thoroughly and sampled to prepare an updated inventory of grass species.
2. **Phytolith analysis:** The grass species listed as above shall be put to detailed phytolith analysis to add an important anatomical character to the taxonomic description of grasses. Quantification of silica content of different parts (root, culm, leaves and inflorescence) of each species will be carried out. This will help us to identify grasses of higher silica content.
3. **Elemental analysis:** Elemental analysis of phytolith morphotypes in each grass species shall be carried out with the help Scanning Electron Microscope/ Energy Dispersive using X-ray (Analysis) (SEM/EDX).
4. **Identification keys:** Based upon the shapes and sizes of phytolith types, both manual and electronic keys for identification of subfamilies, genera and species shall be developed.

METHODOLOGY

To achieve the objectives listed above following methods and techniques shall be employed.

1. Collection and preservation:

Extensive field surveys shall be undertaken to study grass species in their natural habitats. To randomize the process of survey and cover the entire expanse of the territory, a grid map of the study area shall be prepared. Specimens of each species shall be collected from various locations in the study area and dry preserved to prepare herbarium sheets and dry collections for phytolith analysis. Accession numbers will be allotted to the species that are not identified in the first instance. During the field surveys, notes shall be taken on the economic and ethnobotanical significance, distribution range and the flowering and fruiting phenology of the grass species.

2. Phytolith analysis

i) ***In-situ* Location:** Phytoliths shall be located in epidermal cells by clearing solution method of Clarke (1959). Leaf segments will be washed and immersed in a clearing solution of Lactic acid and Chloral hydrate (3:1) and kept at 70^0 C for 2 days. Cleared segments will be mounted in fresh solution and observed under light microscope.

ii) Dry Ashing Method: The method of Carnelli *et al*. (2001) shall be followed for dry ashing of the material. The material will be rinsed and cut into small pieces and heated to ashes in porcelein crucibles in a Muffle Furnace maintained at 470 ^{0}C for 48 hours. The crucibles will be taken out, cooled and the contents transferred to test tubes. Sufficient amount of Hydrogen peroxide (30%) will be added to submerge the contents and the test tubes will be kept at 80 ^{0}C for 1 hour. The test tubes shall be taken out from the incubator; the mixture will decanted and rinsed twice with distilled water. Hydrochloric acid (10%) will be added to the pellet and incubated again for 1 hour. Thereafter, the mixture will be washed with distilled water and centrifuged at 7500 rpm for 10 minutes. The supernatant will be decanted and the pallet washed twice with distilled water. The centrifugation process will be repeated four times till the pallet is clear. Finally, the pallet will be dried for 24 hours at 60 ^{0} C to a powder form. In this form the material will be taken in small bits and mounted on glass slides in DPX for optical microscopy. Olympus Micro Image Projection System (MIPS-USB 0262) shall be used for microphotography. Photographs would be taken at a uniform magnification for ease of comparison. Phytoliths will be classified into types and subtypes according to the International Code of Phytolith Nomenclature (Madella *et al.*, 2005).

3. Morphometry and Statistical analysis

Morphometric measurement of various types of phytoliths will be done with Image J software (version 1.46r). It is a user-friendly software that allows measurements of overall size and other dimensional aspects of microscopic objects from their microphotographs. Phytoliths of each type from different grass species in the sample shall be photographed with the help of a Micro Image Projection System (MIPS, Olympus) and stored in separate files for various species. Thereafter, dimensions of phytoliths will be recorded with the help of the Image J software. The software not only records size dimensions but also calculates other morphometric parameters *viz.*, aspect ratio, surface area, roundedness and solidity.

4. Scanning Electron Microscopy

Details of shape and surface features of phytoliths shall be studied with the help of Scanning Electron Microscopy. Dry ash will be spread uniformly over the stubs with the help of double-sided adhesive tape. The stubs will be put under a stereoscope for uniform spreading of the ash. Silver paint would be applied on the edges of the stub. The samples would be dried at 40^{0}C overnight. Next day, stubs shall be coated with graphite using a vacuum evaporator (JEOL-

JEE-4X). They would subsequently be coated with gold by a sputter coater (QUORUM) and imaged under SEM (CARL ZEISS EVO 40) at an accelerating voltage of 40KV.

5. Biochemical architecture

Elemental analysis of phytoliths shall be carried out with Scanning Electron Microscope-Energy Dispersive X-ray analysis (SEM-EDX). Infrared spectra of silica powder shall be obtained on a Fourier Transform Infrared (FTIR) Spectrophotometer (System92035, Perkin-Elmer, England). X-ray Diffraction (XRD) studies shall be performed on powder XRD diffractometer (Bruker D8 Advance). Similarly, High Resolution Transmission Electron Microscopy (HRTEM) and Selected Area Electron Diffraction (SAED) of the samples shall be worked out using Transmission Electron Microscopy to reveal the differences in phytoliths at atomic level. Facilities for this work are available in Guru Nanak Dev University, Amritsar.

Achievements from the project

Intensive work on the grasses was required because of very scare information of grasses available in the literature. Phytoliths emerged as a new identification tool for grasses with this we can identify grasses as vegetative stage. This in hand information of grasses will further benefit to the agricultural for removing weeds at the vegetative stage. Phytolith also play a role in monitoring environmental and climate change.

List of grasses species studied in the present work.

1. *Arundo donax* L.
2. *Bracharia ramosa* (L.) Stapf.
3. *Brachiaria reptans* (L.) Gardn. & Hubb.
4. *Bromus catharticus* Vahl
5. *Bromus inermis* Leyss.
6. *Cenchrus setigerus* Vahl.
7. *Dichanthium annulatum* (Forssk.) Stapf.
8. *Digitaria abludens* (Roem & Schult.) Veldkamp.
9. *Digitaria ciliaris* (Retz.) Koeler
10. *Echinochloa colonum* (L.) Link.
11. *Echinochloa crusgalli* (L.) P. Beauv.
12. *Lolium temulentum* L.
13. *Panicum antidotale Retz.*

14. *Panicum maximum* Jacq.
15. *Phalaris minor* Retz.
16. *Phragmites karka* (Retz.) Trin. ex Steud.
17. *Setaria pumila* (Poir.) Roem. & Schult.
18. *Setaria verticillata* (L.) P. Beauv.
19. *Setaria. viridis* (L.) P. Beauv.
20. *Sorghum halepense* (L.) Pers.

Contribution to the Society

Apart from taxonomic diversity, grasses occupy a place of privilege both in economy and ecology particularly in the tropical/subtropical parts of the globe including the Indian sub-continent. Even though the alpine-temperate type of grass cover of the North-western Himalayan region is a rich repository of grasses, floristic works in the region have not devoted enough attention and coverage to the group. In the present work exploration of grasses was done in the region and grasses are dominant in this area. The proposed project has both academic and applied relevance. Identification of grasses at vegetative stage was very difficult for researchers, teachers and students. Phytolith morphotypes play important role in identification of grass species at vegetative stage, even single individual morphotype can identify the grass species. The taxonomic keys were also made which would help the students and teachers for identification. In addition to academic relevance phytoliths play a role in carbon sequestration, environmental monitoring and climate change. In addition to this evolutionary relationships of past agricultural practices can also be traced through phytoliths lodged in the soil.

Summary of the findings

Grasses are the dominant elements in the North Western Himalayan Region. Correct and rapid identification at the vegetative stage of grasses with the phytolith morphotypes will be helpful in programs of weed control and their removal at early stage will helpful in agriculture. Even though the full potential of phytoliths in understanding the taxonomy and phylogeny of the grasses must come through future research involving an assessment of inter-population and intra-population variations and construction of representative master profiles for each species, the present work has made an initial contribution. We have made plant collections from single

locations and homogenized the material part-wise but this limitation has been partly made good by following a multiproxy and multi-organ approach in carrying out the present work. In the larger context of plant systematics, concerted and coordinated efforts of a multidisciplinary nature are required to develop integrated and robust phytolith profiles of different groups of plants and their application in the characterization and diagnosis of plant taxa. We found in our work that the reed grasses *Arundo donax* L. and *Phragmites karka* (Retz.) Trin. ex Steud. could be diagnosed from each other by the presence of long trapezoids, narrow bilobates, orbicular, polylobate, spiral and rugose elongate morphotypes in the former and polyhedral, tracheids, cylindric, cross, dendritic,quadrilobate and the rondel types in the latter. The grasses are also show marked differences by physicochemical characters of phytolith morphotypes. The taxonomic keys developed on phytolith morphotypes would help grasses identification both by students and researchers.

Whether any Ph.D. Enrolled/produced out of the Project

Yes, one student has been registered for Ph.D.

List of Publications

Papers Published

Bhat, M.A., Shakoor, S.A., Badgal, P. and Soodan, A.S. (2018) Taxonomic Demarcation of *Setaria pumila* (Poir.) Roem. & Schult., *S. verticillata* (L.) P. Beauv., *and S. viridis* (L.) P. Beauv. (Cenchrinae, Paniceae, Panicoideae, Poaceae) From Phytolith Signatures. *Frontiers in Plant Science*, 9:864. **(IF 4.298)**

Bhat, M.A., Shakoor, S.A., and Soodan, A.S. (2018). Taxonomic description and annotation of *Poa albertii* Regel (Poaceae: Pooideae, Poeae, Poinae) from North Western Himalayas, India. *Annals of Plant Sciences*, 7.3 2096-2100.

Shakoor, S.A., **Bhat, M.A.** and Soodan, A.S. 2016. Taxonomic Demarcation of *Arundo donax* L. *and Phragmites karka* (Retz.) Trin. ex Steud. (Arundinoideae, Poaceae) from Phytolith Signatures. *Flora*, 224:130-153. **(IF: 1.6)**

Papers Presented at Conferences

Bhat, M.A., Shakoor, S.A., Badgal, P., Chowdhary, P. and Soodan, A.S. (2018). Taxonomic Demarcation of *Setaria pumila* (Poir.) Roem. & Schult., *S. verticillata* (L.) P.Beauv. and *S. viridis* (L.) P. Beauv. (Panicoideae, Poaceae) from Phytolith Profiles.Poster presented at **National Seminar on Emerging Trends in Plant and Environmental Sciences** (Mar. 29-30), organized by Department of Botanical and Environmental Sciences, Guru Nanak Dev University, Amritsar.

Bhat, M.A., Badgal, P., Chowdhary, P. and Amarjit Singh Soodan (2018). Taxonomic demarcation of *Bromus catharticus* Vahl and *Bromus inermis* Leyss. (Pooideae, Poaceae) by morphological and chemical characterization of foliar phytoliths at **21st Punjab Science Congress** (Feb. 7-9) organized by Punjab Agricultural University, Ludhiana.

Bhat, M.A., Badgal, P. and Soodan, A.S. (2017). *Catapodium rigidum* (L.) C.E. Hubb. (Poaceae, Pooideae, Poeae) A new plant record from Kashmir Himalayas, India. at **National Seminar on Himalayan Biodiversity Characterization and Bioprospection for Sustainable Utilization** organized by Department of Botany,(Sept. 18-19) at University of Kashmir, Srinagar.

Bhat, M.A., Shakoor, S.A. and Soodan, A.S. 2016. Taxonomic Demarcation of *Bromus catharticus* Vahl. and *Bromus inermis* Leyss. (Pooideae, Poaceae) from Foliar Phytoliths. Paper presented at XXVI meeting of Indian Association of Angiosperm Taxonomy and **International Seminar on Conservation and Sustainable Utilization of Biodiversity** organized by Indian Association of Angiosperm Taxonomy (Calicut) India at Department of Botany, Shivaji University Kolhapur (Maharashtra) India.

Flora 224 (2016) 130–153

Contents lists available at ScienceDirect

Flora

journal homepage: www.elsevier.com/locate/flora

Taxonomic demarcation of *Arundo donax* L. and *Phragmites karka* (Retz.) Trin. ex Steud. (Arundinoideae, Poaceae) from phytolith signatures

Sheikh Abdul Shakoor, Mudassir Ahmad Bhat, Amarjit Singh Soodan*

Plant Systematics and Biodiversity Laboratory, Department of Botanical and Environmental Sciences, Guru Nanak Dev University, Amritsar, Punjab 143005, India

ARTICLE INFO

Article history:
Received 4 May 2016
Received in revised form 23 June 2016
Accepted 18 July 2016
Edited by Alessio Papini
Available online 21 July 2016

Keywords:
Morphometry
Morphotypes
Phytoliths
Poaceae
Reed grasses
Silica

ABSTRACT

Morphological and chemical characterization of phytoliths from aerial and underground parts of *Arundo donax* L. and *Phragmites karka* (Retz.) Trin. ex Steud. was undertaken to substantiate their taxonomic demarcation with reference to one representative species of each genus. Thirty phytolith morphotypes including some new ones were recovered. Apart from individual types, diagnostic phytolith assemblages unique to *Arundo donax* L. included long trapezoids, narrow bilobates, orbicular, polylobate, spiral and rugose elongate morphotypes. *Phragmites karka* (Retz.) Trin. ex Steud. was marked by an assemblage of polyhedral, tracheid, cylindric, cross, dendritic, quadrilobate and the rondel morphotypes. Morphometric data for shape descriptors were analysed by descriptive statistics and *t*-test (for independent-samples) using Paleontological Statistics (PAST) software. Estimation of total silica content revealed higher values for *Phragmites karka* (Retz.) Trin. ex Steud. than *Arundo donax* L. from most of the parts. Elemental analysis of phytolith morphotypes from various parts in both the species revealed the presence of Aluminium (Al), Calcium (Ca), Chlorine (Cl), Copper (Cu), Iron (Fe), Magnesium (Mg), Nitrogen (N), Potassium (K) and Titanium (Ti) in small amounts in addition to major elements including Carbon (C) and Oxygen (O) and Si (Silicon). Principal Component Analysis (PCA) of elemental composition grouped *Arundo donax* L. (leaf) and *Phragmites karka* (Retz.) Trin. ex Steud. (leaf) together in a single group. The Si (wt%) amounts varied significantly among various parts of *Arundo donax* L. ($p \leq 0.05$), whereas differences with Phragmites karka (Retz.) Trin. ex Steud. parts were insignificant. Similarly, Si (wt%) between the various parts of both species showed significant differences ($p \leq 0.05$). Chemical characterization of silica from leaf and synflorescence of both the species using X-ray Diffraction (XRD) showed polymorphic forms of silica and zeolites. Fourier Transform-Infrared (FTIR) Spectroscopy has confirmed the presence of silanol group and siloxane linkages in all the samples.

1. Introduction

Arundo donax L. (giant reed) and *Phragmites karka* (Retz.) Trin. ex Steud. (tall reed) both of subfamily Arundinoideae (family Poaceae) share distribution in moist (water-logged) habitats in temperate and tropical parts of the globe.

Grasses are prolific accumulators of Silicon in the form of biomineralized bodies called phytoliths (Lanning et al., 1958; Rovner, 1971; Piperno, 1988; Mulholland, 1989; Twiss, 1992; Wang and Lu, 1993; Chauhan et al., 2011; Ge et al., 2016). Phytoliths are three dimensional structures of hydrated amorphous silica produced in plant groups including Pteridophytes, Gymnosperms and Angiosperms (Piperno, 2006). Within angiosperms, they are most abundant in commelinid monocotyledons, notably the family Poaceae (Ma and Yamaji, 2006; Currie and Perry, 2007).

Plants absorb monosilicic acid (H_4SiO_4) from the soil and polymerize it to amorphous silica ($SiO_2 \cdot nH_2O$) in intercellular and intracellular locations in various parts of the body (Smithson, 1958; Yoshida et al., 1962; Krishnan et al., 2000). These silica deposits have been implicated in several biological functions ranging from mechanical strength and resistance to grazing and herbivory (Stebbins 1972, 1981; Coughenour, 1985; Epstein, 1994, 1999; Massey et al., 2006), through disease control (Gould and Shaw, 1983; Mazumdar, 2011) and alleviation of abiotic stress from metal toxicity, salinity, drought and high temperature (Hodson et al., 1985; Hodson and Evans, 1995; Lux et al., 2002, 2003; Hattori

* Corresponding author.
E-mail addresses: assoodan@gmail.com, assoodan@gndu.co.in (A.S. Soodan).

http://dx.doi.org/10.1016/j.flora.2016.07.011
0367-2530/

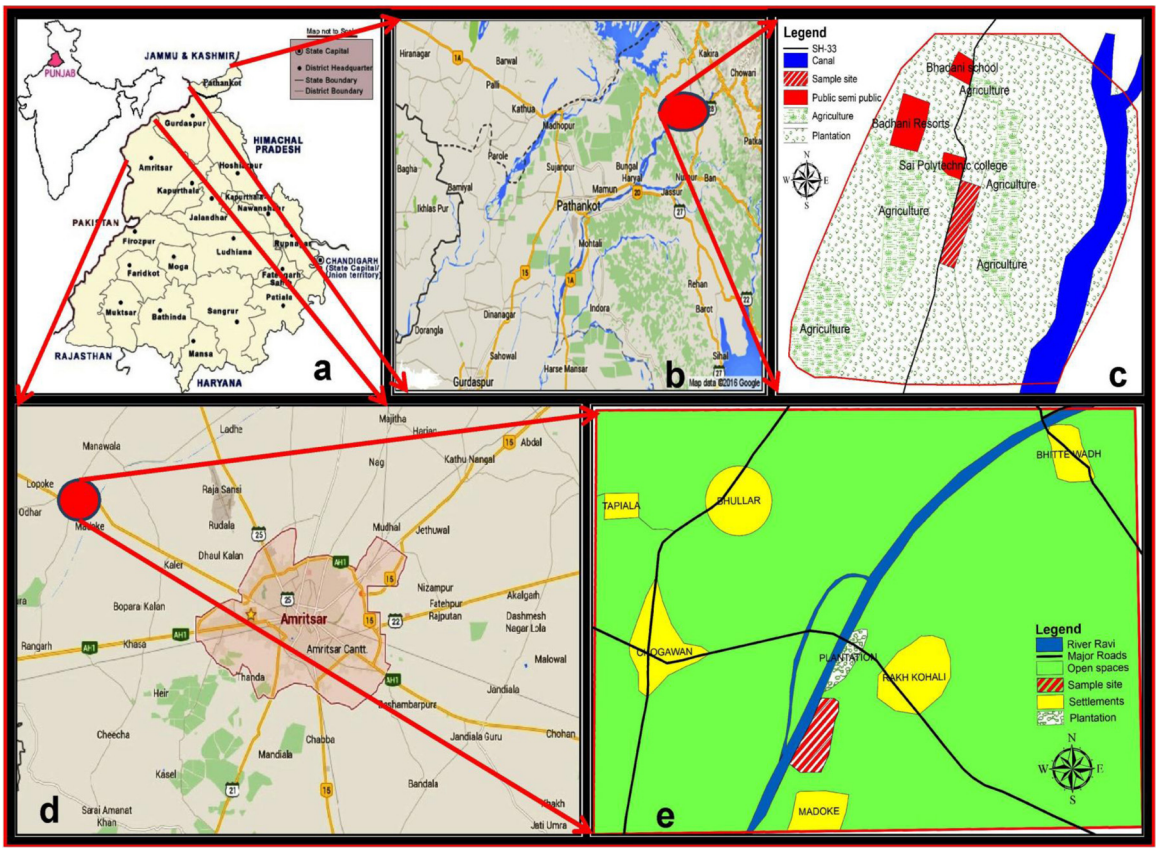

Fig. 1. Distribution of sampling sites for *Arundo donax* L. (b, c) and *Phragmites karka* (Retz.) Trin. ex. Steud. (d, e).

Table 1
Schemes for classification of phytolith morphotypes.

Phytolith Morphotypes	Acronym	Madella et al. (2005)	Twiss et al. (1969)	Lu and Liu (2003)
Bulliform cell	BFC	+ (Cuneiform bulliform cell)[a]	–	–
Bilobate	BL	+ (Dumbbell)	+ (Dumbbell)	+ (Dumbbell)
Clavate	CL	+	–	–
Cross	CR	+	+	+
Cubic	CUB	+	–	–
Cylindrical	CYD	+	–	–
Dendritic	DT	+	–	–
Echinate elongate	EE	+	+ (Elongate spiny)	–
Flat Tower	FT	–	–	+
Globular Echinate	GE	+	–	––
Horned Tower	HT	+	–	–
Long Trapezoid	LTZ	+	–	–
Nodular Bilobate	NBL	–	+ (Complex dumbbell)	–
Orbicular	ORB	+	+	–
Parallepipedal bulliform cell	PBFC	+	–	–
Polyhedral	PH	–	–	–
Polylobate	PL	+ (Cylindrical polylobate)	+ (Regular complex dumbbell)	–
Prickle	PRK	+	–	–
Quadrilobate	QL	+	–	–
Rondel	RD	+	–	+
Rugose elongate	RE	–	–	–
Rectangular	RT	+	+	–
Saddle	SD	+	–	+
Smooth elongate	SmE	+ (Elongate)	+ (Elongate, Smooth)	–
Sinuate elongate	SnE	–	+ (Elongate, Sinous)	–
Spiral	SPR	–	–	–
Scutiform	STF	+	–	–
Tracheids	TRCHD	+	–	–
Triangular	TRN	–	–	–
Trapezoid	TZ	+ (Trapeziform)	+ (Elliptical)	+ (Wavy trapezoids)

[a] Terms in parenthesis give the original names proposed by authors named in the column heads.

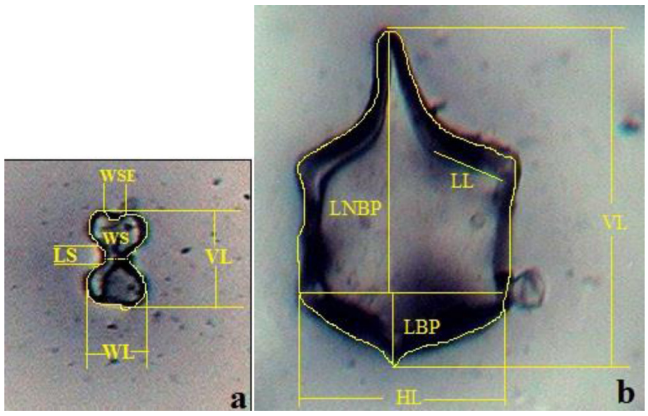

Fig. 2. Morphometric parameters of two prominent phytolith morphotyes from leaves of *Arundo donax* L. and *Phragmites karka* (Retz.) Trin. ex Steud. (a) Bilobate (VL = Vertical length; WL = Width of lobe; LS = Length of shank; WS = Width of shank; WSE = Width of scooped end) (b) Bulliform cell (VL = Vertical length; HL = Horizontal length; LL = Lateral length; LBP = Length of base portion; LNBP Length of non-base portion).

et al., 2005). They have been reported to check transpiration and at the same time reduce heat load of exposed parts of the plant body (Jones and Handreck, 1967; Sangster and Parry, 1971; Krishnan et al., 2000). Siliceous material collected from hollow internodes in the culms of some bamboos *viz. Bambusa arundinacea* (Retz.) Willd., *Bambusa vulgaris* L. *etc* finds reference as 'tabasheer' in Unani system of medicine for its therapeutic use in tuberculosis, diabetes, and malignancy (Singhal et al., 2013).

In grasses, phytoliths are deposited in cell lumina and extracellular spaces of specific cell types, especially leaf epidermal cells of leaves and reproductive bracts (Bonnett, 1972; Ball et al., 2001; Holst et al., 2007; Zhang et al., 2011; Rudall et al., 2014; Weisskopf and Lee, 2014). Phytoliths assume characteristic shapes in the host cells often moulded by the cell lumen. Some early studies brought to light the taxonomic significance of phytoliths. Prat (1936) and Metcalfe (1960) employed phytoliths as one of the anatomical features in characterization and identification of grass species. Smithson (1958) compared phytoliths from epidermal cells of grasses and argued that a combination of six phytolith morphotypes could distinguish Festucoid from Panicoid grasses. Twiss et al. (1969) compared shapes of phytoliths in seventeen grass species and categorized them into four classes and 26 types that were employed as markers to distinguish the subfamilies, Festucoideae, Chlorodoideae and Panicoideae. Thomasson (1978, 1980) used epidermal patterning of silica cells as one of the anatomical characters to classify grasses of the Miocene epoch. Krishnan et al. (2000) studied shapes and sizes of phytoliths of a large number of Indian grasses and developed taxonomic keys for species identification. Rudall et al. (2014) highlighted the heritability of phytolith shapes and their taxonomic significance. Recently, Shakoor et al. (2014) and Jattisha and Sabu (2015) have elucidated taxonomic significance of foliar phytoliths as diagnostic markers in some grasses of Punjab (India) and Southern parts of India respectively.

Ball et al. (2009, 2015) suggested a hierarchical approach to species diagnosis in which the first step involves a search for unique (marker) phytolith morphotypes produced in a given taxon. The next stage is to look for unique frequencies of particular phytolith

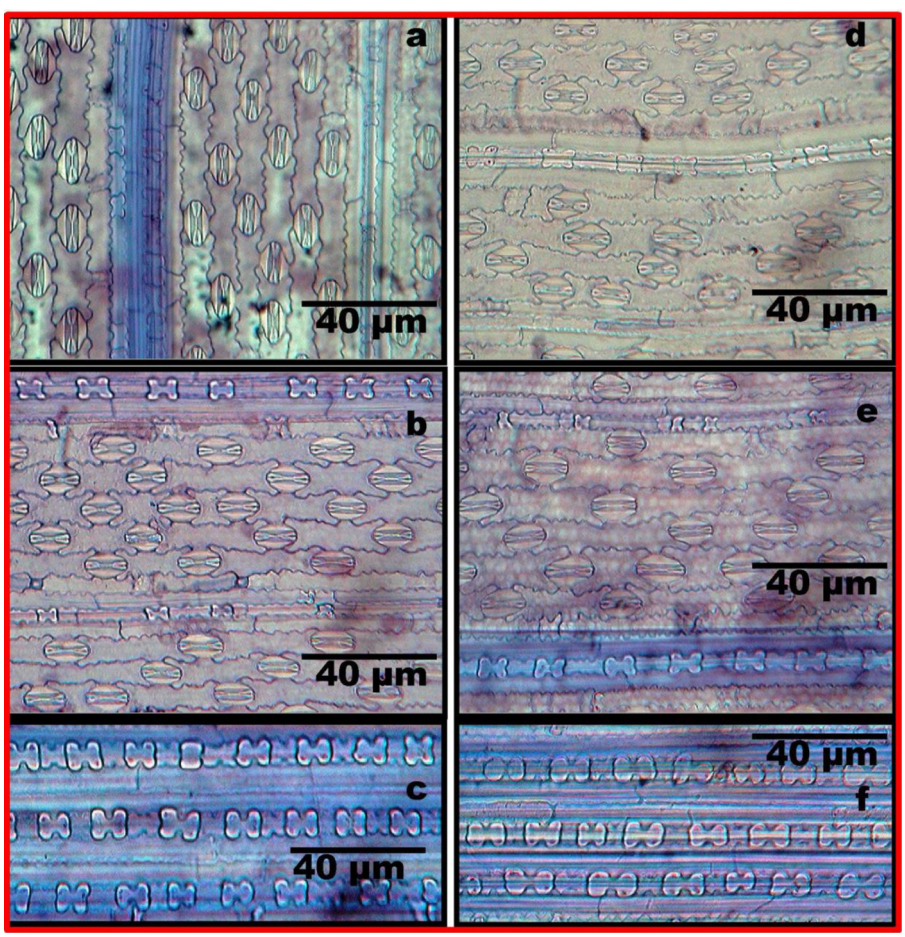

Fig. 3. *In-situ* location of phytoliths in leaf epidermis of *Arundo donax* L. (adaxial surface (a–c) and abaxial surface (d–f)).

Table 2a
Morphometric measurements of phytolith types in *Arundo donax* L.

Phytolith Morphotypes	Plant Part									
	Root					Culm				
	Length (μm)	Width(μm)	Area (μm^2)	Perimeter (μm)	Aspect ratio (μm)	Length (μm)	Width (μm)	Area (μm^2)	Perimeter (μm)	Aspect ratio (μm)
BFC	76.10 ± 7.44*	41.77 ± 0.91	2288 ± 26.26	205 ± 13	1.71 ± 0.33	–	–	–	–	–
BL	–	–	–	–	–	–	–	–	–	–
CL	92.39 ± 24.94	18.83 ± 03.71	1636.48 ± 739.40	208.03 ± 52.82	4.19 ± 0.54	50.98 ± 4.18	10.45 ± 1.86	437.18 ± 44.69	119.21 ± 7.96	4.91 ± 0.89
CUB	22.14 ± 02.13	16.77 ± 01.99	367.56 ± 96.65	75.38 ± 11.12	1.17 ± 0.08	–	–	–	–	–
EE	90.72 ± 14.73	11.31 ± 0.50	917.57 ± 164.47	227.17 ± 35.54	7.96 ± 1.25	51.39 ± 6.53	8.81 ± 1.55	466.59 ± 120.74	129.20 ± 18.53	5.14 ± 0.20
FT	–	–	–	–	–	–	–	–	–	–
GE	22.49 ± 03.62	20.02 ± 3.80	457.62 ± 162.27	76.87 ± 13.82	1.24 ± 0.06	–	–	–	–	–
HT	–	–	–	–	–	–	–	–	–	–
LTZ	–	–	–	–	–	–	–	–	–	–
NBL	–	–	–	–	–	–	–	–	–	–
ORB	–	–	–	–	–	–	–	–	–	–
PBFC	–	–	–	–	–	–	–	–	–	–
PL	–	–	–	–	–	–	–	–	–	–
PRK	–	–	–	–	–	–	–	–	–	–
RE	–	–	–	–	–	34.82 ± 1.89	8.85 ± 1.27	313.47 ± 33.03	92.66 ± 2.77	1.09 ± 0.27
RT	–	–	–	–	–	27.63 ± 3.61	8.72 ± 0.83	270.81 ± 56.60	76.99 ± 8.89	2.96 ± 0.30
SD	–	–	–	–	–	28.01 ± 2.07	11.22 ± 0.53	263.60 ± 20.90	74.72 ± 5.05	2.32 ± 0.40
SmE	63.08 ± 5.08	10.28 ± 1.30	665.38 ± 74.54	148.08 ± 10.68	5.86 ± 0.77	62.08 ± 9.63	6.92 ± 0.90	392.59 ± 64.02	138.72 ± 18.02	9.60 ± 1.95
SnE	72.95 ± 5.81	10.41 ± 1.12	741 ± 87.98	168 ± 12.45	6.91 ± 0.88	85.78 ± 22.86	12.20 ± 1.04	1149.09 ± 395.3	198.90 ± 48.35	6.09 ± 1.31
SPR	–	–	–	–	–	–	–	–	–	–
STF	45.13 ± 5.04	21.50 ± 1.96	796.61 ± 101.85	120.12 ± 9.49	1.89 ± 0.27	37.34 ± 3.71	17.69 ± 2.11	542.82 ± 99.45	104.52 ± 8.97	1.58 ± 0.16
TRN						19.60 ± 2.72	13.63 ± 2.66	232.91 ± 95.44	64.27 ± 9.74	1.14 ± 0.03
TZ	42.14 ± 6.01	26.19 ± 4.05	962.44 ± 277.77	128.42 ± 16.82	1.56 ± 0.11	35.80 ± 4.68	21.62 ± 4.52	711.66 ± 172.75	110.48 ± 13.06	1.48 ± 0.17

Phytolith Morphotypes	Plant Part									
	Leaf					Synflorescence				
	Length(μm)	Width (μm)	Area (μm^2)	Perimeter (μm)	Aspect ratio(μm)	Length(μm)	Width(μm)	Area (μm^2)	Perimeter (μm)	Aspect ratio(μm)
BFC	68.26 ± 4.47	51.99 ± 3.72	2375.3 ± 247.73	201.45 ± 8.98	1.39 ± 0.09	–	–	–	–	–
BL	27.58 ± 3.06	13.37 ± 1.57	297.90 ± 72.22	90.77 ± 10.03	2.28 ± 0.16	15.57 ± 0.90	8.19 ± 0.52	108.05 ± 12.04	52.60 ± 431	2.23 ± 0.25
CL	58.22 ± 7.55	11.74 ± 1.61	538.11 ± 86.20	134.57 ± 14.62	5.32 ± 1.04	74.25 ± 20.16	9.58 ± 1.63	598.52 ± 162.41	169.95 ± 42.59	7.54 ± 1.86
CUB	13.54 ± 0.48	12.48 ± 0.69	185.77 ± 20.44	55.93 ± 2.09	1.49±0.20	12.10 ± 0.70	11.08 ± 0.72	159.66 ± 29.88	48.57 ± 4.47	1.43 ± 0.07
EE	–	–	–	–	–	61.65 ± 6.90	8.48 ± 0.74	479.79 ± 62.26	154.04 ± 20.67	6.55 ± 0.50
FT	26.02 ± 4.48	16.28 ± 2.19	369.30 ± 74.58	77.38 ± 8.36	1.32 ± 0.07	–	–	–	–	–
GE	30.95 ± 1.10	25.31 ± 0.63	681.51 ± 39.31	97.71 ± 2.97	1.23 ± 0.03	23.24 ± 3.63	18.88 ± 2.62	384.20 ± 79.39	75.54 ± 8.01	1.26 ± 0.04
HT	18.41 ± 3.01	10.07 ± 1.14	177.41 ± 35.60	61.82 ± 5.75	1.62 ± 0.20	22.82 ± 4.05	10.06 ± 1.12	218.04 ± 41.04	64.04 ± 6.02	2.10 ± 0.40
LTZ	57.24 ± 2.97	16.81 ± 1.54	895.09 ± 101.10	180.64 ± 15.71	2.63 ± 0.13	–	–	–	–	–
NBL	28.70 ± 1.37	9.49 ± 0.68	214.42 ± 16.19	82.41 ± 4.56	3.21 ± 0.027	–	–	–	–	–
ORB	29.95 ± 2.13	25.03 ± 2.10	614.46 ± 79.12	87.40 ± 5.98	1.21 ± 0.02	11.70 ± 2.52	9.12 ± 3.18	159 ± 74.64	43 ± 9.9	1.15 ± 0.05
PBFC	51.68 ± 7.05	29.92 ± 3.16	1350.02 ± 261.65	157.03 ± 17.71	1.94 ± 0.21	–	–	–	–	–
PL	–	–	–	–	–	25.22 ± 2.35	9.25 ± 1.32	220.31 ± 28.09	75.81 ± 6.90	2.73 ± 0.30
PRK	–	–	–	–	–	26.85 ± 3.46	6.27 ± 0.78	120.28 ± 18.21	66.90 ± 6.59	4.65 ± 0.62
RE	–	–	–	–	–	–	–	–	–	–
RT	–	–	–	–	–	–	–	–	–	–
SD	–	–	–	–	–	12.36 ± 1.09	8.98 ± 0.99	131.86 ± 15.88	48.87 ± 3.84	1.72 ± 0.21
SmE	134.87 ± 85.44	11.24 ± 2.50	3493.47 ± 3081.88	299.03 ± 181.23	6.84 ± 1.01	59.59 ± 7.63	6.86 ± 1.36	378.12 ± 103.71	135.30 ± 15.89	9.68 ± 0.58
SnE	83.15 ± 5.30	11.15 ± 1.37	904 ± 143.14	199.83 ± 14.15	7.14 ± 0.75	64.92 ± 5.40	9.42 ± 1.08	654.24 ± 10.21	164.23 ± 11.20	6.72 ± 0.74
SPR	–	–	–	–	–	221.16 ± 16.74	9.20 ± 0.32	2413.01 ± 576.91	558.29 ± 59.58	8.02 ± 1.11
STF	–	–	–	–	–	61.34 ± 10.36	28.06 ± 4.37	1389.63 ± 411.02	161.77 ± 25.52	1.94 ± 0.23
TRN	–	–	–	–	–	–	–	–	–	–
TZ	37.12 ± 6.20	20.51 ± 1.19	647.14 ± 136.04	103.88 ± 13.74	1.74 ± 0.25	29.46 ± 3.01	19.22 ± 3.31	507.99 ± 100.44	92.07 ± 7.82	1.29 ± 0.10

BFC = Bulliform cell; BL = Bilobate; CL = Clavate; CUB = Cubic; EE = Echinate elongate; FT = Flat tower; GE = Globular echinate; HT = Horned tower; LTZ = Long trapezoids; NBL = Narrow bilobate; ORB = Orbicular; PBFC = Parallepipedal bulliform cell; PL = Polylobate; PRK = Prickle; RE = Rugose elongate; RT = Rectangular; SD = Saddle; SmE = Smooth elongate; SnE = Sinuate elongate; SPR = Spiral; STF = Scutiform; TRN = Triangular; TZ = Trapezoid.
* = mean ± Standard Error; (–) = Absence of morphotype.

Table 2b
Morphometric measurements of phytolith types in *Phragmites karka* (Retz.) Trin. ex Steud.

Phytolith Morphotypes	Plant Part									
	Root					Culm				
	Length (μm)	Width(μm)	Area (μm^2)	Perimeter (μm)	Aspect ratio (μm)	Length (μm)	Width (μm)	Area (μm^2)	Perimeter (μm)	Aspect ratio (μm)
BFC	*112.21 ± 2.04	53.67 ± 0.98	3698.20 ± 186.57	302.15 ± 6.43	2.05 ± 0.06	–	–	–	–	–
BL	–	–	–	–	–	15.14 ± 0.98	11.49 ± 1.00	186.57 ± 0.08	61.86 ± 1.01	1.31 ± 0.03
CL	155.82 ± 31.93	17.68 ± 2.44	2425.69 ± 686.40	335.52 ± 65.53	8.45 ± 1.86	54.50 ± 5.11	9.22 ± 1.82	547.14 ± 102.49	133.79 ± 9.76	5.24 ± 0.67
CR	–	–	–	–	–	–	–	–	–	–
CUB	13.23 ± 1.21	12.94 ± 1.55	163.36 ± 22.63	52.74 ± 4.16	1.12 ± 0.06	–	–	–	–	–
CYD	–	–	–	–	–	–	–	–	–	–
DT	–	–	–	–	–	–	–	–	–	–
EE	93.27 ± 23.89	6.81 ± 1.30	703.27 ± 273.98	214.73 ± 50.61	10.19 ± 1.33	44.18 ± 6.53	5.21 ± 0.44	267.62 ± 34.85	121.66 ± 14.05	7.06 ± 1.26
FT	14.73 ± 0.73	11.30 ± 1.07	130.98 ± 13.98	51.23 ± 3.10	1.55 ± 0.06	15.84 ± 1.14	7.25 ± 0.45	129.94 ± 16.83	50.39 ± 3.07	1.85 ± 0.16
GE	34.61 ± 3.68	29.51 ± 3.08	836.20 ± 156.52	110.61 ± 11.75	1.27 ± 0.04	–	–	–	–	–
HT	15.87 ± 0.81	6.57 ± 0.56	136.94 ± 08.71	57.48 ± 2.87	1.96 ± 0.19	14.97 ± 0.89	7.57 ± 0.66	129.94 ± 10.64	54.48 ± 2.33	1.76 ± 0.12
PBFC	14.73 ± 0.73	11.30 ± 1.07	130.98 ± 13.98	51.23 ± 3.10	1.55 ± 0.06	–	–	–	–	–
PH	25.27 ± 1.19	21.80 ± 1.88	492.16 ± 73.68	84.55 ± 6.36	1.20 ± 0.07	–	–	–	–	–
PRK	–	–	–	–	–	–	–	–	–	–
QL	–	–	–	–	–	–	–	–	–	–
RD	–	–	–	–	–	–	–	–	–	–
RT	48.98 ± 1.73	18.67 ± 1.65	865.21 ± 83.70	131.52 ± 3.12	2.69 ± 0.37	43.74 ± 3.84	17.68 ± 1.81	834.74 ± 159.19	124.67 ± 11.64	2.41 ± 0.24
SD	–	–	–	–	–	9.54 ± 0.88	7.25 ± 0.45	75.46 ± 12.16	34.30 ± 3.11	1.39 ± 0.04
SmE	64.21 ± 14.94	7.17 ± 1.15	419.52 ± 83.53	145.24 ± 27.82	10.66 ± 3.66	87.73 ± 21.57	11.03 ± 1.55	1047.11 ± 357	202.19 ± 47.81	7.70 ± 1.11
SnE	–	–	–	–	–	76.47 ± 10.81	11.78 ± 1.51	932.88 ± 216.96	188.30 ± 25.94	6.91 ± 0.93
STF	46.04 ± 7.01	7.17 ± 1.15	419.51 ± 83.53	145.24 ± 27.82	10.66 ± 3.66	83.13 ± 23.65	24.82 ± 3.87	2094.88 ± 934.42	212.45 ± 52.26	2.71 ± 0.38
TRCHD	–	–	–	–	–	74.03 ± 4.28	16.36 ± 1.64	1300.60 ± 29.86	192.84 ± 4.44	3.36 ± 0.23
TRN	–	–	–	–	–	–	–	–	–	–
TZ	34.04 ± 3.09	24.84 ± 2.97	706.29 ± 152.73	101.84 ± 10.45	1.34 ± 0.11	33.42 ± 2.03	22.30 ± 1.38	686.19 ± 43.80	111.33 ± 4.49	1.41 ± 0.09

Phytolith Morphotypes	Plant Part									
	Leaf					Synflorescence				
	Length (μm)	Width (μm)	Area (μm^2)	Perimeter (μm)	Aspect ratio(μm)	Length(μm)	Width(μm)	Area (μm^2)	Perimeter (μm)	Aspect ratio(μm)
BFC	98.04 ± 1.46	64.37 ± 0.45	4296.12 ± 205.95	285.12 ± 5.98	1.37 ± 0.03	–	–	–	–	–
BL	18.26 ± 0.51	12.74 ± 1.12	201.97 ± 19.74	68.46 ± 3.02	1.53 ± 0.16	12.66 ± 1.24	9.05 ± 0.77	95.24 ± 14.93	45.92 ± 3.72	1.69 ± 0.17
CL	42.42 ± 7.83	13.13 ± 2.47	608.44 ± 192.19	111.56 ± 20.82	2.72 ± 0.19	42.42 ± 4.04	10.55 ± 2.99	436.13 ± 138.25	105.73 ± 12.05	4.69 ± 1.31
CR	–	–	–	–	–	18.55 ± 1.46	17.44 ± 1.67	257.46 ± 31.62	92.54 ± 10.91	1.21 ± 0.05
CUB	14.24 ± 2.29	10.30 ± 1.73	183.33 ± 54.17	51.33 ± 7.55	1.30 ± 0.06	–	–	–	–	–
CYD	52.21 ± 11.94	4.17 ± 0.50	306.52 ± 47.53	114.24 ± 21.82	12.66 ± 2.76	–	–	–	–	–
DT	–	–	–	–	–	65.68 ± 7.24	6.99 ± 0.61	435.33 ± 86.87	186.73 ± 20.53	7.94 ± 1.52
EE	62.46 ± 6.43	12.07 ± 0.65	1531.99 ± 768.58	197.57 ± 43.78	4.78 ± 0.73	–	–	–	–	–
FT	12.13 ± 0.62	8.27 ± 0.45	101.08 ± 6.45	45.39 ± 1.20	1.33 ± 0.06	–	–	–	–	–
GE	–	–	–	–	–	–	–	–	–	–
HT	13.49 ± 1.58	9.60 ± 1.38	135.56 ± 22.59	52.49 ± 6.86	1.32 ± 0.09	–	–	–	–	–
PBFC	–	–	–	–	–	–	–	–	–	–
PH	–	–	–	–	–	–	–	–	–	–
PRK	96.41 ± 23.62	41.44 ± 11.12	2487.86 ± 746.81	226.37 ± 52.02	2.72 ± 0.36	45.84 ± 4.42	10.89 ± 0.92	428.88 ± 59.54	117.96 ± 9.74	3.74 ± 0.30
QL	–	–	–	–	–	14.71 ± 1.27	11.65 ± 1.48	185.89 ± 11.84	70.95 ± 4.39	1.17 ± 0.06
RD	–	–	–	–	–	11.34 ± 0.77	7.30 ± 1.08	79.31 ± 12.25	39.03 ± 3.02	1.49 ± 0.08
RT	–	–	–	–	–	–	–	–	–	–
SD	17.96 ± 1.56	13 ± 1.47	235.85 ± 52.94	58.68 ± 7.0	1.19 ± 0.04	12.45 ± 0.51	8.83 ± 0.47	106.84 ± 12.52	43.78 ± 3.10	1.57 ± 0.14
SmE	90.36 ± 15.16	07.29 ± 0.82	641 ± 125.56	199.55 ± 29.83	12.22 ± 1.89	57.25 ± 8.77	10.47 ± 0.82	614.91 ± 141.18	140.29 ± 18.58	5.55 ± 0.73
SnE	52.74 ± 3.74	19.77 ± 3.09	1007.90 ± 91.23	152.22 ± 3.68	2.95 ± 0.70	45.08 ± 4.85	9.12 ± 2.44	418.26 ± 105.76	113.95 ± 9.54	4.59 ± 0.94
STF	43.71 ± 4.90	20.28 ± 4.16	755.85 ± 208.33	119.38 ± 14.33	2.03 ± 0.19	49.16 ± 8.21	20.31 ± 2.53	844.75 ± 258.84	132.97 ± 22.74	2.13 ± 0.09
TRCHD	56.22 ± 5.68	17.75 ± 2.26	847.05 ± 132.50	147.17 ± 10.87	3.06 ± 0.31	–	–	–	–	–
TRN	20.66 ± 6.17	13.68 ± 4.22	383.97 ± 247.57	76.99 ± 24.33	1.32 ± 0.09	–	–	–	–	–
TZ	36.71 ± 3.22	24.32 ± 2.64	712.63 ± 117.56	110.61 ± 9.83	1.32 ± 0.09	51.51 ± 8.47	34.02 ± 7.23	1562.69 ± 487.23	158.43 ± 24.55	1.33 ± 0.08

BFC = Bulliform cell; BL = Bilobate; CL = Clavate; CR = Cross; CYD = Cylindrical; CUB = Cubic; DT = Dendritic; EE = Echinate elongate; FT = Flat tower; GE = Globular echinate; HT = Horned tower; PBFC = Parallepipedal bulliform cell; PH = Polyhedral; PRK = Prickle; QL = Quadrilobate; RD = Rondel; RT = Rectangular; SD = Saddle; SmE = Smooth elongate; SnE = Sinuate elongate; STF = Scutiform;TRCHD = Tracheids; TRN = Triangular; TZ = Trapezoid.
* = mean ± Standard Error: (–) = Absence of morphotype.

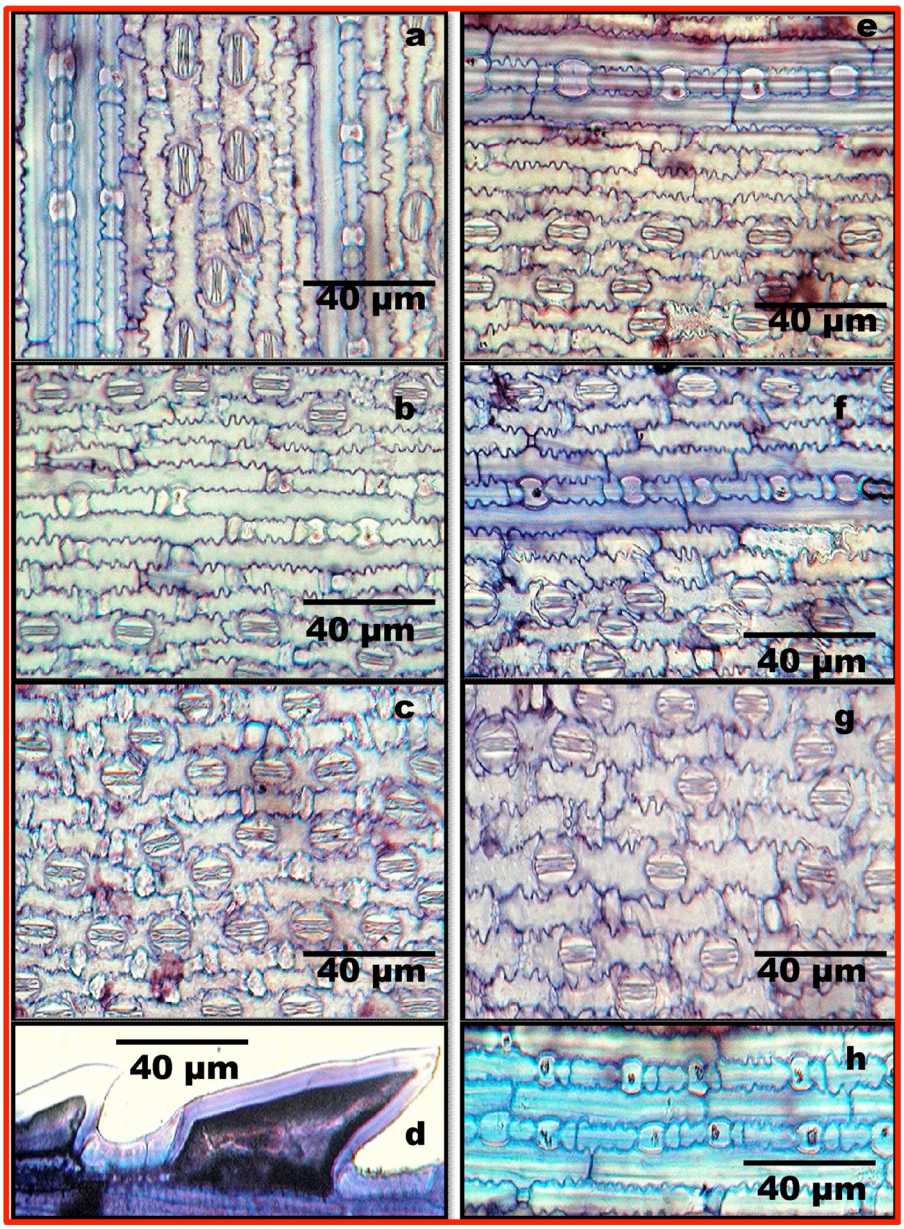

Fig. 4. *In-situ* location of phytoliths in leaf epidermis of *Phragmites karka* (Retz.)Trin ex. Steud. (adaxial surface (a–c) and abaxial surface (d–f)).

morphotypes. The occurrence of a phytolith type with higher (or lesser) frequency than the rest of the taxa could be diagnostic for that taxon. At the third stage, morphometric data of the phytoliths are employed for identification. Morphometry characterizes phytoliths in terms of size dimensions (*e.g.* length, width, area, perimeter, *etc.*) and could be employed alone or in combination with shape descriptors (*e.g.* roundness, solidity, form factor, convexity, *etc.*). Biochemical characterization of phytoliths including the crystal structure, elemental composition and bonding relationships are additional parameters added in recent literature (Hodson et al., 2005; Kamenik et al., 2013).

The present study aimed at developing diagnostic phytolith signatures of *Arundo donax* L. and *Phragmites karka* (Retz.) Trin. ex Steud. through an analytical study of the morphological, morphometric, elemental and chemical bonding diversity of phytoliths produced by underground (root) and aerial (culm, leaf and synflorescence) parts of these reed grasses.

2. Material and methods

2.1. Area of study

Arundo donax L. was collected from a large and pure stand at Badani in district Pathankot (32.34°N and 75.76°E) respectively (Fig. 1b and c). The collection site is located in the Shiwalik foothills at 332 m (asl) and experiences an annual rain fall of 1113 mm *Phragmites karka* (Retz.) Trin. ex Steud. was collected from an embankment of river Ravi at Rakh Kohali in district Amritsar (31.64°N and 74.83°E) respectively (Fig. 1d and e). The site located at 234 m (asl), receives an annual rainfall of 681 mm. Specimens were collected at the flowering stage and different underground (root) and overground (culm, leaf and synflorescence) parts were separated, cut to size and preserved in 70% ethanol at 4 °C.

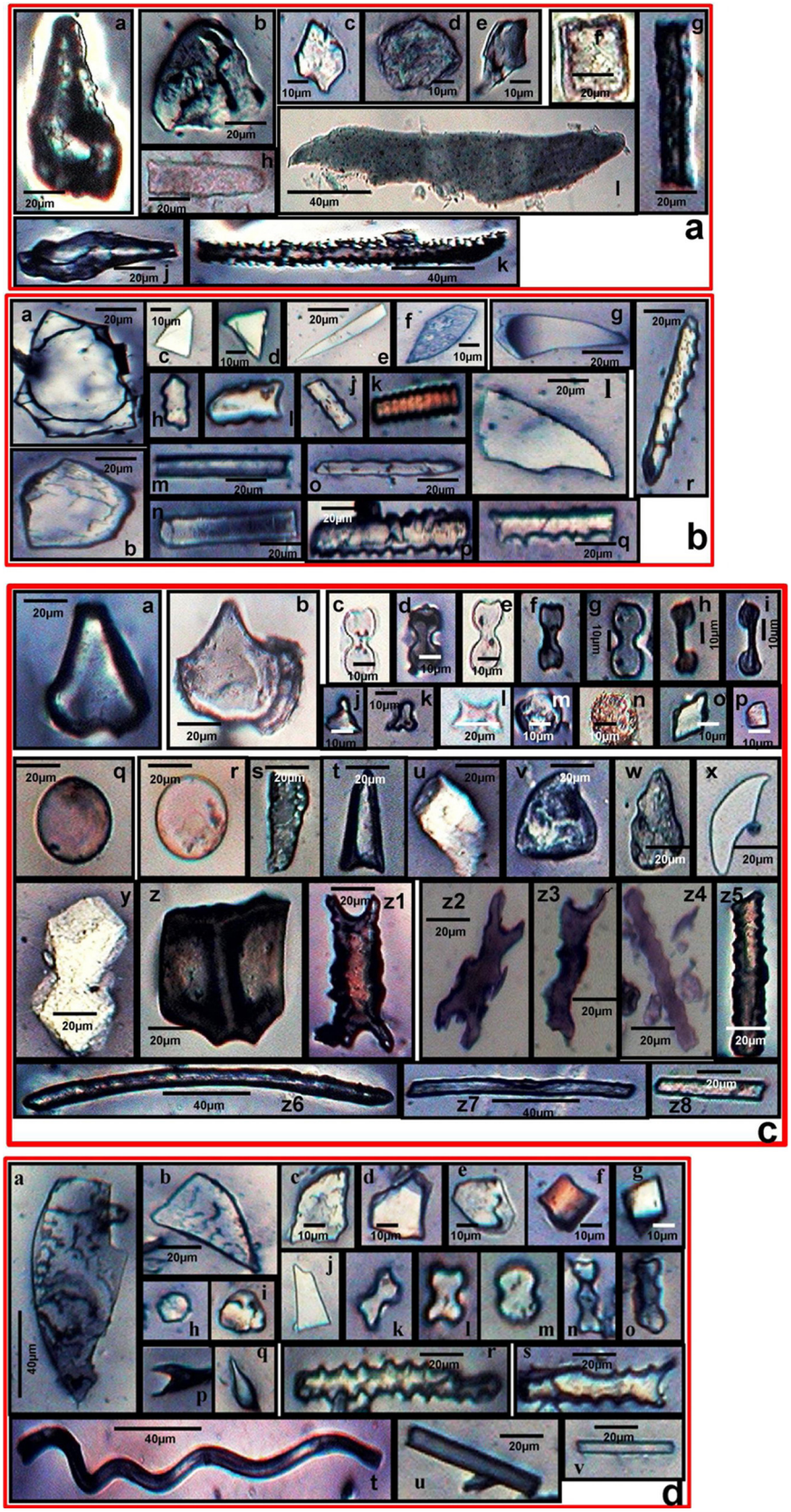

Fig. 5. Phytolith morphotypes from various parts of *Arundo donax* L. 4a (Root): Bulliform (a); Trapezoids (b, c); Globular echinate (d); Scutiform (e); Cubic (f); Sinuate elongate (g); Clavate (h–j); Echinate elongate (k). 4b (Culm):Trapezoids (a, b); Triangular (c, d); Clavate (e–g); saddles (h, i); Rectangular (j); Rugose elongate (k); Scutiform (l); Smooth elongate (m, n); Sinuate elongate (o); Echinate elongate (p–r). 4C (Leaf):Bulliform cells (a,b); Bilobates (c-g); Narrow bilobates (h, i); Flat towers (j, k); Horned tower (l); Globular echinate (m, n); Cubic (o, p); Orbicular (q, r); Clavate (s, t); Trapezoids (u–w); Scutiform (x); Parallepipedal bulliform cells (y, z); Long Trapezoids (Z1–Z3); Sinuate elongates (z4, z5); Smooth elongate (z6–z8). 4d (Synflorescence): Scutiform (a, b); Trapezoids (c–e); Cubic (f, g); Globular echinate (h, i); Clavate (J); Bilobates (k, l); Saddle (m); Polylobates (n, o); Prickle (p, q); Echinate elongate (r, s); Spiral (t) Smooth elongate (u, v).

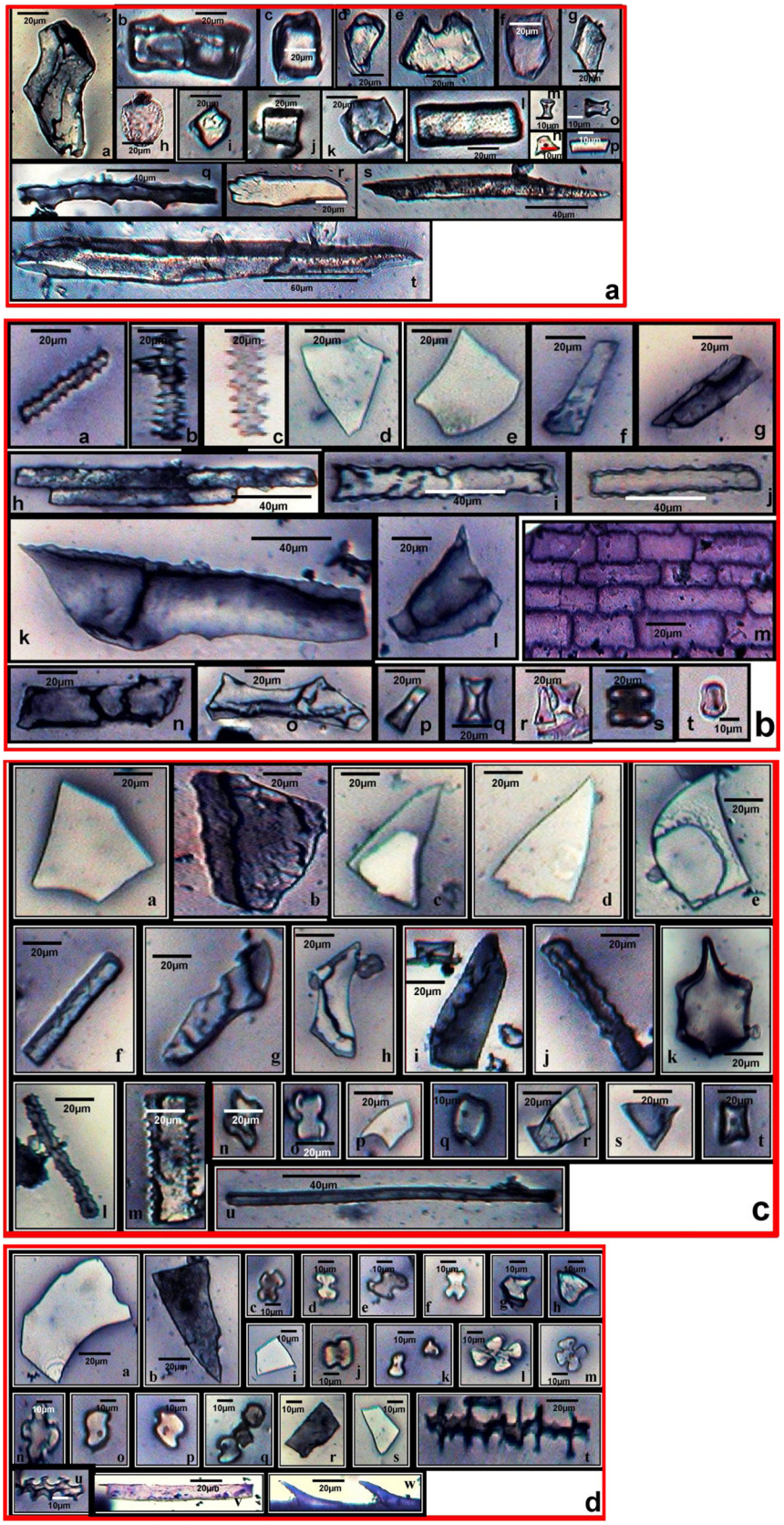

Fig. 6. Phytolith morphotypes from various parts of *Phragmites karka*(Retz.) Trin. ex Steud. 5a(Root): Parallepipedal bulliform cells (a, c); Trapezoids (d–g); Globular echinate (h); Cubic (I, j); Polyhedral (k); Rectangular (l); Flat tower (m, n); Horned tower (o); Smooth elongate (p); Echinate elongate (p); Clavate (q–s). 5b (Culm): Echinate elongate (a–c); Trapezoids (d, e); Clavate (f, g); Sinuate elongate (h–j); Scutiform (k, l); Rectangular (m); Tracheids (n, o) Flat tower (p, q1); Horned tower (q2, r); Bilobate (s); saddle (t). 5c (Leaf): Trapezoids (a, b); Scutiform (c–e); Cylindric (f); Tracheids (g, h); Clavate (i); Sinuate elongate (j); Bulliform cell (k); Echinate elongate (l, m); Bilobates (n, o); Prickle (p); Saddle (q); Cubic (r); Triangular (s); Flat tower (t); Smooth elongate (u). 5d (Synflorescence): Scutiform (a, b); Bilobates (c–f); Trapezoids (g–i); Rondels (j–k); Crosses (l, m); Quadrilobate (n); Saddles (o–q); Dendritic (r, s); Smooth elongate (t); Prickles (u).

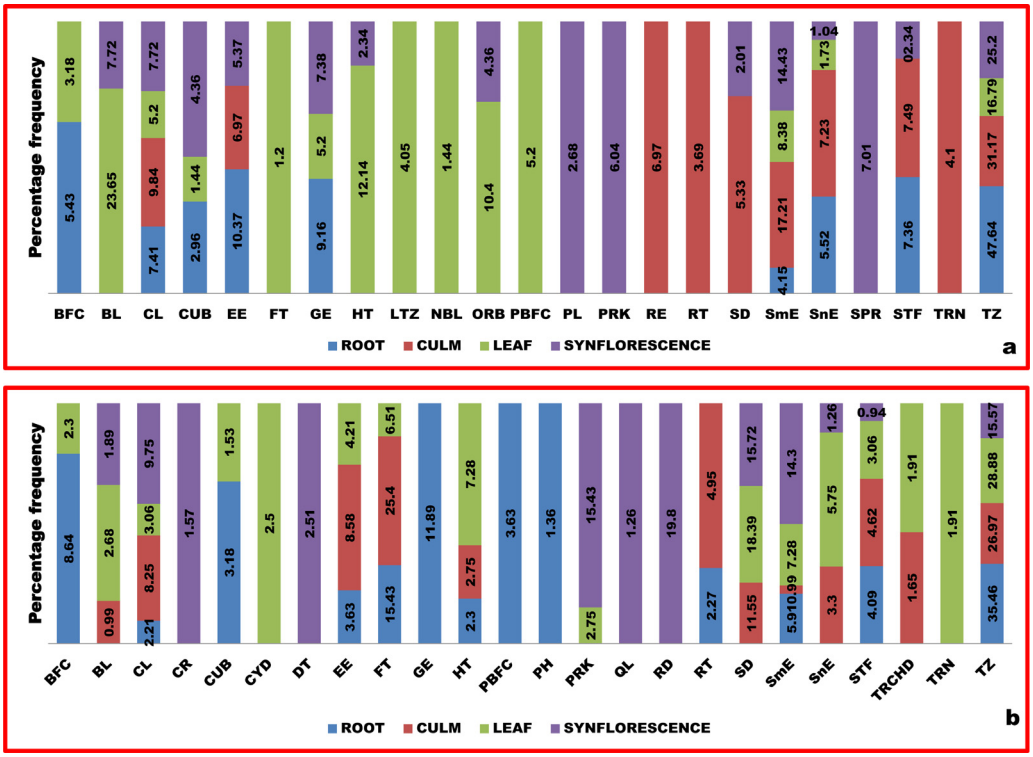

Fig. 7. Stack bars showing the percentage frequency of different phytolith types in various parts of (a) *Arundo donax* L. and (b) *Phragmites karka* (Retz.) Trin. ex Steud. (Values in stack bars indicate their respective percentage frequency in different parts) Abbreviations for types are given in Table 1a & b.

2.2. Phytolith analysis

2.2.1. In-situ location

Leaf samples for *in-situ* location of phytoliths were prepared according to the method of Clark (1959) with some modifications. Leaf blades from both fresh and preserved material were washed thoroughly under running tap water to remove adhering dust and other artifacts. Leaf segments from mature leaves were boiled in distilled water for 5–10 min in test tubes (50 ml). After cooling, leaf segments were put in ethanol and heated gently (80 °C) in a water bath till they were decolorized. Thereafter, leaf segments were immersed in a solution of lactic acid and chloral hydrate (3:1 v/v) and heated again for 20–30 min in a water bath. Lactic acid softened the leaf segments for taking epidermal peelings. After clearing, leaf segments were placed on clean ceramic tiles with the adaxial surface upwards and epidermal layer was peeled off from middle part of mature leaf blades. Epidermal peelings were taken in a watch glass and stained in Gentian violet. The watch glass was heated gently over a spirit lamp for 3–5 min (in small intervals) for deep staining. Excess stain was removed and peelings passed through a dehydration series of Ethanol (30% through 50%, 70%, 90% and absolute ethanol) and were mounted in DPX for light microscopy and microphotography with a Micro Image Projection System Camera (MIPS-USB 0262).

2.2.2. Dry ashing method

Carnelli et al. (2001) protocol was employed for dry ashing of the plant material. About 10–20 plants of each species were dismembered into root, culm, leaf and synflorescence and each part rinsed under tap water thoroughly. The parts were dried, weighed, cut into small pieces and transferred to porcelain crucibles. The crucibles were incinerated at 550 °C for 4–6 h to ashes in a muffle furnace. During incineration, the material turned to white ash. The crucibles were taken out of the furnace, cooled and ash contents transferred to test tubes. Sufficient quantities of hydrogen peroxide (30%) were added to submerge the ash and test tubes were kept at 80 °C for 1 h in a water bath. The mixture was decanted and rinsed twice in distilled water. Hydrochloric acid (10%) was added to the pellet and incubated at 80 °C for 1 h. Thereafter, the mixture were washed in distilled water and centrifuged for 15 min at 7500 rpm. The supernatant was decanted off and the pellet was washed twice in distilled water. The process was repeated (four times) till the pellet was clear. Finally, the pellet was dried for 24 h at 60 °C to a powder form and weighed. The silica content (%) was calculated by the formula: ash content/dry mass × 100.

A small amount (0.05 mg) of dried ash was dipped in 10 ml of Gentian violet in a watch glass. A drop of dry ash mixture in Gentian violet was put on a glass slide and covered with a cover slip. The slides were heated gently and excess stain drained off in the folds of a filter paper. Ten slides were prepared for each sample. Morphotypes of phytoliths were identified by their shape and size. Frequency data of different morphotypes were recorded with the help of a marked observation area (1.24 mm^2) on the coverslip. Olympus Micro Image Projection System (MIPS-USB 0262) was employed for microphotography of various morphotypes at a uniform magnification (40×). The morphotypes were named according to the schemes of Twiss et al. (1969), Lu and Liu (2003) and the International Code of Phytolith Nomenclature 1.0 (Madella et al., 2005) (Table 1).

2.3. Morphometry

Morphometric measurements of morphotypes were made in Image J software (version 1.46r.). The software not only recorded dimensions but also calculated values of other descriptors of size (surface area) and shape (aspect ratio, roundness, circularity and solidity). Besides, the study includes some additional morphometric parameters for two key phytolith types *viz.*, bilobate and bulliform cell phytoliths. These parameters included vertical length, width of lobe, length and width of shank and width of

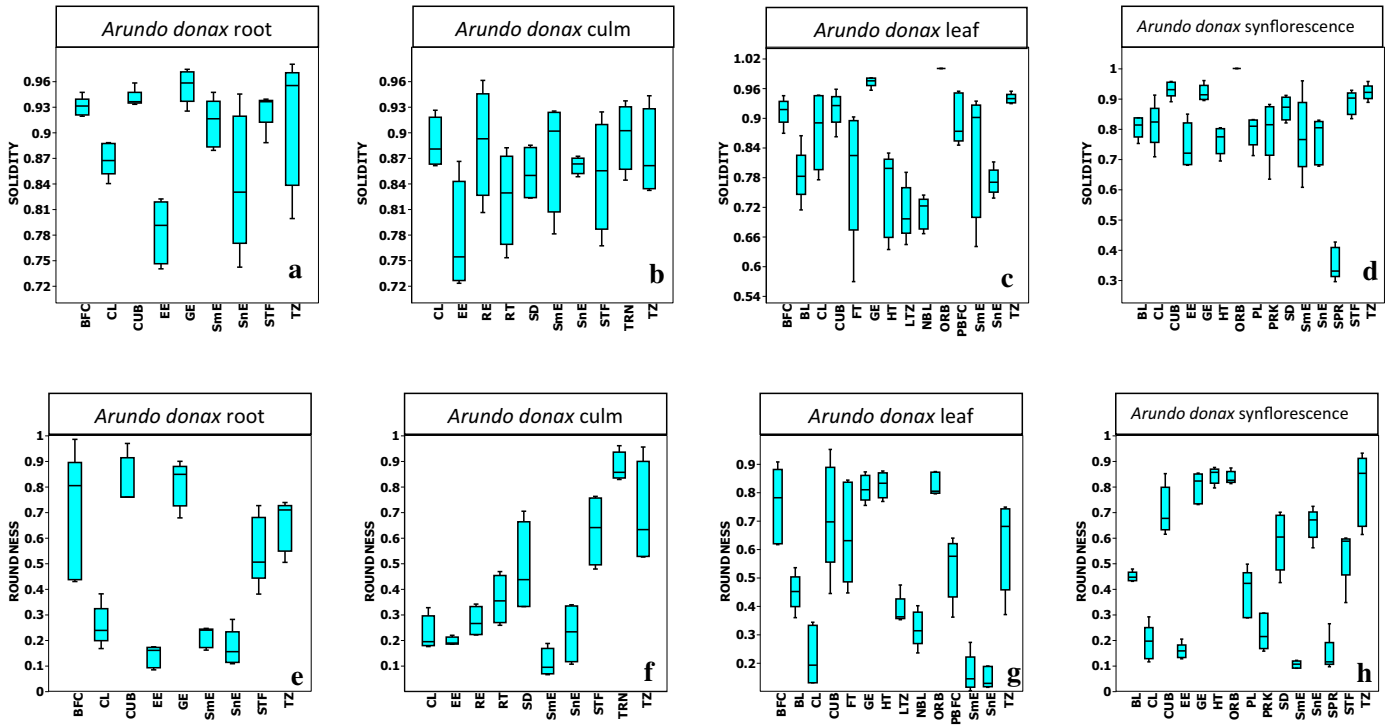

Fig. 8. Box-Whisker plots for median, percentile and range of shape descriptors (solidity and roundness) of phytoliths in *Arundo donax* L.

scooped end for bilobate phytolith and vertical length, horizontal length, lateral length, length of base portion and length of non-base portion for bulliform cell phytoliths respectively (Fig. 2a and b).

2.4. Scanning Electron Microscopy (SEM)

Insights into ultra-structural details were gained through Scanning Electron Microscopy (SEM). Dry ash was spread evenly over the stubs, dried overnight at 40 °C, coated with graphite and gold by a sputter coater (QUORUM) and imaged under SEM (CARL ZEISS EVO 40) at an accelerating voltage of 40 kV.

2.5. Chemical architecture

Elemental analysis of morphotypes was carried out with Scanning Electron Microscope-Energy Dispersive X-ray analysis (SEM/EDX). Infrared spectra of silica powder were obtained on an Fourier Transform Infrared (FTIR) Spectrophotometer (System 92035, Perkin-Elmer, England) at room temperature using the standard KBr method. The functional group spectra were recorded over a wavelength range of 500 cm^{-1} to 4000 cm^{-1}. X-ray Diffraction (XRD) studies were performed on powder XRD system (Bruker D8 Advance) using Cu Kα radiation (k = 1.5418 Å) in the 2θ (Bragg's angle) range of 10–70. The data were analysed for presence of different polymorphic structures of silica and other compounds using the origin pro 8 software and following the notation of Joint Committee on Powder Diffraction.

2.6. Statistical analysis

Principal Component Analysis of elemental composition data was carried out with the help of paleontological statistics (PAST) software (Hammer et al., 2001). Morphometric comparison of morphotypes were made by *t*-test for unpaired data arrays. Silicon content (Si wt%) of phytoliths as revealed by SEM-EDX analysis were compared within and between the species using one-way and two-way analysis of variance (ANOVA).

3. Results and discussion

3.1. Epidermal patterns

After spikelet structure, epidermal cell patterns and cytology are the most important characters for taxonomic characterization and diagnosis of grasses (Prat, 1936; Metcalfe, 1960; Srivastava, 1978; Hilu 1984). Leaf epidermis of grasses is a matrix of several kinds of longitudinal epidermal long cells and short cells arranged in diagnostic patterns in the costal and intercostal regions (Metcalfe, 1960). The short cells differentiate into cork cell pairs, microhairs, macrohairs, prickles and stomata (McWhorter et al., 1993). Orientation and patterning of silica cells among different kinds of epidermal cells has provided an additional evidence for taxonomic characterization of grasses (Rudall et al., 2014; Jattisha and Sabu, 2015). Silica cells in grass leaf epidermis are oriented both axially (parallel) and transversely (perpendicular) to the long axis of the leaf blade. Fernández Pepi et al. (2012b) reported that leaf epidermis in eight species of the genus *Festuca* L. namely, *F. cirrosa* (Speg.) Parodi, *F. contracta* Kirk., *F. gracillima* Hook. f., *F. magellanica* Lam., *F. monticola* Phil., *F. purpurescens* Banks & Sol. ex Hook. f., *F. pyrogea* Speg. and *F. thermarum* Phil. had long cells with sinous margins, separated intermittently with rectangular to irregular (contorted) short cells that contain crescent shaped silica bodies in the intercostal but sinuate trapezoid ones in the costal zone.

Leaf epidermal patterns of some taxa of subfamily Arundinoideae (including *Arundo* spp. and *Phragmites* spp.) have been dealt by Renvoize, (1986). The subfamily showed presence of saddle or dumb-bell shaped to nodular phytoliths with occasional presence of square or oblong types in varying proportions in 1–4 rows in the costal zones of both upper and lower epidermis. The cleared epidermal peelings revealed diagnostic patterns and distribution of phytoliths that could be employed in diagnosis of the arundinoid reed grasses under reference. Adaxial surface of *Arundo donax* L. leaf

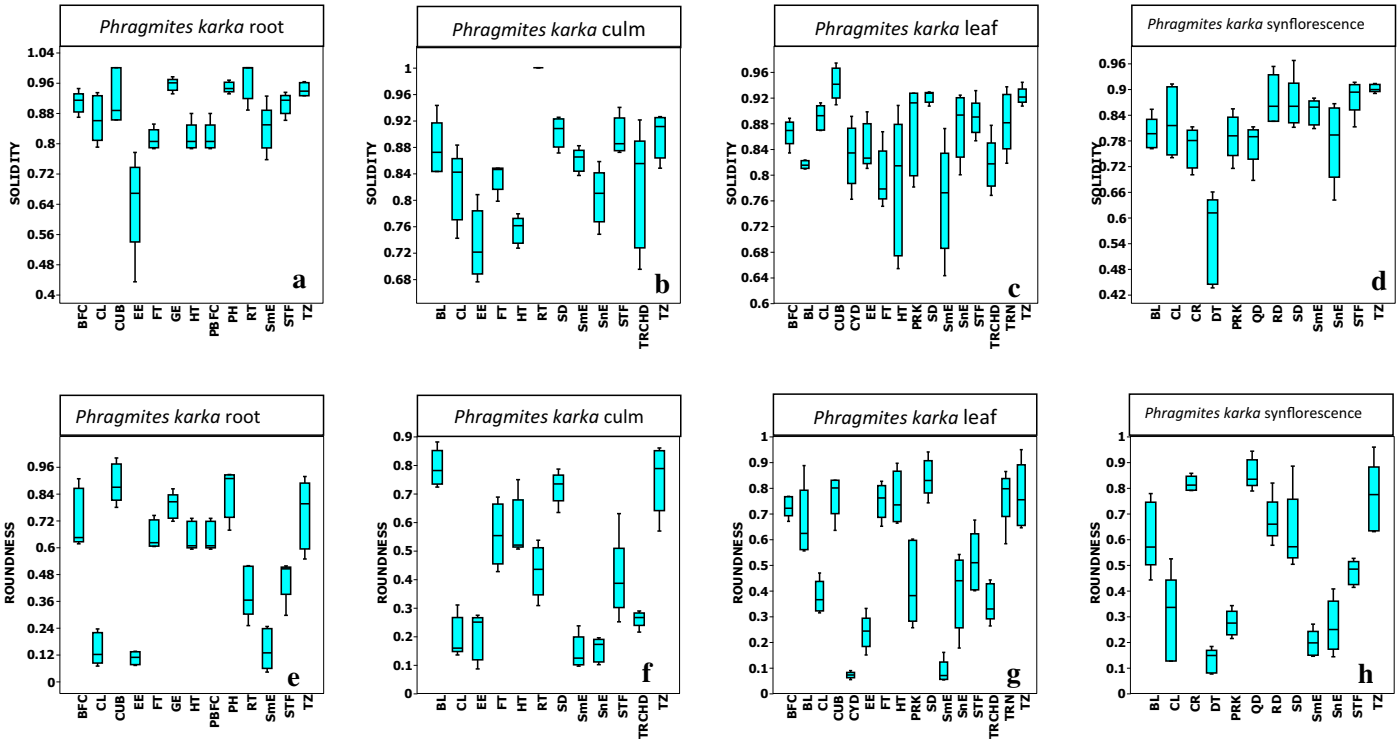

Fig. 9. Box-Whisker plots for median, percentile and range of shape descriptors (solidity and roundness) of phytoliths in *Phragmites karka* (Retz.)Trin. ex Steud.

Table 3a
Comparison of morphometric parameters of bulliform cell phytoliths of *Arundo donax* L. and *Phragmites karka* (Retz.) Trin ex. Steud.

	Phytolith morphotypes		
	Bulliform cells (BFC)		
Species	*Arundo donax* L.	*Phragmites karka* (Retz.) Trin ex. stued	P-value
Morphometric parameters			
Area	2338.5 ± 300.05	4296.1 ± 205.98	0.001*
Perimeter	201.95 ± 10.98	285.12 ± 5.98	0.001*
Vertical length (Length)	69.01 ± 5.39	98.04 ± 1.46	0.001*
Horizontal length (Width)	49.67 ± 3.55	64.38 ± 0.45	0.014
Length of base portion	36.38 ± 6.49	23.55 ± 3.08	0.112
Length of non-base portion	35.99 ± 5.59	77.53 ± 0.62	0.002**
Lateral length	25.32 ± 5.33	24.63 ± 1.07	0.902

*represents significance at $p \leq 0.001$ and **represents significance at $p \leq 0.01$

Table 3b
Comparison of morphometric parameters of bilobate phytoliths of *Arundo donax* L. and *Phragmites karka* (Retz.) Trin ex. Steud.

	Phytolith morphotypes		
	Bilobates (BL)		
Species	*Arundo donax* L.	*Phragmites karka* (Retz.) Trin ex. stued	P-value
Morphometric parameters			
Area	297.90 ± 72.22	201.97 ± 19.74	0.247
Perimeter	90.77 ± 10.03	68.46 ± 3.02	0.077
Vertical length (Length)	27.58 ± 3.06	18.26 ± 0.52	0.034*
Width of lobe	13.36 ± 1.57	12.74 ± 1.12	0.756
Length of shank	9.87 ± 0.94	4.85 ± 0.63	0.004**
Width of shank	5.42 ± 1.21	6.05 ± 0.18	0.643
Width of scooped end	5.81 ± 0.83	6.86 ± 0.42	0.309

*represents significance at $p \leq 0.05$ and **represents significance at $p \leq 0.01$.

in the costal region revealed 1–4 chains of axially arranged bilobate phytoliths with narrow shanks, scooped ends and extended lobes, and were spaced and separated by intervening silica cork cells. It also revealed intermittent presence of saddle silica cells with a frequency of less than five percent. The intercostal region comprised of 1–2 rows of bilobate silica cells separated regularly by epidermal long cells having an echinate outline. It also had 5–6 rows of stomata with low dome which is believed to be an advanced character (Ellis, 1979; Shouliang et al., 1996). The stomata in each stomatal file were separated by interstomatal cells (Fig. 3a–c).

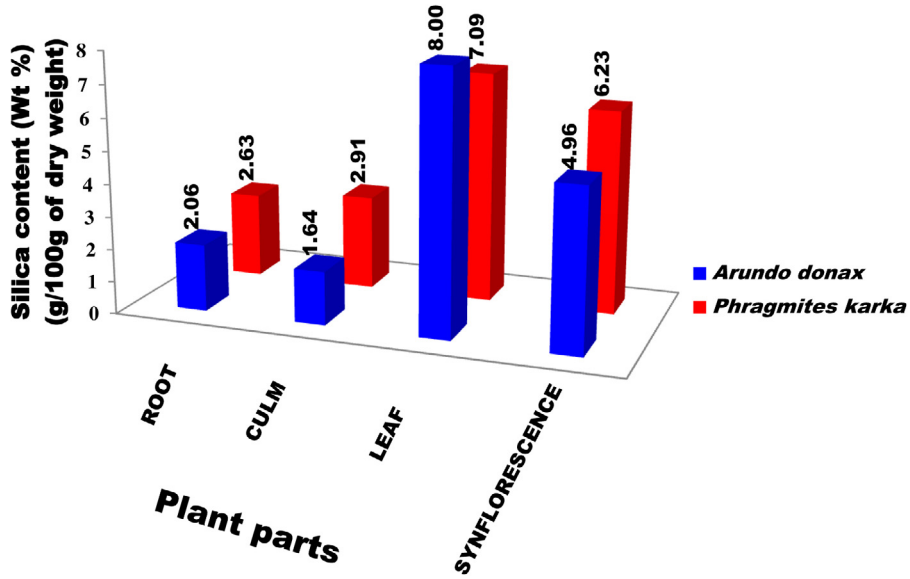

Fig. 10. 3D bar-chart showing the silica content in various parts of *Arundo donax* L. and *Phragmites karka* (Retz.) Trin. ex Steud. (g/100 g) (Data points at the top of each bar represent percentage silica content).

The abaxial surface of the *Arundo donax* L. had 1–4 rows of bilobate phytoliths arranged axially in the costal region and separated by silica short cells. But these bilobates had comparatively thick shanks as compared to the ones on adaxial surface. They were further marked out from the adaxial ones in lacking extended lobes and scooped ends. The intercostal region was marked by 1–2 rows of bilobate/irregular bilobates in both axial and transverse orientation (Fig. 3d–f). The adaxial surface had a higher frequency of stomata and was further distinguished by the presence of microhair. As regards the distribution of phytoliths, leaf epidermal profile of *Phragmites karka* (Retz.) Trin. ex Steud. presented a different scenario. In the costal region on the adaxial surface leaf blade had 1–3 rows of saddle shaped silica cells with each saddle separated by a silica cork cell and epidermal long cells with echinate outlines. Similar epidermal patterning of saddles occured on the abaxial surface as well (Fig. 4a–f). The intercostal region on both adaxial and abaxial surfaces revealed a similar pattern of epidermal cells; both had 2–6 rowed stomatal files of low domed stomata (Fig. 4c, d). But adaxial surface had a higher frequency of silica cork cells as compared to the abaxial surface. The margins of adaxial surface of *Phragmites karka* (Retz.) Trin. ex Steud. also showed the presence of prickle hairs with barbs as long as or slightly longer than the base.

3.2. Phytolith morphotypes

Dry ashing yielded about thirty phytolith morphotypes recognized and classified by their diagnostic shapes and sizes. The present study has added the 'spiral' type to the world catalog of phytolith morphotypes. The morphotypes were grouped into five categories namely, long cells, short cells, bulliform cells, prickle hairs and tracheids. The first four types are known to have an epidermal location while the last one belongs to the vascular system (Gu et al., 2013). The short cell group included 17 morphotypes (bilobate, cross, cubic, flat tower, granular echinate, horned tower, nodular bilobate, orbicular, polyhedral, polylobate, quadrilobate, rondel, rugose elongate, saddle, scutiform, trapezoid and triangular); long cells included 9 types (clavate, cylindric, dendritic, echinate elongate, long trapezoids, smooth elongate, sinuate elongate, spiral and rectangular); the bulliform cells only two types. The first one comprised of bulliform cells (also called as motor cells, fan cells, cuneiform bulliform cells) and the second type of parallepipedal bulliform cells. The prickle hairs (prickle) and tracheids (tracheid) were each represented by a single type named in parenthesis.

Earlier studies in grasses have dealt with documentation of phytoliths from overground parts mainly the leaf (Sangster and Parry, 1969; Twiss et al., 1969; Lau et al., 1978; Perry et al., 1984; Hodson and Sangster, 1988; Ollendorf et al., 1988; Whang et al., 1998; Krishnan et al., 2000; Dietrich et al., 2003; Ponzi and Pizzolongo, 2003), but also the culm and the synflorescence (Bonnett, 1972; Ball et al., 1999; Lu and Liu, 2003; Portillo et al., 2006; Ball et al., 2009; Tripathi et al., 2012). The present study has enlarged the scope of phytolith analysis in grasses by including phytolith profiles of underground parts (roots) as well. Between the two species *Phragmites karka* (Retz.) Trin. ex Steud. revealed a greater diversity of phytolith morphotypes (24) with an overlapping representation of types from root (13), culm (12), leaf (16) and synflorescence (12). *Arundo donax* L. also had nearly the same number (23) morphotypes with similar representation from root (9), culm (10), leaf (14) and synflorescence (15). Overall, the order of numerical representation would be leaf > synflorescence > culm > root in both the species (Tables 2a and 2b).

Some of the morphotypes were common to both the species while others are found only in one of this pair of arundinoid grasses. The shared types included the clavate, trapezoid and smooth elongate morphotypes from all their parts (Tables 2a and 2b). As both these reed grasses belong to the subfamily (Arundinoideae), the presence of shared types was only to be expected. But phytolith profiles of these reeds also revealed morphotypes that mark one species from the other. Marker morphotypes isolated from various parts of *Arundo donax* L. include the long trapezoids (Fig. 5c-z1-z3) and narrow bilobates (Fig. 5c–h, i), from leaf, orbicular (Fig. 5c–q, r and Fig. 14w) from both leaf and synflorescence, polylobate (Fig. 5d–n) and spiral (Figs. 5 d–t and 1 4r) from the synflorescence and rugose elongate morphotype from the culm (Fig. 5b–k). Similarly, *Phragmites karka* (Retz.) Trin. ex Steud. yielded unique and diagnostic phytolith assemblages from different parts of the plant body. They included the polyhedral (Fig. 6a–k) from the root, tracheids (Fig. 6b–n, o and c–g, h) from both culm and leaf, cylindric (Figs. 6 c–f and 1 5t) from leaf, and cross (Fig. 6d–l and m), dendritic (Fig. 6d–t and u), quadrilobate (Fig. 6d–n) and rondel (Figs. 6 d–j and k; 15 u and v) from the synflorescence.

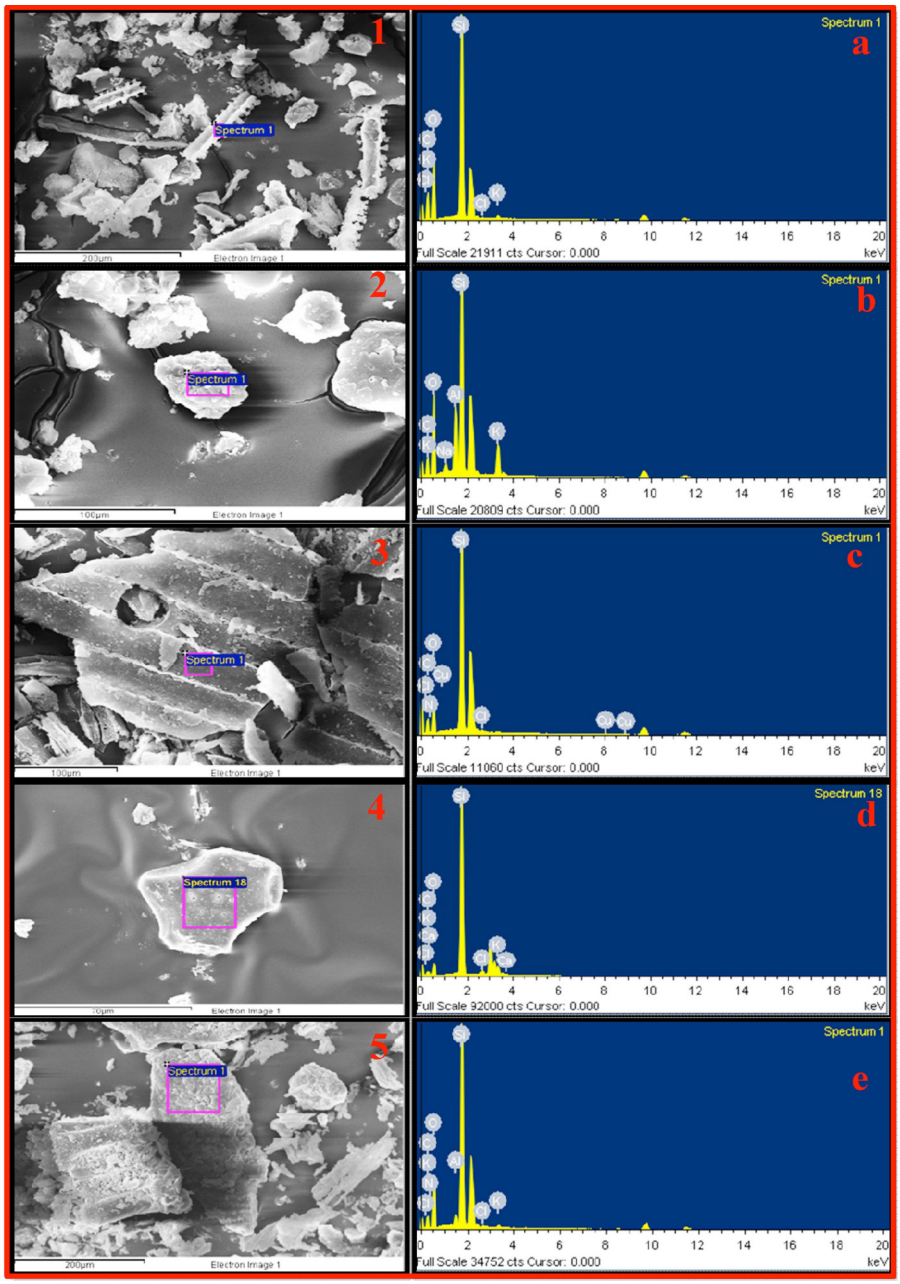

Fig. 11. SEM-EDX spectra of phytoliths isolated from different parts of *Arundo donax* L. Root (1-a, 2-b); Culm (3-c); Leaf (4-d) and Synflorescence (5-e).

Dore (1960) and Piperno (1983) reported diagnostic differences in phytolith profiles from leaves of *Arundo donax* L. and *Phragmites communis* (L.) Trin. mainly in the presence of saddles from *Phragmites communis* (L.) Trin. in contrast to bilobates and crosses in *Arundo donax* L. However, the reported differences between the phytolith profiles of leaves of this pair of arundinoid grasses required further confirmation as their findings contradicted the reports of saddle morphotypes from *Arundo donax* L. (Metcalfe, 1960) and later Chauhan et al. (2011). Our findings support the contention that saddles do not diagnose the genus *Phragmites spp* from *Arundo spp*. Although, we did not recover saddles from the leaf dry ash of *Arundo donax* L. but they were visualized *in-situ* in the leaf epidermis (Fig. 3c). Moreover saddles have been recovered even from the dry ash of culm (5.33%) and synflorescence (2.01%) of this species. However, saddles were recovered with a much higher frequencies from leaf (18.39), culm (11.55%) and synflorescence (15.72%) respectively of *Phragmites karka* (Retz.) Trin. ex Steud. (Fig. 7a and b) lending further credence to earlier reports that emphasize the relevance of frequency data in taxonomic diagnosis and analysis (Jattisha and Sabu, 2012; Szabo et al., 2014; Ball et al., 2015). The present results do not support the reports of cross morphotypes from *Arundo donax* L. (Ollendorf et al., 1988). In our work, recovery of cross morphotypes from the synflorescence of *Phragmites karka* (Retz.) Trin. ex Steud. and their absence from all the parts of *Arundo donax* L. both from *in-situ* visualization as also dry ash seems to provide a diagnostic difference. The above results clearly highlight the importance of studying phytolith profiles from all (underground and aerial) parts before their evaluation and use in taxonomic diagnosis, as also in studies related to reconstruction of past vegetation types, where soil phytolith profiles are used to make interpretations (Gosh et al., 2011; An et al., 2015; Biswas et al., 2016).

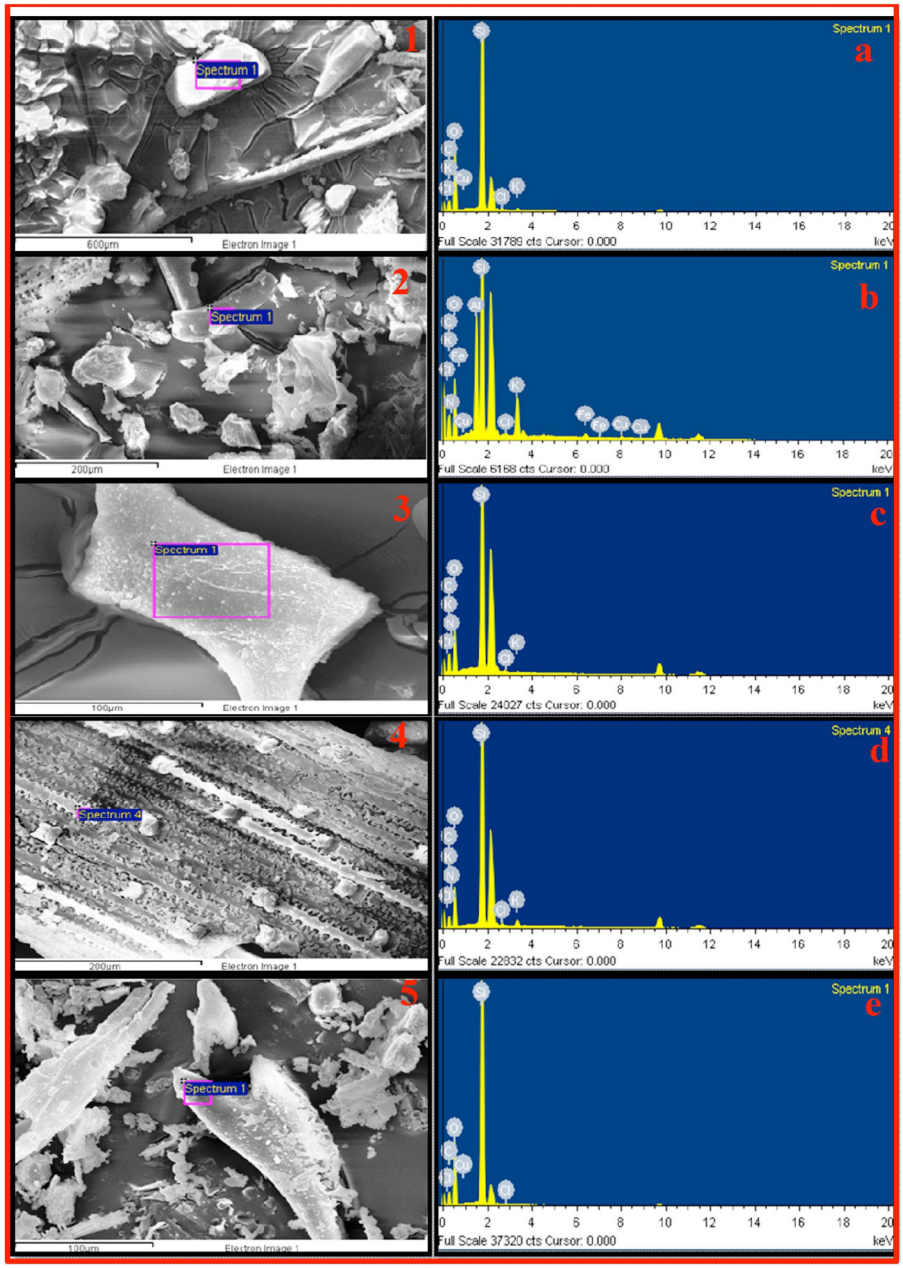

Fig. 12. SEM-EDX spectra of phytoliths isolated from different parts of *Phragmites karka* (Retz.) Trin. ex Steud. Root (1-a, 2-b); Culm (3-c); Leaf (4-d) and Synflorescence (5-e).

3.3. Frequency distribution

Arundo donax L. and *Phragmites karka* (Retz.) Trin. ex Steud. showed considerable variation in percentage frequency occurrences of various morphotypes (Fig. 7a and b). For example, frequency of bilobates was higher by several orders of magnitude in *Arundo donax* L. leaf (24.85%) and synflorescence (7.72%) as compared to *Phragmites karka* (Retz.) Trin. ex Steud. culm (0.99%), leaf (2.68%) and synflorescence (1.89%) respectively (Fig. 7a and b). Comparison of the frequency of shared phytoliths types in at least one part of these reed grasses showed significant differences. In this scenario, the frequency of flat towers were significantly lesser in leaves (1.2%) of *Arundo donax* L. as compared to the leaves (6.04%) of *Phragmites karka* (Retz.) Trin. ex Steud. ($p \leq 0.05$; χ^2 test) Besides the later species also showed their presence in the root (15.43) and culm (25.4%). Similarly, the frequency of prickles in the synflorescence of *Arundo donax* L. was much lesser (6.04%) than in *Phragmites karka* (Retz.) Trin. ex Steud (15.43%). in addition to their presence (2.75%) in the leaves of latter named species and their absence from the leaves of the former. Both the reed grasses showed the presence of smooth elongate type of phytoliths in all their parts but their percentage frequency in culm showed highly significant differences ($p \leq 0.001$; χ^2 test) with *Arundo donax* L. (17.21%) and *Phragmites karka* (Retz.) Trin. ex Steud. (0.99%), other body parts showed slightly lesser differences in their percentage frequency occurrences (Fig. 7). Similarly, other phytolith morphotypes revealed significant differences in percentage frequency occurrence (Fig. 7a and b). The diagnostic significance of frequency data of phytoliths of plant species has been highlighted in several studies (Honaine et al., 2006; Jattisha and Sabu, 2012; Szabo et al., 2014; Fernández Pepi et al., 2012b; Ball et al., 2015). Recently, Huan et al. (2015) highlighted the significance of percentage frequency data in discriminating the wild and domesticated rice plants on the basis of bulliform phytolith signatures.

Table 4
Elemental composition of phytolith from various parts of *Arundo donax* L. and *Phragmites karka* (Retz.) Trin ex Steud.

Species	*Arundo donax*							
Plant Part	Root		Culm		Leaf		Synflorescence	
Elements	WT%	AT%	WT%	AT%	WT%	AT%	WT%	AT%
Carbon (C)	27.66 ± 3.78	38.97 ± 3.82	42.86 ± 4.33	53.54 ± 4.06	25.30 ± 1.06	37.41 ± 1.66	28.86 ± 3.17	40.48 ± 3.48
Nitrogen (N)	1.67 ± 1.02	2.46 ± 1.09	2.07 ± 0.95	2.30 ± 0.05	0.66 ± 0.66	0.80 ± 0.80	0.96 ± 0.63	1.67 ± 0.84
Oxygen (O)	27.65 ± 7.65	36.94 ± 4.31	35.20 ± 1.85	33.52 ± 2.22	32.25 ± 2.15	35.32 ± 2.60	34.29 ± 2.04	38.61 ± 2.41
Silicon (Si)	27.34 ± 6.90	18.164.73	18.44 ± 3.21	10.22 ± 2.02	38.18 ± 1.86	24.65 ± 2.01	28.64 ± 3.04	16.10 ± 1.27
Chlorine (Cl)	1.69 ± 1.62	0.02 ± 0.02	0.36 ± 0.11	0.16 ± 0.05	2.12 ± 0.52	1.08 ± 0.26	0.20 ± 0.17	0.12 ± 0.08
Potassium (K)	5.77 ± 4.06	1.27 ± 0.65	–	–	0.90 ± 0.28	0.42 ± 0.14	2.44 ± 1.42	1.34 ± 0.61
Calcium (Ca)	–	–	–	–	0.31 ± 0.12	o.14 ± 0.06	0.03 ± 0.03	0.01 ± 0.01
Aluminum (Al)	1.70 ± 1.56	2.80 ± 1.93	–	–	0.22 ± 0.22	0.14 ± 0.14	3.37 ± 2.24	2.72 ± 1.46
Sodium (Na)	9.50 ± 9.05	0.28 ± 0.20	–	–	–	–	0.07 ± 0.07	0.06 ± 0.05
Titanium (Ti)	0.11 ± 0.11	0.04 ± 0.04	–	–	–	–	0.04 ± 0.04	0.02 ± 0.01
Iron (Fe)	0.24 ± 0.24	0.08 ± 0.08	–	–	–	–	0.27 ± 0.27	0.11 ± 0.09
Copper (Cu)	–	–	1.07 ± 0.14	0.26 ± 0.04	–	–	0.77 ± 0.20	0.25 ± 0.04
Magnesium (Mg)	–	–	–	–	0.035 ± 0.03	0.02 ± 0.02	0.08 ± 0.08	0.08 ± 0.06
Species	*Phragmites karka*							
Plant Part	Root		Culm		Leaf		Synflorescence	
Elements	WT%	AT%	WT%	AT%	WT%	AT%	WT%	AT%
Carbon (C)	22.93 ± 1.02	34.96 ± 1.50	31.92 ± 3.12	42.49 ± 3.16	24.64 ± 2.78	36.68 ± 2.61	32.95 ± 3.83	45.56 ± 5.27
Nitrogen (N)	2.45 ± 1.03	3.13 ± 1.31	5.13 ± 1.11	5.89 ± 1.25	3.60 ± 1.06	4.40 ± 1.26	11.16 ± 6.51	4.09 ± 0.84
Oxygen (O)	36.07 ± 3.32	39.93 ± 3.05	35.30 ± 1.24	35.68 ± 1.71	34.73 ± 2.84	37.37 ± 3.88	35.86 ± 1.24	36.93 ± 2.80
Silicon (Si)	32.12 ± 2.28	18.93 ± 2.38	26.95 ± 2.55	15.64 ± 1.71	32.03 ± 0.99	18.70 ± 0.96	23.53 ± 3.85	13.05 ± 2.92
Chlorine (Cl)	0.35 ± 0.18	0.17 ± 0.09	0.22 ± 0.07	0.10 ± 0.03	0.75 ± 0.28	0.33 ± 0.15	0.03 ± 0.03	0.01 ± 0.01
Potassium (K)	2.58 ± 1.00	1.16 ± 0.45	0.42 ± 0.05	0.17 ± 0.02	1.47 ± 0.36	0.64 ± 0.15	0.04 ± 0.04	0.02 ± 0.02
Calcium (Ca)	–	–	–	–	1.17 ± 1.17	0.53 ± 0.53	–	–
Aluminum (Al)	2.00 ± 2.00	1.30 ± 1.30	0.06 ± 0.06	0.03 ± 0.03	1.17 ± 1.17	1.06 ± 1.06	–	–
Sodium (Na)	–	–	–	–	0.21 ± 0.21	0.17 ± 0.17	–	–
Titanium (Ti)	–	–	–	–	–	–	–	–
Iron (Fe)	0.32 ± 0.32	0.10 ± 0.10	–	–	0.20 ± 0.20	0.06 ± 0.06	–	–
Copper (Cu)	1.18 ± 0.24	0.32 ± 0.07	–	–	–	–	1.41 ± 0.11	0.32 ± 0.05
Magnesium (Mg)	–	–	–	–	0.04 ± 0.04	0.03 ± 0.03	–	–

WT% = Weight percentage; AT% = Atomic percentage; The entries in the table indicate mean± Standard error; (—) = Absence of eleme

3.4. Morphometric measurements

Apart from frequency distribution, morphometric data on size dimensions and shape descriptors of the morphotypes have also been employed for taxonomic resolution of plant species (Ball et al., 1993; Ball et al., 1996; Whang et al., 1998; Krishnan et al., 2000; Portillo et al., 2006; Ball et al., 2009). In the present study, we have collected data on size parameters (length, width, area and perimeter) and shape descriptors like aspect ratio (Tables 2a and 2b), roundness and solidity of different phytolith morphotypes from plant parts of both the species (Figs. 8 and 9). A discussion of results of statistical comparisons of size and shape descriptors would greatly add to the volume of the paper. Here we include comparison of only two key morphotypes, namely the bilobates and bullifrom cells (Figs. 8 and 9). Using *t*-test for bulliform cell morphotype, surface area, perimeter, vertical length showed significant differences ($p \leq 0.001$) and length of non-base portion highly significant differences ($p \leq 0.01$) between the two species (Table 3a). Similarly, for bilobate morphotypes, differences in vertical length ($p \leq 0.01$) and length of shank ($p \leq 0.05$) was found to be statistically significant (Table 3b).

The morphometric data of shape descriptors (aspect ratio, solidity and roundness) assigned quantitative values to shapes of phytolith morphotypes and made them amenable to comparison (Tables 2a and 2b, Figs. 8 and 9). For example, aspect ratio more than unity signifies that a particular morphotype is longer than wide. It ranged from >1–3 for short cell types whereas for long cell types, it ranged from >5 to <11 (Tables 2a and 2b). Similarly, the value of roundness was unity for perfect circles and decreased with an increase along any of the dimensions. The orbicular phytoliths showed roundness values of >0.8 (Fig. 8g and h). Expectedly, roundness value of elongate types (smooth elongate, sinuate elongate *etc*), hardly exceeded 0.60 (Figs. 8 e–h and 9 e–h). The data confirms inverse relationship between aspect ratio and roundness. Another important shape descriptor was solidity which is a measure of the ratio between the total surface area to the convex area of a type. Accordingly, orbicular and convex polygonal (eg. the perfect rectangles) showed the perfect solidity value of unity which gets confirmed from Box-Whisker plots that show mean, median and percentiles at the same position (Figs. 8 c and d and 9 b). Expectedly, values of solidity were lowest for echinate elongate and dendritic morphotypes as these types bore surface indentations that increase surface area without affecting the convex area of these types (Figs. 8 a and b and 9 a, b and d).

3.5. Scanning Electron Microscopy

SEM of phytoliths of *Arundo donax* L. and *Phragmites karka* (Retz.) Trin. ex Steud. in both *in-situ* and isolated state revealed subtle differences in structure (Figs. 14 and 15). For example, the surface of the trapezoidal phytoliths from root of *Arundo donax* L. was rough as compared to those from the root of *Phragmites karka* (Retz.) Trin. ex Steud. (Fig. 15a). Similarly, echinate elongate phytoliths of *Phragmites karka* (Retz.) Trin. ex Steud. (culm) revealed dot like markings on the upper surface in addition to lateral extensions seen in the other species (Fig. 15k). Differences were also detected within the species. For example, the echinate elongate type in *Arundo donax* L. showed one sided knobs from root material (Fig. 14e) as compared to two sided knobs from the synflorescence (Fig. 14v). SEM has revealed ultra structural differences of rectangular phytoliths from the root (Fig. 15a) and the culm (Fig. 15g) of *Phragmites karka* (Retz.) Trin. ex Steud.; phytoliths isolated from the root had smooth

Table 5
Comparison of elemental composition of phytoliths as reflected in the previous and present studies.

Macro-elements									Micro-elements													Number	References	Material	Technique (s)
C	Ca	K	Mg	Na	–	–	–	–	Fe	Mn	Si	–	–	–	–	–	–	–	–	–	–	8(8)[a]	Jones and Milne (1963)	Avena sativa	Colorimetric, Flame and Atomic absorption Spectroscopy
–	Ca	K	Mg	Na	H	O	–	–	–	–	Si	–	–	–	–	–	–	–	–	–	–	7(10)	Jones et al. (1966)	Poaceae Bambooos (Poaceae)	X-ray diffraction
–	Ca	K		–	–		P	–	Fe	–	Si	–	–	–	–	–	–	–	–	–	–	5(11)	Soni et al. (1972)	Cyperus alterni-folius(Cyperaceae)	Electron microprobe analysis
C	Ca	K	Mg	Na	–	–	–	–	Fe	–	Si	Al	Ti	–	–	–	–	–	–	–	–	9(13)	Bartoli and Wilding (1980)	Grasses (Poaceae) and some woody coniferous plants	Cold and Hot water dissolution
–	–	–	–	Na	–	O	P	–	–	–	Si	–	–	Cl	–	–	–	–	–	–	–	5(14)	Lanning and Eleuterius, 1981	Grasses (Poaceae) and Sedges (Cyperaceae)	X-ray diffraction
–	Ca	K	Mg	Na	H	O	P	–	–	–	Si	Al	–	Cl	S	–	–	–	–	–	–	11(15)	Lanning and Eleuterius (1983)	Some grasses (Poaceae) and dicots	SEM-EDX analysis
–	Ca	–	Mg	–	–	–	–	–	Fe	Mn	–	Al	–	–	–	As	Cr	Cu	Ni	Pb	Zn	11(21)	Bujan (2013)	Members of Ericaceae	Energy dispersive miniprobe Multielement analyzer (EMMA-XRF)
C	Ca	K	Mg	–	H	O	–	N	Fe	–	Si	–	–	–	–	–	–	–	–	–	–	9(22)	Tripathi et al. (2012)	Triticum aestivum(Poaceae)	Laser Induced Breakdown Spectroscopy (LIBS)
–	Ca	K	Mg	Na	–	–	–	–	Fe	Mn	Si	Al	Ti	Cl	–	As	Cr	–	–	–	Zn	33(42)	Kamenik et al. (2013)	Hordeum Vulgare	Instrumental Neutron Activation Analysis (INAA)
									Ba Ta	Br Tb	Ce Th	Co U	Cs V	Dy W	Eu Yb	Hf –	La –	Rb –	Sb –	Sc –	Sm –			(Poaceae)	
C	Ca	K	Mg	–	–	O	–	–	Fe	–	Si	Al	–	–	–	–	–	Cu	–	–	–	9(42)	Anala and Nambisan (2015)	Oryza sativa(Poaceae)	SEM-EDX analysis
C	–	–	–	–	–	O	–	–	–	–	Si	–	–	–	–	–	–	–	–	–	–	3(42)	Nylese et al. (2015)	Equisetum hye-male(Pteridophytes)	Variable pressure SEM
C	Ca	K	Mg	Na		O	–	N	Fe	–	Si	Al	Ti	Cl	–	–	–	Cu	–	–	–	13(42)	Present Study	Reed grasses (Arundo donax&Phragmites australis) (Poaceae)	SEM-EDX analysis

[a] Figures in parenthes is give cumulative number of elements.

Table 6
Comparison of Silicon (WT%) in different parts of *Arundo donax* L. and *Phragmites karka* (Retz.) Trin. ex. Steud.

Treatments	Grass species							
	Arundo donax L.				*Phragmites karka* (Retz.) Trin. ex. Stued			
	Root	Culm	Leaf	Synflorescence	Root	Culm	Leaf	Synflorescence
1.	21.72	12.01	47.67	34.82	34.59	30.62	30.37	30.82
2.	22.39	11.42	41.15	27.37	34.48	27.38	33.20	29.85
3.	21.48	20.86	35.83	29.85	37.82	15.77	30.32	25.79
4.	24.19	27.79	32.88	29.82	28.31	31.34	35.14	10.17
5.	54.83	27.19	38.12	25.25	16.82	32.42	33.45	13.21
6.	19.41	11.40	33.25	24.73	40.71	24.18	29.62	31.36
HSD	13.79				11.607			
F-ratio (3, 23)	5.362*				2.034			

Two Way ANOVA	
Treatment	F-ratio (1, 40): 0.05079
Dose	F-ratio (3, 40): 5.42453*
Treatment x Dose	F-ratio (3, 40): 2.54036
HSD	14.54822

*represents the significance at $p \leq 0.05$.

surface whereas those from the culm had a porous surface. Apart from ultrastructural details that help to diagnose the species, SEM has also helped in *in-situ* location of the types that could not be visualized under the light microscope. Bulliform cells in the leaf had deep location and variable contrast making their visualization under light microscope difficult, but, SEM helped to visualize them in sufficient details. Surface features like presence of a depression on their front surface and a somewhat polygonal outline have been figured out (Fig. 14l and m). SEM has also revealed structural features like depressions on the upper surface, thickness of the shank *etc*. in bilobates present in the leaf and synflorescence of *Arundo donax* L. (Fig. 14n-p and s). SEM was useful in demarcation of the rondel (Fig. 15u and v) from other closely related morphotypes *viz*., flat towers (Fig. 15b, h and l) and horned towers (Fig. 15c, n, o, t and u). It emerges from the present studies that phytoliths in reed grasses displayed a wide range ultra-structural variations useful for diagnosis and taxonomic characterization.

3.6. Chemical architecture

3.6.1. Silica content

The amount of silica deposition in the form of phytoliths showed considerable variation among various parts in both the species. *Phragmites karka* (Retz.) Trin. ex Steud. accumulated more silica than *Arundo donax* L. in all parts except leaf (Fig. 10). The quantification of silica showed that leaves in both the species *viz*., *Arundo donax* L. and *Phragmites karka* (Retz.) Trin. ex Steud. accumulated highest percentages of silica (approx. 8.00% and 7.09%) followed by synflorescence (4.96% and 6.22%), culm (1.64% and 2.91%) and root (2.06% and 2.63%) respectively in this pair of grass reeds. The amount of accumulation of silica in underground and aerial parts (particularly leaf and synflorescence) are believed to be controlled by a number of extrinsic and intrinsic factors. The former category includes ambient temperature and humidity besides edaphic factors including soil type, soil moisture and availability of silica which is further controlled by soil pH and the presence of Fe and Al oxides (Jones and Handreck, 1967; Motomura et al., 2002; Zucol and Brea, 2005; Honaine and Osterrieth, 2011). On the other hand, intrinsic factors include phenological state of the plant in the yearly cycle and changes in the availability of silica transporters resulting from metabolic processes related to age and maturity (Parry and Smithson, 1964; Bertoldi and de Pomar, 1971, 1975; Ma and Yamaji., 2006; Massey et al., 2006; Fernández Pepi et al., 2012a). On comparison, aerial parts (particularly, leaf and synflorescence) were found to accumulate higher amounts of silica than underground parts (roots). The higher amount of silicification in aerial parts has been correlated with higher evapotranspiration rates in these parts, such as the leaf lamina and synflorescence bracts. Silica is brought to various plant parts through the transpiration stream. As water evaporates in transpiration, silicic acid becomes supersaturated to solid hydrated silica and gets precipitated as amorphous silica in the form of phytoliths (Jones and Handreck, 1965; Rosen and Weiner, 1994; Raven, 2003).

3.6.2. Elemental composition

SEM-EDX spectra of phytoliths from different parts of *Arundo donax* L. and *Phragmites karka* (Retz.) Trin. ex Steud. revealed their elemental composition (Figs. 11 and 12). Silicon (Si) carbon (C) and oxygen (O) emerged as the major constituents of phytoliths. However, phytoliths from various parts of both the species showed the presence of other elements namely Aluminium (Al), Calcium (Ca), Chlorine (Cl), Copper (Cu), Iron (Fe), Magnesium (Mg), Nitrogen (N), Potassium (K), and Titanium (Ti) in small amounts (Table 4). These elements are present in the cytoplasm of the host cells and during course of silica impregnation are retained and encased within the phytoliths (Jones and Milne, 1963; Bartoli and Wilding, 1980; Smith and Anderson, 2001; Ma and Yamaji, 2006; Bauer et al., 2011). Jones and Milne (1963) reported eight elements *viz*., C, Ca, Fe, K, Mg, Mn, Na and Si from phytoliths of *Avena sativa* L. However, later workers have added several elements through latest detection method of SEM-EDX (Lanning and Eleuterius, 1983; Anala and Nambisan, 2015), Energy Dispersive Miniprobe Multielement Analysis (EMMA-XRF), Neutron Activation Analysis (Kamenik et al., 2013), Laser Induced Breakdown Spectroscopy (LIBS, Tripathi et al., 2012) and Variable Pressure Scanning Electron Microscopy (VPSEM, Nylese et al., 2015) (Table 5). Table 4 brings out the differences in elemental profiles of phytoliths in the reed grasses under comparison. Some elements were restricted to one or the other of the species while others showed differences in percentage (by weight) and atomic weight. For example, Titanium was present in *Arundo donax* L. (root and synflorescence) but was absent from all parts of *Phragmites karka* (Retz.) Trin. ex Steud. The Si (Wt%) amounts among various parts of *Arundo donax* L. showed significant differences ($p \leq 0.05$), while as in *Phragmites karka* (Retz.) Trin. ex Steud. it was found to be insignificant. Similarly, pairwise comparison of Si (Wt%) amount between various parts of the two species showed significant differences ($p \leq 0.05$; Table 6).

Principal Component Analysis (PCA) of elemental composition data of different parts for species demarcation showed two principal components, PC1 (64.391) and PC2 (20.213%) that together

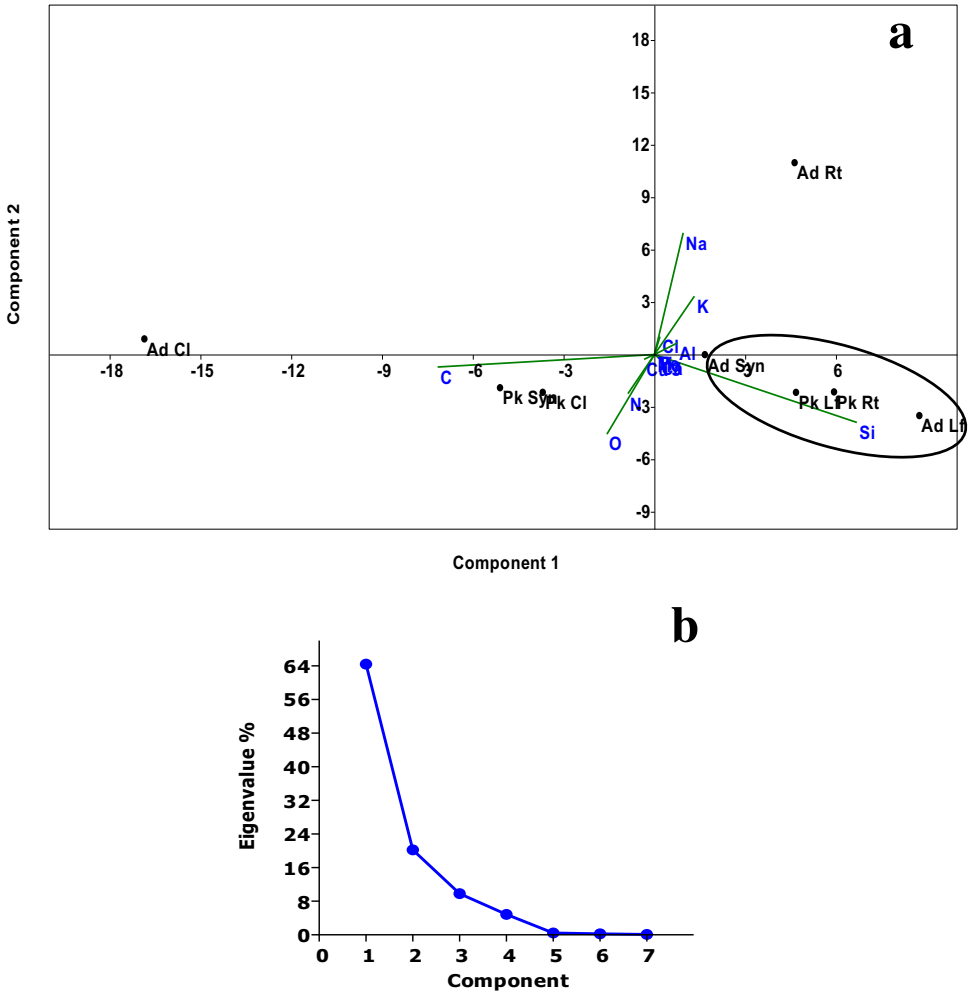

Fig. 13. Principal Component Analysis (PCA) plot showing clustering by elemental composition of plant parts (Si Wt%) (a); Plot of Eigen values% *versus* components showing the variance of each component (b) (Ad Rt = *Arundo donax* root; Ad Cl = *Arundo donax* culm; Ad Lf = *Arundo donax* leaf; Ad Syn = *Arundo donax* synflorescence and Pk Rt = *Phragmites karka* root; Pk Cl = *Phragmites karka* culm; Pk Lf = *Phragmites karka* leaf; Pk Syn = *Phragmites karka* synflorescence).

explained 84.60% of the total variance in the data set (Fig. 13a and b). In PC1 the maximum positive loading was shown by Silicon (Si) whereas Carbon (C) showed the maximum negative loading. Similarly, for PC2 maximum positive loading was shown by Sodium (Na) and maximum negative loading by oxygen (O). However, PCA analysis did not distinguish *Arundo donax* L. (leaf and synflorescence) from *Phragmites karka* (Retz.) Trin. ex Steud. (leaf) on the basis of Silicon (Si) Wt%. PCA grouping of leaf of these species on the basis of Si Wt% seems to have resulted from higher content of Silica in leaf in both the species as compared to other parts.

3.6.3. XRD analysis

Powder diffractograms of phytoliths isolated from leaf and synflorescence of *Arundo donax* L. showed peaks characteristic of various crystalline polymorphic phases of silica ranging from quartz, coesite, cristobalite, tridymite and other silicates (Fig. 16a). These phases have identical chemical composition (SiO_2) but different physical structures and symmetries. They show distinct lattice systems ranging from anorthic (triclinic), through monoclinic, orthorhombic, hexagonal and cubic. The present studies lend further credence to the existence of polymorphic silica in plants. Gonzalez-Espindola et al. (2010, 2014) carried out X-Ray Diffraction (XRD) analysis of silica extracted from agro-industrial wastes and the grass species *Stenotaphrum secundatum* (Walt.) O. Kuntze. The authors reported the presence of various polymorphic phases of silica like α-quartz, coesite, cristobalite and tridymite.

Silica shows several polymorphs depending on temperature and pressure (Holm et al., 1967). A high ashing temperature (600 °C) maintained for 4–6 h could have transformed the amorphous silica into the crystalline phases. The diffractogram of phytoliths of *Arundo donax* L. (synflorescence) showed a unique peak corresponding to orthorhombic ferrierite primitive in addition to the peaks obtained from leaf phytoliths (Fig. 16b). Ferrierite is a zeolite (Aluminosilicate) that binds a number of cations *viz*., Na^+, K^+, Ca^{2+}, Mg^{2+} *etc*. Earlier, Kow et al. (2014) carried out XRD analysis of phytoliths from the cogon grass (*Imperata cylindrica* (L.) P. Beauv.). X-ray diffraction studies broughtout that purity and amorphicity of silica was modified significantly by the presence of Potassium (K).

The presence of Al, Na, Ca, Mg, K in phytoliths from the synflorescence of *Arundo donax* L. could be deduced from the existence of a ferrierite phase in SEM-EDX spectra. *Phragmites karka* (Retz.) Trin ex Steud. showed lesser number of silica polymorphic phases as compared to *Arundo donax* L. X-ray diffractograms of *Phragmites karka* (Retz.) Trin ex Steud. (leaf) showed five peaks indicating quartz, tridymite and other crystalline phases (Fig. 16c) while diffractograms from the synflorescence showed only three peaks (Fig. 16d).

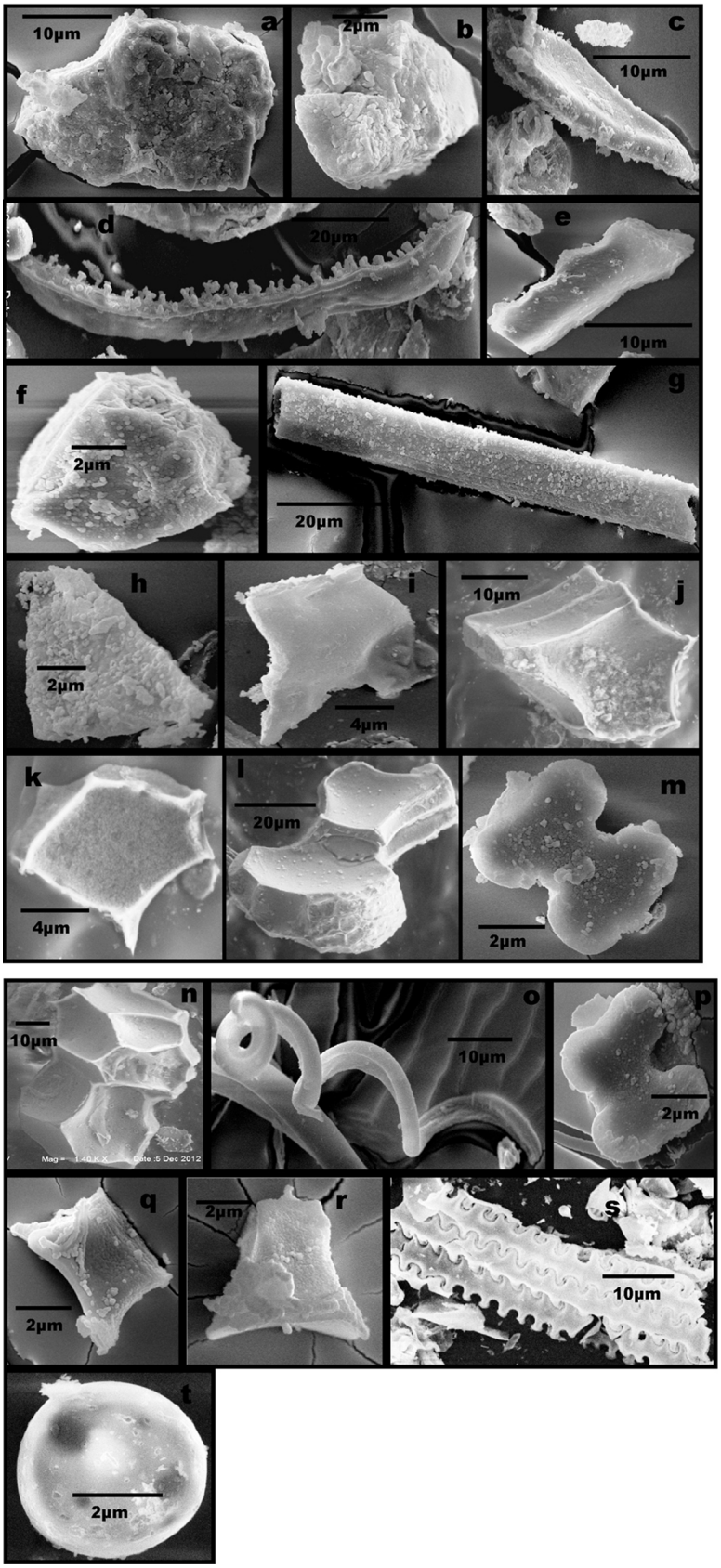

Fig. 14. Scanning Electron Micrographs (SEM) of phytolith morphotypes from various parts of *Arundo donax* L. (Root): Trapezoids (a, b); Clavate (c); Echinate elongate (d). Culm: Sinuate elongate (e); Trapezoid (f); Smooth elongate (g); Triangular (h); Scutiform (i). Leaf: Bulliform cells (j, k); Bilobates (l, m); Parallepipedal bulliform cell (n). Synflorescence: Spiral (o); Bilobate (p); Horned tower (q, r); Echinate elongate (s) and Orbicular (t).

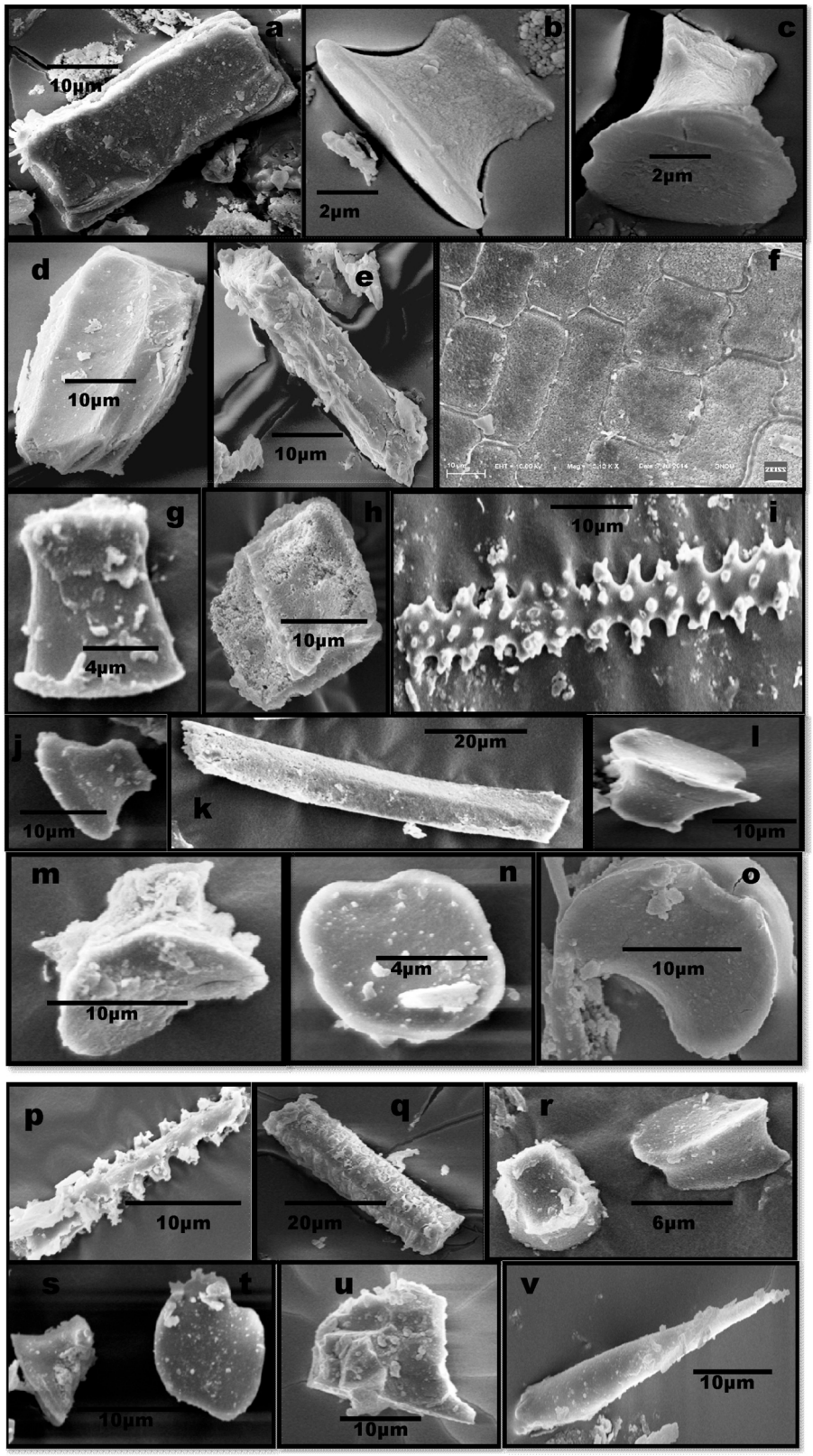

Fig. 15. Scanning Electron Micrographs (SEM) of phytolith morphotypes from various parts of *Phragmites karka* (Retz.) Trin. ex Steud. (Root): Rectangular (a); Flat tower (b); Horned tower (c); Trapezoids (d); Smooth elongate (e). Culm: Rectangular (f); Flat tower (g); Trapezoid (h); Echinate elongate (i). Leaf; Flat tower (j); Smooth elongate (k); Horned tower (l, m); Saddles (n, o); Echinate elongate (p); Cylindric (q). Synflorescence: Rondel (r, s); Saddle (t); Scutiform (u); Prickle (v).

3.6.4. FT-IR spectroscopy

FTIR spectra of phytoliths isolated from leaf and synflorescence of both *Arundo donax* L. (Fig. 17a and b) and *Phragmites karka* (Retz.) Trin ex Steud. (Fig. 17c and d) showed a wide peak range between 3435 cm^{-1} to 3450 cm^{-1}. These peaks have been ascribed to H—OH stretching frequency of Silanol (Si—OH) group and traces

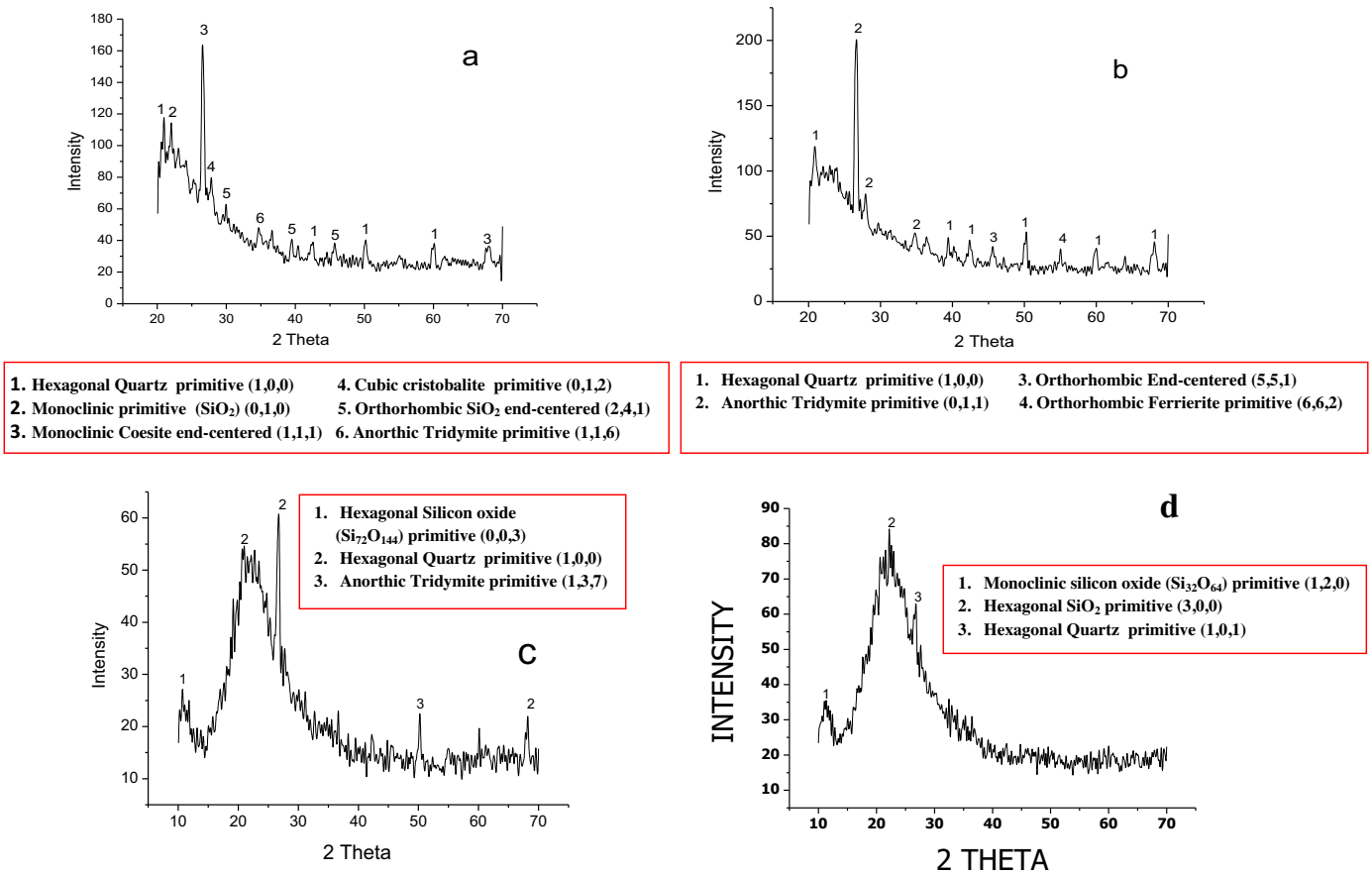

Fig. 16. X-ray diffraction pattern of phytoliths (a) *Arundo donax* L. leaf (b) *Arundo donax* L. synflorescence (c) *Phragmites karka* (Retz.) Trin. ex. Steud. leaf (d) *Phragmites karka* (Retz.) Trin. ex. Steud. Synflorescence.

of adsorbed water as reported earlier (Gonzalez-Espindola et al., 2010, 2014; Pijarn et al., 2010; Long-Gui et al., 2011; Kow et al., 2014; Li et al., 2015). The spectra also showed a peak between 1625 cm^{-1} to 1635 cm^{-1} which are known to correspond to H—OH bending modes of adsorbed water molecules (Pijarn et al., 2010; An et al., 2011; Long-Gui et al., 2011; Gonzalez-Espindola et al., 2014; Kow et al., 2014). Spectra of phytoliths from different parts except *Arundo donax* L. (synflorescence) showed another peak between 1384 cm^{-1} and 1385 cm^{-1} indicative of carbonate mineral phases namely calcite, dolomite and aragonite (Fig. 17a, c, d) in conformity with earlier reports (Gonzalez-Espindola et al., 2014). The peak between 800 cm^{-1} to 803 cm^{-1} detected in all the spectra corresponded to symmetric vibration modes of Si-O-Si bond in Siloxane group. This band has also been associated with the presence of quartz (Kow et al., 2014; Mourhly et al., 2015). Similarly, all the samples in the present study showed peaks between 1095 cm^{-1} to 1100 cm^{-1} and 468 cm^{-1} to 470 cm^{-1} which have been ascribed to asymmetric stretching vibration and bending modes of Si—O—Si (Karunakaran et al., 2013; Mourhly et al., 2015). Phytoliths isolated from synflorescences of both the species showed unique peaks between 2145 cm^{-1} to 2147 cm^{-1}(Fig. 17b and d). These peaks may be associated with vibrations of carbon impurity in the samples. In addition, FTIR spectra of phytoliths from *Arundo donax* L. (leaf) showed two more peaks at 2962.94 cm^{-1} and 1260.65 cm^{-1}(Fig. 17a) which were missing in the leaf spectra of *Phragmites karka* (Retz.) Trin. ex Steud. The peak at 2962.94 cm^{-1} corresponds to the asymmetric stretching modes of aliphatic methylene group (R_2CH_2), indicating the presence of aliphatic long chain hydrocarbons (Long-Gui et al., 2011; Watling et al., 2011). In another study, plant ash from archaeological sites showed similar bands that were indicative of thermal degradation of phytolith occluded carbon (Phytoc) (Watling et al., 2011). Similarly, the peak at 1260.45 cm^{-1} corresponds to the presence of Si-CH_3 group (Long-Gui et al., 2011). The present studies have confirmed the presence of silanol group and siloxane linkages in all the samples. Even though, carbonate minerals detected in leaf of *Arundo donax* L. were shared with leaf and synflorescence of *Phragmites karka* (Retz.) Trin. ex Steud. but aliphatic methylene group was present only in the leaf of *Arundo donax* L.

4. Conclusion

The reed grasses yielded more than thirty phytolith morphotypes including the 'spiral' which is probably a new addition to the world phytolith catalog. The reed grasses *Arundo donax* L. and *Phragmites karka* (Retz.) Trin. ex Steud. could be diagnosed from each other by the presence of long trapezoids, narrow bilobates, orbicular, polylobate, spiral and rugose elongate morphotypes in the former and polyhedral, tracheids, cylindric, cross, dendritic, quadrilobate and the rondel types in the latter. *In-situ* location of phytoliths in foliar parts also showed marked differences. *Arundo donax* L. showed an axial arrangement of bilobate phytoliths whereas *Phragmites karka* (Retz.) Trin ex Steud. revealed transverse arrangement of saddle shaped silica cells. The latter named species also showed the presence of silica cork cell in the intercostal regions but they were not found in *Arundo donax* L. The present study has also brought out the significance of frequency distribution data in various body parts and morphometry of phytolith types in taxonomic characterization. SEM of phytoliths revealed some differences of diagnostic significance. The total amount of silica was

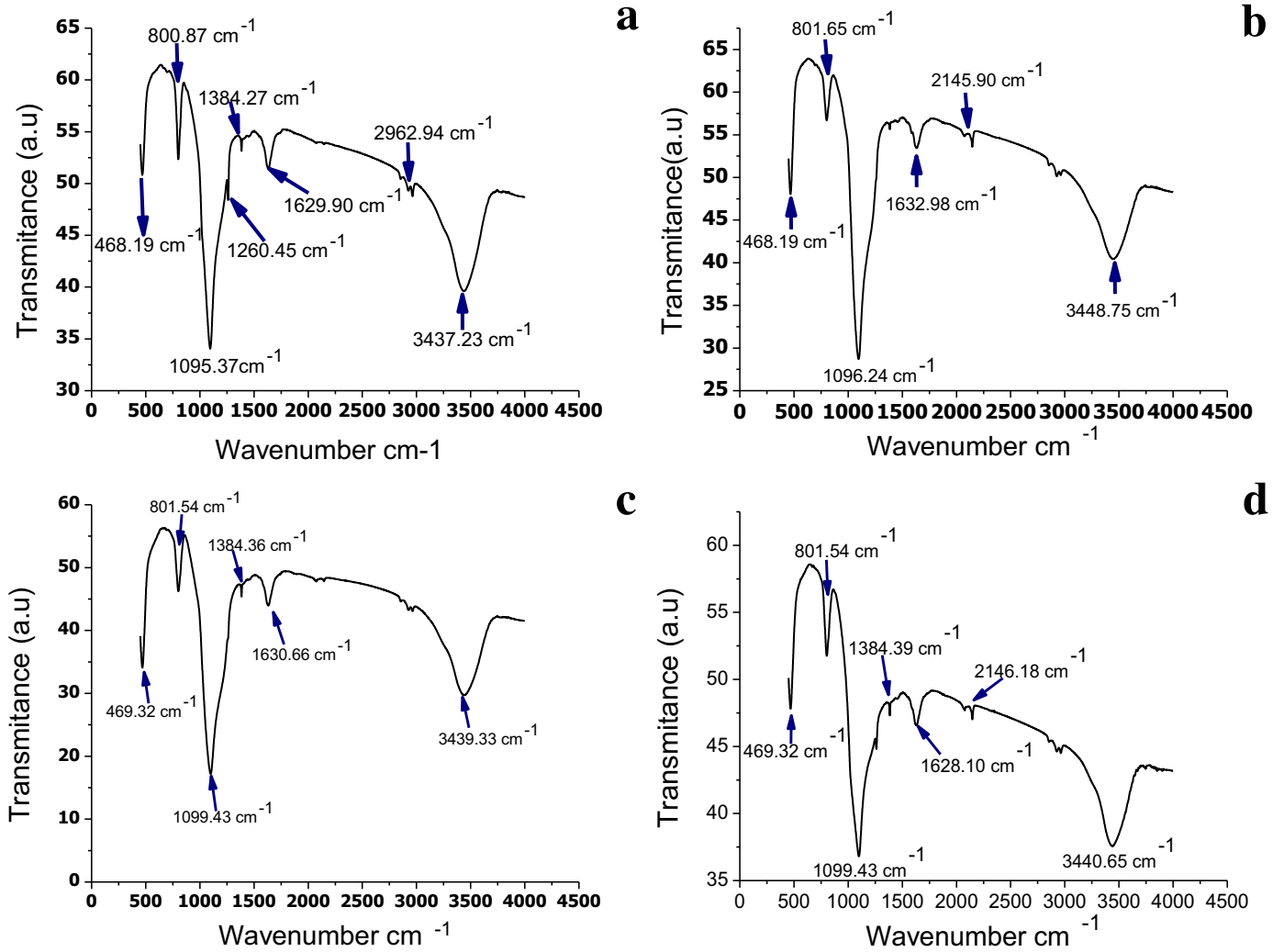

Fig. 17. FTIR spectra of phytoliths (a) *Arundo donax* L. leaf (b) *Arundo donax* L. synflorescence (c) *Phragmites karka* (Retz.) Trin. ex. Steud leaf (d) *Phragmites karka* (Retz.) Trin. ex. Steud synflorescence.

higher in *Phragmites karka* (Retz.) Trin. ex Steud. as compared to *Arundo donax* L. Among the parts, leaf of both the species showed highest amounts of silica followed by the synflorescence, culm and root. PCA of elemental composition data of phytoliths supported silica quantification results that leaves have higher silica content as compared to other plant parts in both the species. Chemical characterization of phytoliths from leaf and synflorescence using XRD analysis showed silica in crystalline phases namely, quartz, coesite, cristobalite and tridymite. *Arundo donax* L. synflorescence was marked by the presence of Ferrierite (a zeolite). Similarly, the FTIR analysis indicated aliphatic methylene groups in leaves of this species.

Acknowledgements

The authors are thankful to Head, Department of Botanical and Environmental Sciences and Incharge, Emerging Life Sciences Laboratory, Guru Nanak Dev University Amritsar, Punjab (India) for Scanning Electron Microscopy (SEM) and Electron Dispersive X-Ray analysis (EDX). We wish to thank Prof. Atul Khanna, Department of Physics and Prof. Kamaljeet Singh, Department of Chemistry (Centre for Advanced Studies) of the same university for X-Ray Diffraction studies (XRD) and FTIR analysis respectively. The first author is thankful to the University Grants Commission, New Delhi for financial assistance under a Basic Scientific Research (BSR) fellowship. The authors wish to thank two anonymous reviewers for a critical and constructive review of the original manuscript.

References

An, D., Guo, Y., Zou, B., Zhu, Y., Wang, Z., 2011. A study on the consecutive preparation of silica powders and active carbon from rice husk ash. Biomass Bioenergy 35, 1227–1234.

An, X., Lu, H., Chu, G., 2015. Surface soil phytoliths as vegetation and altitude indicators: a study from the southern Himalaya. Sci. Rep. 5, 15523.

Anala, R., Nambisan, P., 2015. Study of morphology and chemical composition of phytoliths on the surface of paddy straw. Paddy Water Environ. 13, 521–527.

Ball, T.B., Brotherson, J., Gardner, J.S., 1993. A typologic and morphometric study of variation in phytoliths from einkhorn wheat (*Triticum monococcum* L.). Can. J. Bot. 71, 1182–1192.

Ball, T.B., Gardener, J.S., Brotherson, J.D., 1996. Identifying phytoliths produced by the inflorescence bracts of three species of wheat (*Triticum monococcum* L., *T. dicoccom* Schrank., and *T. aestivum* L.) using computer-assisted image and statistical analyses. J. Archaeol. Sci. 23, 619–632.

Ball, T.B., Gardner, J.S., Anderso, n.N., 1999. Identifying inflorescence phytoliths from selected species of wheat (*Triticum monoccum, T., dicoccon, T. dicoccoides*, and *T. aestivum*) and barley (*Hordeum vulgare* and *H. spontaneum*). Am. J. Bot. 86, 1615–1623.

Ball, T.B., Gardner, J.S., Anderson, N., 2001. An approach to identifying inflorescence phytoliths from selected species of wheat and barley phytoliths. Appl. Earth Sci. Hum. Hist., 289–301.

Ball, T.B., Ehlers, R., Standing, M.D., 2009. Review of typologic and morphometric analysis of phytoliths produced by wheat and barley. Breed. Sci. 59, 505–512.

Ball, T.B., Davis, A.L., Evett, R., Ladwig, J.L., Tromp, M., Out, W.A., Portillo, M., 2015. Morphometric analysis of phytoliths: recommendations towards standardization. J. Archaeol. Sci. (in press).

Bartoli, F., Wilding, L.P., 1980. Dissolution of biogenic opal as a function of its physical and chemical properties. Soil Sci. Soc. Am. J. 44, 873–878.

Bauer, P., Elbaum, R., Weiss, I.M., 2011. Calcium and silicon mineralization in land plants: transport structure and function. Plant Sci. 180, 746–756.

Bertoldi, de Pomar, H., 1971. Ensayo de clasificación morfológica de los silicofito litos. Ameghiniana 8, 317–328.

Bertoldi, de Pomar, H., 1975. Los silicofitolitos: sinopsis de su conocimiento. Darwiniana 19, 173–206.

Biswas, O., Gosh, R., Paruya, K.D., Mukherjee, B., Thapa, K.K., Bera, S., 2016. Can grass phytoliths and indices be related on during vegetation and climate interpretations in the eastern Himalayas? Studies from Darjeeling and Arunachal Pradesh, India. Quat. Sci. Rev. 134, 114–132.

Bonnett, O.T., 1972. Silicificd cells of grasses: a major source of plant opal in Illinois soils. Agricultural Experiment Station, Bulletin 142, University of Illinois at Urbana-Champaign. Coll. Agric. 742, 32.

Bujan, E., 2013. Elemental composition of phytoliths in modern plants (Ericaceae). Quat. Int. 287, 114–120.

Carnelli, A.L., Madella, M., Theurillat, J.P., 2001. Biogenic silica production in selected alpine plant species and plant communities. Ann. Bot. 87, 425–434.

Chauhan, D.K., Tripathi, K.D., Kumar, D., Kumar, Y., 2011. Diversity, distribution and frequency based attributes of phytolith in *Arundo donax* L. Int. J. Innov. Plant Chem. Sci. 1, 22–27.

Clark, J., 1959. Preparation of leaf epidermis for topographic study. Stain Technol. 35, 35–39.

Coughenour, M.B., 1985. Graminoid responses to grazing by large herbivores: adaptations: exaptations and interacting processes. Ann. Missouri Bot. Gard. 72, 852–863.

Currie, H.A., Perry, C.C., 2007. Silica in plants: biological: biochemical and chemical studies. Ann. Bot. 100, 1383–1389.

Dietrich, D., Hinke, S., Baumann, W., Fehlhaber, R., Baucker, E., Ruhle, G., Wienhaus, O., Marx, G., 2003. Silica accumulation in *Triticum aestivum* L. and *Dactylis glomerata* L. Anal. Bioanal. Chem. 376, 399–404.

Dore, W.G., 1960. Silica deposits in leaves of Canadian grasses. Can. Soc. Agron. 6, 96–99.

Ellis, R.P., 1979. A procedure for standardizing comparative leaf anatomy in the Poaceae: II. The epidermis as seen in surface view. Bothalia 12, 641–671.

Epstein, E., 1994. The anomaly of silicon in plant biology. Proc. Natl. Acad. Sci. U. S. A. 91, 11–17.

Epstein, E., 1999. Silicon. Annu. Rev. Plant Physiol. Plant Mol. Biol. 50, 641–664.

Fernández Pepi, M.G., Arriaga, M.O., Zucol, A.F., 2012a. Leaf anatomy and biomineralization in *Empetrum rubum* Valh ex Willd. (Ericaceae). Bot. Complut. 36, 113–121.

Fernández Pepi, M.G., Zucol, A.F., Arriaga, M.O., 2012b. Comparative phytolith analysis of *Festuca* (Pooideae: poaceae) species native to tierra del fuego, Argentina. Can. J. Bot. 90, 1113–1124.

Ge, Y., Lu, H., Zhang, J., Wang, C., He, K., Huan, X., 2016. Phytolith analysis for the identification of barnyard millet (*Echinochloa sp.*) and its implications. Archeol. Anthropol. Sci., http://dx.doi.org/10.1007/s12520-016-0341-0.

Gonzalez-Espindola, A., Harnendez-Martinez, A.L., Chaves-Angeles, C., Catano, M.V., Santos-Velasco, C., 2010. Novel crystalline SiO_2 nanoparticles via annelids bioprocessing of agro-industrial wastes. Nanoscale Res. Lett. 5, 1408–1417.

Gonzalez-Espindola, A., Ramirez-Fuentes, R., Harnendez-Martinez, L.A., Catano, M.V., Santos- Velasco, C., 2014. Structural characterization of silica particles extracted from grass *Stenotaphrum secundatum*: biotransformation via annelids. Adv. Mater. Sci. Eng., 956945.

Gosh, R., Naskar, M., Bera, S., 2011. Phytolith assemblages of grasses from Sunderbans, India and their implications for the reconstruction of deltaic environment. Palaeogeogr. Palaeoclimatol. Palaeoecol. 311, 93–102.

Gould, F.W., Shaw, R.B., 1983. Grass Systematics Collage Station. Texas A and M University Press, College Station.

Gu, Y., Zhao, Z., Pearsall, M.D., 2013. Phytolith morphology research on wild and domesticated rice species in East Asia. Quat. Int. 247, 141–148.

Hammer, Ø., Harper, D.A.T., Ryan, P.D., 2001. PAST: paleontological statistics software package for education and data analysis. Palaeontol. Electronica 4, 1–9.

Hattori, T., Inanaga, S., Tanimoto, E., Lux, A., Luxova, M., Sugimoto, Y., 2005. Silicon–induced changes in viscoelastic properties of Sorghum root cell walls. Plant Cell Physiol. 44, 743–749.

Hilu, W.K., 1984. Leaf epidermes of *Andropogon* sect. *Leptopogon* (Poaceae) in North America. Syst. Bot. 9, 247–257.

Hodson, M.J., Evans, D.E., 1995. Aluminium/silicon interactions in higher plants. J. Exp. Bot. 46, 161–171.

Hodson, M.J., Sangster, A.G., 1988. Observation on the distribution of mineral elements in the leaf of wheat (*Triticum aestivum* L.) with particular reference to silicon. Ann. Bot. 62, 463–471.

Hodson, M.J., Sangaster, A.G., Parry, D.W., 1985. An ultrastructural study on the developmental phases and silicification of the glume of *Phalaris canariensis* L. Ann. Bot. 55, 649–655.

Hodson, M.J., White, P.J., Mead, A., Broadley, M.R., 2005. Phylogenetic variation in the silicon composition of plants. Ann. Bot. 96, 1027–1046.

Holm, J.L., Kleppa, O.J., Westrum Jr., Edgar, F., 1967. Thermodynamics of polymorphic transformations in silica: thermal properties from 5 to 1070 K and pressure-temperature stability fields for coesite and stishovite. Geochim. Cosmochim. Acta 31, 2289–2307.

Holst, I., Moreno, J.E., Piperno, D.R., 2007. Identification of teosinte, maize, and Tripsacum in Mesoamerica by using pollen, starch grains, and phytoliths. Proc. Natl. Acad. Sci. 104, 17608–17613.

Honaine, M.F., Osterrieth, M.L., 2011. Silicification of the adaxial epidermis of leaves of a panicoid grass in relation to leaf position and section and environmental conditions. Plant Biol. 14, 596–604.

Honaine, M.F., Zucol, A.F., Osterrieth, M.L., 2006. Phytolith assemblages and systematic associations in grassland species of the South-Eastern Pampean Plains, Argentina. Ann. Bot. 98, 1155–1165.

Huan, X., Lu, H., Wang, C., Tang, X., Zuo, X., Ge, Y., He, K., 2015. Bulliform phytolith research in wild and domesticated rice paddy soil in South China. PLoS One 10 (10), e0141255.

Jattisha, P.I., Sabu, M., 2012. Phytoliths as a tool for the identification of some chloridoideae grasses in Kerala. ISRN Bot., 246057.

Jattisha, P.I., Sabu, M., 2015. Foliar phytoliths as an aid to the identification of Paniceae (Panicoideae: poaceae) grasses in South India. Webbia: J. Plant Taxon. Geogr. 70, 115–131.

Jones, L.H.E., Handreck, K.A., 1965. Studies of silica in the oat plant, III: uptake of silica from soils by the plant. Plant Soil 23, 79–96.

Jones, L.H.P., Handreck, K.A., 1967. Silica in soils, plants, and animals. In: Norman, A.G. (Ed.), Advances in Agronomy, 19. Academic Press, New York, pp. 107–147.

Jones, L.H.P., Milne, A.A., 1963. Studies of silica in the oat plant I: chemical and physical properties of the silica. Plant Soil 68, 207–220.

Jones, L.H.P., Milne, A.A., Sanders, J.V., 1966. Tabashir: an opal of plant origin. Science 151, 464–466.

Kamenik, J., Mizera, J., Randa, Z., 2013. Chemical composition of plant silica phytoliths. Environ. Chem. Lett. 11, 189–195.

Karunakaran, G., Suriyaprabha, R., Manivasakan, P., Yuvakkumar, R., Rajendran, V., Prabu, P., Kannan, N., 2013. Effect of nanosilica and silicon sources on plant growth promoting rhizobacteria, soil nutrients and maize seed germination. IET Nanobiotechnol., 1–8.

Kow, K.W., Yusoff, R., Aziz-Abdul, A.R., Abdullah, E.C., 2014. Characterisation of bio-silica synthesized from cogon grass. Powder Technol. 254, 206–2013.

Krishnan, S., Samson, N.P., Ravichandran, P., Narasimhan, D., Dayanandan, P., 2000. Phytoliths of Indian grasses and their potential use in identification. Bot. J. Linn. Soc. 132, 241–252.

Lanning, F.C., Eleuterius, L.N., 1981. Silica and ash in several marsh plants. Gulf Res. Rep. 7, 47–52.

Lanning, F.C., Eleuterius, L.N., 1983. Silica and ash in tissues of some coastal plants. Ann. Bot. 51, 835–850.

Lanning, F.C., Ponnaiya, B.W., Crumpton, C.F., 1958. The chemical nature of silica in plants. Plant Physiol. 33, 339–343.

Lau, E., Goldoftas, M., Baldwin, V.D., Dayanandan, P., Srinivasan, J., Kaufman, P.B., 1978. Structure and localization of silica in the leaf and internodal epidermal system of the marsh grass, *Phragmites australis*. Can. J. Bot. 56, 1096–1701.

Li, X., Jiang, P., Wang, Z., Huang, Y., 2015. Phosphotungstate-based ionic silica nanoparticles network for alkenes expoxidation. Catalysts 6, 1–13.

Long-Gui, X., Changyun, D., Yun, Liang, Hui-Pi, P., Hu, Jian, Zhuoru, Y., 2011. Preparation and characterization of raspberry-like SiO_2 particles by the sol-gel method. Nanomater. Nanotechnol. 1, 79–83.

Lu, H., Liu, K., 2003. Phytoliths of common grasses in the coastal environments of southeastern USA, Estuarine. Coastal Shelf Sci. 58, 587–600.

Lux, A., Luxová, M., Hattori, T., Inanaga, S., Sugimoto, Y., 2002. Silicification in sorghum (*Sorghum bicolor*) cultivars with different drought tolerance. Physiol. Plant. 115, 87–92.

Lux, A., Luxova, M., Abe, J., Tanimoto, E., Hattori, T., Inanaga, S., 2003. The dynamics of silicon deposition in the *Sorghum* root endodermis. New Phytol. 158, 437–441.

Ma, J.F., Yamaji, N., 2006. Silicon uptake and accumulation in higher plants. Trends Plant Sci. 11, 39–397.

Madella, M., Alexandre, A., Ball, T., 2005. International code for phytolith nomenclature. Ann. Bot. 10, 109–172.

Massey, F.P., Ennos, A.R., Hartley, S.E., 2006. Silica in grasses as a defence against insect herbivores: contrasting effects on folivores and a phloem feeder. J. Anim. Ecol. 75, 595–603.

Mazumdar, J., 2011. Phytoliths of pteridophytes. S. Afr. J. Bot., http://dx.doi.org/10.1016/j.sajb.2010.07.020.

McWhorter, C.G., Ouzts, C., Paul, R.N., 1993. Micromorphology of johnsongrass (*Sorghum halepense*) leaves. Weed Sci. 41, 583–589.

Metcalfe, C.R., 1960. Anatomy of the Monocotyledons: I. Gramineae. Oxford University Press, London.

Motomura, H., Mita, N., Suzuki, M., 2002. Silica accumulation in long-lived leaves of *Sasa veitchii* (Carrie're) rehder (Poaceae, bambusoideae). Ann. Bot. 90, 149–152.

Mourhly, A., Khachani, M., Hamidi, E.A., Kacimi, M., Halim, M., Arsalane, S., 2015. The synthesis and characterization of low-cost mesoporous silica SiO_2 from local pumice rock. NanoMater. Nanotechnol. 5, 1–7.

Mulholland, S.C., 1989. Phytolith shape frequencies in North Dakota grasses: a comparison to general patterns. J. Archaeol. Sci. 16, 489–511.

Nylese, T.L., Berry, A., Oscher, S., 2015. Elemental analysis of silicon in plant material with variable-pressure SEM. Microscopy Today 23, 26–31.

Ollendorf, A., Susan, C., Mulholland George, R.J.R., 1988. Phytolith analysis as a means of plant identification: *Arundo donax* and *Phragmites communis*. Ann. Bot. 61, 209–214.

Parry, D.W., Smithson, F., 1964. Types of opaline silica deposition in the leaves of British grasses. Ann. Bot. 26, 169–185.
Perry, C.C., Mann, S., Williams, R.J.P., 1984. Structural and analytical studies of the silicified microhairs from the lemma of the grass *Phalaris canariensis* L. Proc. R. Soc. Lond. Ser. B 222, 427–438.
Pijarn, N., Jaroenworaluck, A., Sunsaneeyametha, W., Stevens, R., 2010. Synthesis and characterisation of nanosized-silica gels formed under controlled conditions. Powder Technol. 203, 462–468.
Piperno, D.R., 1983. The Application of Phytolith Analysis to the Reconstruction of Plant Subsistence and Environments in Prehistoric Panama. Ph.D. Dissertation, Temple University. University Microfilms, Ann Arbor.
Piperno, D.R., 1988. Phytolith Analysis: An Archaeological and Geological Perspective (280 pp.). Academic Press, San Diego.
Piperno, D.R., 2006. Phytoliths: A Comprehensive Guide for Archaeologists and Paleoecologists. AltaMira Press, Lanham, Maryland, pp. 89–102.
Ponzi, R., Pizzolongo, P., 2003. Morphology and distribution of epidermal phytoliths in *Triticum aestivum* L. Plant Biosyst. 137, 3–10.
Portillo, M., Ball, T., Manwaring, J., 2006. Morphometric analysis of inflorescence phytoliths produced by *Avena sativa* L. and *Avena strigosa* Schreb. Econ. Bot. 60, 121–129.
Prat, H., 1936. La systematique des graminees. Ann. Sci. Nat. Bot. 18, 165–258.
Raven, J.A., 2003. Cycling silicon—the role of accumulation in plants. New Phytol. 158, 419–430.
Renvoize, S.A., 1986. A survey of leaf-blade anatomy in grasses. VIII. Arundinoideae. Kew Bull. 41, 323–338.
Rosen, A.M., Weiner, S., 1994. Identifying ancient irrigation: a new method using opaline phytoliths from Emmer wheat. J. Archeol. Sci. 21, 125–132.
Rovner, I., 1971. Potential of opal phytolith for use in paleoecological reconstruction. Quat. Res. 1, 343–359.
Rudall, J.P., Prychid, J.C., Gregory, T., 2014. Epidermal patterning and silica phytoliths in grasses: an evolutionary history. Bot. Rev. 80, 59–71.
Sangster, A.G., Parry, D.W., 1969. Some factors in relation to bulliform cell silicification in the grass leaf. Ann. Bot. 33, 315–323.
Sangster, A.G., Parry, D.W., 1971. Silica deposition in the grass leaf in relation to transpiration and the effect of dinitrophenol. Ann. Bot. 35, 667–677.
Shakoor, S.A., Bhat, M.A., Mir, S.H., Soodan, A.S., 2014. Investigations into phytoliths as diagnostic markers for the grasses (Poaceae) of Punjab. Univ. J. Plant Sci. 2, 107–122.
Shouliang, C., Yuexing, J., Zhujun, W., Xintian, L., 1996. Systematic evolutionary study of Poaceae (Gramineae) and its relatives using leaf epidermis. Proc. IFCD 2, 417–425.
Singhal, P., Bal, L.M., Satya, S., Sudhakar, P., Naik, S.N., 2013. Bamboo shoots: a novel sourcefor food and medicine. Crit. Rev. Food Sci. Nutr. 53, 517–534.
Smith, F.A., Anderson, K.B., 2001. Characterization of organic compounds in phytoliths: improving the resolving power of phytolith δC as a tool for paleological reconstruction of C3 and C4 grasses. In: Meunier, J.D., Colin, F. (Eds.), Application in Earth Sciences and Human History. August Aime Balkema Publishers, Rotterdam, Netherlands, pp. 317–327.
Smithson, F., 1958. Grass opal in British soils. J. Soil Sci. 9, 148–154.
Soni, S.L., Kaufman, P.B., Bigelow, W.C., 1972. Electron microprobe analysis of silica cells in leaf epidermal cells of *Cyperus alternifolius*. Plant Soil 36, 121–128.
Srivastava, A.K., 1978. Study of leaf epidermis in the genus *Digitaria* Rich (Gramineae). J. Indian Bot. Soc. 37, 155–160.
Stebbins, G.L., 1972. The evolution of the grass family. In: Youngner, V.B., McKell, C.M. (Eds.), The Biology and Utilization of Grasses. Academic Press, New York.
Stebbins, G.L., 1981. Coevolution of grasses and large herbivores. Ann. Missouri Bot. Gard. 68, 75–86.
Szabo, L.Z., Kovacs, S., Peto, A., 2014. Phytolith analysis of *Poa pratensis* (Poaceae) leaves. Turk. J. Bot. 38, 851–863.
Thomasson, J.R., 1978. Epidermal patterns of the lemma in some fossil and living grasses and their phylogenetic significance. Science 199, 975–977.
Thomasson, J.R., 1980. Paleoericoma (Gramineae: stipeae) from the Miocene of Nebraska: taxonomie and phylogenetic significance. Syst. Bot. 5, 233–240.
Tripathi, D.K., Kumar, R., Pathak, A.K., Chauhan, D.K., Rai, A.K., 2012. Laser-induced breakdown spectroscopy and phytolith analysis: an approach to study the deposition and distribution pattern of silicon in different parts of wheat (*Triticum aestivum* L.) plant. Agric. Res. 1, 352–361.
Twiss, P.C., Suess, E., Smith, R.M., 1969. Morphological classification of grass phytoliths. Soil Sci. Soc. Am. Proc. 33, 109–115.
Twiss, P.C., 1992. Predicted world distribution of C3 and C4 grass phytolith. In: Rapp, G., Mulholland, S.C. (Eds.), Phytoliths Systematic. Emerging Issues. Advances in Archaeological and Museum Science. , 1st ed. Plenum Press, New York, pp. 113–128.
Wang, Y.J., Lu, H.Y., 1993. The Study of Phytolith and Its Application. China Ocean Press, Beijing.
Watling, M.K., Parr, J.F., Rintoul, L., Brown, L.C., Sullivan, A.L., 2011. Raman: infrared and XPS study of bamboo phytoliths after chemical digestion. Spectrochim. Acta 80, 106–111.
Weisskopf, A., Lee, G.-A., 2014. Phytolith identification criteria for foxtail and broomcorn millets: a new approach to calculating crop ratios. Archaeol. Anthropol. Sci., 1–14.
Whang, S., Kim, S.K., Hess, W.M., 1998. Variation of silica bodies in leaf epidermal long cells within and among seventeen species of *Oryza* (Poaceae). Am. J. Bot. 85, 461–466.
Yoshida, S., Ohnishi, Y., Kitagishi, K., 1962. Histochemistry of silicon in rice plant III. The presence of cuticle-silica double layer in the epidermal tissue. Soil Sci. Plant Nutr. 8, 1–5.
Zhang, J.P., Lu, H.Y., Wu, N.Q., Yang, X.Y., Diao, X.M., 2011. Phytolith analysis for differentiating between foxtail millet (*Setaria italica*) and green foxtail (*Setaria viridis*). PLoS One 6, e19726.
Zucol, A.F., Brea, M., 2005. Sistemática de fitolitos pautas para un sistema clasificatorio. Un caso en estudio en la Formación Alvear (Pleistoceno inferior), Entre Ríos, Argentina. Ameghiniana 42, 685–704.

frontiers in Plant Science

ORIGINAL RESEARCH
published: 22 June 2018
doi: 10.3389/fpls.2018.00864

Taxonomic Demarcation of *Setaria pumila* (Poir.) Roem. & Schult., *S. verticillata* (L.) P. Beauv., and *S. viridis* (L.) P. Beauv. (Cenchrinae, Paniceae, Panicoideae, Poaceae) From Phytolith Signatures

Mudassir A. Bhat, Sheikh A. Shakoor, Priya Badgal and Amarjit S. Soodan*

Plant Systematics and Biodiversity Laboratory, Department of Botanical and Environmental Sciences, Guru Nanak Dev University, Amritsar, India

Background and Aims: The role and significance of phytoliths in taxonomic diagnosis of grass species has been well documented with a focus on the types found in foliar epidermis and the synflorescence. The present paper is an attempt to broaden the scope of phytoliths in species diagnosis of grasses by developing phytolith signatures of some species of the foxtail genus *Setaria* P. Beauv. through *in situ* location and physico-chemical analysis of various phytolith morphotypes in different parts of the plant body.

Methods: Clearing solution and dry ashing extraction methods were employed for *in situ* location and isolation of phytolith morphotypes respectively. Ultrastructural details were worked out by Scanning Electron Microscopy (SEM) and Transmission Electron Microscopy. Morphometric and frequency data of phytolith morphotypes were also recorded. Biochemical architecture of various phytolith types was worked out through SEM-EDX, XRD, and FTIR analysis. Data were analyzed through Principal Component Analysis and Cluster Analysis.

Key Results: *In situ* location of phytoliths revealed species specific epidermal patterns. The presence of cystoliths (calcium oxalate crystals) in the costal regions of adaxial leaf surface of *S. verticillata* (L.) P. Beauv. is the first report for the genus *Setaria*. Our results revealed marked variations in epidermal ornamentation and undulation patterns with a novel "Λ" (Lamda) type of undulated ornamentation reported in *S. verticillata*. Dry ashing method revealed species specific clusters of phytolith morphotypes.

Conclusions: The study revealed that phytoliths can play a significant role in resolution of taxonomic identity of three species of *Setaria*. Each species was marked out by a unique assemblage of phytolith morphotypes from various parts of the plant body. Apart from *in situ* location and epidermal patterning, diagnostic shapes, frequency distribution, size dimensions, and biochemical architecture emerged as complementary traits that help in developing robust phytolith signatures for plant species.

Keywords: grasses, morphotypes, phytoliths, *Setaria* spp., silica, taxonomic demarcation

OPEN ACCESS

Edited by:
Terry B. Ball,
Brigham Young University,
United States

Reviewed by:
Jennifer Bates,
University of Cambridge,
United Kingdom
Lisa K. Kealhofer,
Santa Clara University, United States

***Correspondence:**
Amarjit S. Soodan
assoodan@gmail.com

Specialty section:
This article was submitted to Plant Physiology, a section of the journal Frontiers in Plant Science

Received: *21 February 2018*
Accepted: *04 June 2018*
Published: *22 June 2018*

Citation:
Bhat MA, Shakoor SA, Badgal P and Soodan AS (2018) Taxonomic Demarcation of Setaria pumila (Poir.) Roem. & Schult., S. verticillata (L.) P. Beauv., and S. viridis (L.) P. Beauv. (Cenchrinae, Paniceae, Panicoideae, Poaceae) From Phytolith Signatures. Front. Plant Sci. 9:864. doi: 10.3389/fpls.2018.00864

INTRODUCTION

The foxtail genus, *Setaria* P. Beauv., so named by the presence of sterile bristles that subtend spikelets in a close panicle, belongs to the "bristle clade" (subtribe Cenchrinae, tribe Paniceae, subfamily Panicoideae) of the grass family Poaceae (Morrone et al., 2012). The genus has a labile morphology requiring additional characters for the resolution of phylogenetic relations among the 113 odd species of the genus (Clayton et al., 2016 onwards). One of the species, the foxtail millet *Setaria italica* (L.) P. Beauv. has been cultivated along with other millets in dryland farming system since prehistoric times (Madella et al., 2016; Weisskopf and Lee, 2016). Some other species of the genus also serve as significant sources of forage and fodder (Aliscioni et al., 2011; Marinoni et al., 2013). Several studies have attempted to resolve the infrageneric (Stapf and Hubbard, 1934; Webster, 1987; Pensiero, 1999) and intergeneric (Webster, 1993, 1995; Veldkamp, 1994; Morrone et al., 2014) relations of the genus. Molecular studies on the chloroplast gene ndhF have revealed polyphyletic nature of the genus with three well supported clades (Kellogg et al., 2009). Even though leaf blade anatomy has traditionally been employed for taxonomic characterization of grasses (Prat, 1936, 1948; Metcalfe, 1960; Ellis, 1979, 1984), the role of anatomical characters in grass taxonomy and phylogeny has been, so to say, rediscovered in the recent past (Ingram, 2010) with *Setaria* P. Beauv. as a model genus (Aliscioni et al., 2016). Apart from epidermal cell patterns and vasculature, phytoliths in leaf epidermis and other parts of the plant body have been utilized for species characterization and taxonomic analysis of grass taxa.

Phytolith studies have been utilized both for characterization of individual *Setaria* species (Rovner, 1971; Hodson et al., 1982) as also for taxonomic demarcation among species within the genus (Zhang et al., 2011; Layton and Kellogg, 2014; Wang et al., 2014; Madella et al., 2016) and from related genera (Hunt et al., 2008; Lu et al., 2009; Out et al., 2014; Wang et al., 2014; García-Granero et al., 2016; Madella et al., 2016). The ever increasing role of phytoliths in the resolution of intrageneric and intergeneric taxonomy of the genus can be ascribed to the simple fact that even among grasses, *Setaria* spp. show exceptional levels of silica accumulation in the form of phytoliths in all parts of the plant body. During the present investigations, an attempt has been made to supplement the information available on the phytolith profiles of three closely related species of the foxtail grass genus through a multiproxy approach and the development of phytolith signatures as additional evidence for their taxonomic demarcation. Analysis of several aspects of phytoliths from different parts of the plant body of the selected species was done through a battery of techniques employed in a logical sequence from *in situ* location of phytolith morphotypes in foliar epidermis to advanced level of physico-chemical analysis involving sophisticated instruments and methodology. In this context, the present study marks a significant advance toward developing a comprehensive and robust framework for the use of data on morphotype diversity, distribution in different parts of the plant body and their ultrastructural and biochemical characterization in identification and taxonomic demarcation of plant taxa.

Silica and Phytolith Production in Plants

Plants absorb monosilicic acid (H_4SiO_4), which is released to the soil by weathering of siliceous minerals, by action of an aquaporin-like channel Low-silicon 1 (*Ls1*) and a proton antiporter Low-silicon 2 (*Ls2*) and polymerizes it into amorphous silica ($SiO_2.nH_2O$) in cell lumens (internal casts), intercellular spaces, and cell walls (external casts) of the parenchymatous tissue (Baker, 1959b; Jones and Handreck, 1967; Rovner, 1971; La Roche, 1977; Bombin, 1984; Piperno, 1988; Mulholland, 1989; Ma et al., 2011; Ma and Yamaji, 2015). A number of unknown silica transporters are believed to be involved in directing silica transfer to different silicification sites (Kumar et al., 2017). Being hard and resistant to dessication and disfiguration, these amorphous silica bodies are commonly called phytoliths [phyton ($\varphi\upsilon\tau o\nu$) = plant + lithos ($\lambda\iota\theta o\varsigma$) = stone]. As casts (both internal and external) of plant cells, phytoliths vary in shape, size, frequency, surface ornamentation and other structural features (Ollendorf et al., 1988; Piperno, 1988, 2006; Lu and Liu, 2003; Lu et al., 2009; Zhang et al., 2011; Szabo et al., 2015; Ge et al., 2016). Genetic control of shape, size and frequency of phytoliths has been demonstrated in some monocots (e.g., *Zea mays* L.) and dicots (e.g., *Cucurbita* spp. L.) (Bozarth, 1987; Piperno et al., 2000).

Phytoliths have been implicated in several biological functions including that of providing an endoskeletal framework which prevents wilting (Parry and Smithson, 1958a) and offering resistance to herbivory (Rovner, 1971; Stebbins, 1972, 1981; Coughenour, 1985; Epstein, 1994, 1999), and alleviating biotic (Jones and Handreck, 1967; Gould and Shaw, 1983; Mazumdar, 2011) and abiotic (Hodson et al., 1985; Hodson and Evans, 1995; Lux et al., 2003; Hattori et al., 2005) stress. Phytoliths have also been reported to play a role in checking the rate of transpiration and at the same time reducing the heat load of plants growing in exposed habitats (Jones and Handreck, 1967; Sangster and Parry, 1971; Krishnan et al., 2000).

Ecological functions played by phytoliths include a role in biogeochemical and bio-cycling of silicon in terrestrial ecosystems (Conley, 2002; Gerard et al., 2008; Borrelli et al., 2010; Struyf and Conley, 2012) and sequestration of occluded carbon (Rajendiran et al., 2012; Parr and Sullivan, 2014; Alexandre et al., 2015; Ru et al., 2018; Yang et al., 2018). Isotopic dating of phytolith occluded carbon (PhytOC) has been employed to determine the age of sediments and that of elements of vegetation trapped in these sediments (Parr and Sullivan, 2014). The use of phytoliths in dating of plant fossils can be attributed to the fact that upon death and *in situ* decay of the plant body, phytoliths are released into the soil where they stay through the millenia resisting deformation and destruction by the vagries of geological and climatic conditions. Their long time persistence in the soil make them ideal plant microfossils which have been recovered from sediments as far back as 60 mya in the Cenozoic (Jones, 1964), including the glacials (Twiss et al., 1969; Fredlund et al., 1985) and the Holocene (Baker, 1959a; Crawford, 2009). Phytoliths have been recovered from diverse habitats including swamps (Baker, 1959a), arid zones (Pease and Anderson, 1969), humid areas (Jones and Beavers, 1964) and vegetation types including grasslands and forests (Wilding and Drees, 1973).

Owing to widespread production across several plant groups and excellent preservation as microfossils, phytoliths have found an ever increasing role as proxies in diverse fields of scientific enquiry including archeaobotany of the centers of civilization and cultivation (Schellenberg, 1908; Pearsall, 1978; Rovner, 1983; Piperno, 1984; Shillito, 2013; Gao et al., 2018), paleoecology and paleoclimatology (Rovner, 1971; Carbone, 1977; Fox et al., 1996; Piperno, 2006; Albert et al., 2007), the mapping of ancient land use patterns, and vegetation structure (Gross, 1973; Pearsall and Trimble, 1984; Fisher et al., 1995). Phytolith profiles of present day crop species and soil samples of ancient sites have been compared and calibrated for developing historical calendars for the origin of agriculture and routes of spread and diversification of crop species and calculating the crop ratios (Rovner, 1983; Piperno, 1998, 2009; Pearsall et al., 2003; Albert and Henry, 2004; Fuller et al., 2007; Itzstein-Davey et al., 2007; Tsartsidou et al., 2007; Hunt et al., 2008; Crawford, 2009; Lu et al., 2009; Zhang et al., 2010, 2012; Zhao, 2011; Chen et al., 2012; Madella et al., 2014, 2016; Weisskopf et al., 2014; Out and Madella, 2016; Weisskopf and Lee, 2016), the food and non-food uses of plants in crafts and building materials (Ryan, 2011), agricultural practices (e.g., irrigation, Rosen and Weiner, 1994; Slash-n-burn; Piperno, 1998), paleoagrostology (Piperno and Pearsall, 1998), taphonomy (Madella and Lancelotti, 2012) and colonization of islands and distant lands (Astudillo, 2017).

On account of the wide range of availability and ease of recovery from unused parts of cereals (and other crop species) and the purity of silica obtained, phytoliths have also found a role in nanotechnology (Neethirajan et al., 2009; Qadri et al., 2015). In the contemporary environmental context, phytoliths are being employed as models for assessment of the effects of global warming and climate change (Hongyan et al., 2018).

Phytoliths in Grass Systematics

Notwithstanding the above mentioned applications, phytoliths have found the most significant role in taxonomic characterization and demarcation of plant taxa. At this juncture it would be quite instructive to review the landmarks in plant phytolith research that have provided the framework for the use of phytoliths in grass systematics as well. After the revisionary work of (Netolitsky, 1929), attempts were made to identify the marker morphotypes for plant taxa at different levels of taxonomic hierarchy. Within grasses, branched cells were typically associated with *Nardus stricta* L. (Parry and Smithson, 1958a,b). Twiss et al. (1969) expanded the scope of "marker morphotype" approach to major groups within the family through a study of 26 morphotypes of which eight were ascribed to festucoid group, two to chloridoid, and 11 to panicoid grasses and the rest (five) had no particular subfamilial affiliation. Soon afterwards, Rovner (1971) pointed out that a search for "marker" types for plant taxa would run into difficulty on account of "multiplicity" of types within a single species (more so for taxa at higher ranks) and "redundancy" of occurrence of same types "appearing in related as well as taxonomically unrelated species." Rovner (1971) suggested that assemblages or "type-sets" of phytoliths would provide better taxonomic demarcation among plant species and soil samples.

Apart from types, Mulholland (1989) presented data on frequencies of various types to characterize 19 wild grasses collected from their natural habitats. Piperno and Pearsall (1993) pointed out that phytoliths from reproductive parts proved more useful in separating maize (*Zea mays* L.) from teosinte. This work focused on an organ-specific approach in using phytoliths in taxonomic demarcation of grass species. Pearsall et al. (1995) further narrowed it down to "silicified glumes" as the most revealing in distinguishing cultivated rice (*Oryza sativa* L.) from its wild relatives. Piperno (1998) identified diagnostic morphotypes of phytoliths for the subfamilies Pooideae, Arundinoideae, Chloridoideae, and described the diagnostic and diverse types in the Bambusoideae in great detail. Several subsequent workers have utilized typology and frequency (abundance) approachs to phytolith analysis for taxonomic characterization and demarcation of cultivated and wild grasses (Piperno, 1985; Zhang et al., 2012; Tripathi et al., 2013).

Rudall et al. (2014) employed the shapes of costal phytolith morphotypes and their orientation to elucidate phylogenetic relationships among different grass subfamilies and supported the recognition of three clades within the family. The APP (Anomochloideae, Pharoideae, Puelioideae) clade was treated as the most primitive followed by BEP (Bambusoideae, Ehrhartoideae, Pooideae) and species rich PACCMAD (Panicoideae, Arundinoideae, Chloridoideae, Micrairoideae, Aristidoideae, Danthonioideae) clades. Kealhofer et al. (2015) carried out phytolith analysis of leaf and synflorescence of the foxtail millet [*S. italica* (L.) Beauv.]. In India, Jattisha and Sabu (2015) brought out the taxonomic significance of foliar phytoliths as diagnostic markers in some grasses of South India. More recently, Shakoor et al. (2016) employed phytoliths from underground (root) and aerial (culm, leaf & synflorescence) parts for taxonomic demarcation of two reed grasses, *Arundo donax* L. and *Phragmites karka* (Retz.) Trin. ex Stued.

Parry et al. (1984) marked the biochemical dimension in phytolith characterization by reporting a time dependent accumulation of some elements (K, Cl, P, and S) along with silicon in the silicified microhairs from the lemma of the canary grass, *Phalaris canariensis* L. and giving evidence of genetic control of silicification. In recent years, physico-chemical characterization of phytoliths has been extended to a study of the physical states (as amorphous vs. crystalline), the mineral composition and the study of functional groups and their bonding patterns through sophisticated methods of analysis (Chauhan et al., 2011; Shakoor et al., 2016).

The work reported in this paper is a part of the ongoing program of research on the role of phytoliths in the systematic analysis of grass flora in the area of study. *Setaria* species selected for the present investigations show morphological similarity with one another as well as the foxtail millet *S. italica* (L.) P. Beauv. and are placed closely in keys to species identification of the genus (Layton and Kellogg, 2014). *Setaria viridis* (L.) P. Beauv. had an Asian origin with phylogenetic relations with its domesticated derivative the foxtail millet, *S. italica* with which it remains interfertile (Shi et al., 2008). The second species of the present sample, *S. verticillata* is the polyploid derivative of *S. viridis* (L.) P. Beauv. (Layton and Kellogg, 2014). The third species, *S. pumila*

(Poir.) Roem. & Schult. had an African origin (Rominger et al., 2003) but shares a wide distribution with *S. viridis* and growth in mixed populations and is included in the "*S. viridis* clade" of the genus. The foxtail millet, *Setaria italica* would have been a useful and desirable addition to the material but it is not cultivated in the Punjab plains and was thus unavailable for this work. Even though permanent herbarium sheets of this species were available in the departmental herbarium, sufficient material could not have been extracted from them for the present analysis.

MATERIALS AND METHODS

Area of Study

About twenty plant specimens of *S. pumila* and *S. verticillata* were collected from the campus of Guru Nanak Dev University, (32.64 °N and 74.82 °E) Amritsar, Punjab (**Figures 1a–c**). A similar number of plants of *S. viridis* were collected from the campus of Sher-i-Kashmir University of Agricultural Sciences and Technology, (32.65 °N and 74.81 °E) Srinagar, Jammu & Kashmir (**Figures 1d,e**). The specimens were collected at flowering and fruiting stage. Taxonomic descriptions and illustrations of the species were made from fresh material in the standard formats of grass description proposed by Grass Phylogeny Working Group (GPWG (Grass Phylogeny Working Group)., 2001) and GPWG (Grass Phylogeny Working Group II). (2011) systems and maintained by the online sources (Clayton et al., 2016; GrassBase—The Online World Grass Flora: The Board of Trustees, Royal Botanic Gardens [online]. Available at http://www.kew.org/data/grasses-db.html and 2. Tropicos (2011) http://www.tropicos.org. Name Search.aspx. 3.eflora of China: http://www.efloras.org. Missouri Botanical Garden, St. Louis, MO and Harvard University Herbaria, Cambridge, MA). The species identity of the specimens was established by comparison of the vegetative and reproductive morphology and micromorphometry with standard descriptions available in works of grass floristics of the world (Bor, 1960; Gould, 1968; Cope, 1982; Gould and Shaw, 1983; Clayton and Renvoize, 1986; Watson and Dallwitz, 1992; Kellogg, 2015; Soreng et al., 2017 and the region Sharma and Khosla, 1989; Kumar, 2014). For preparation of herbarium sheets, three dried specimens for each of the species have been deposited in the Herbarium of the Department of Botanical and Environmental Sciences, Guru Nanak Dev University, Amritsar (Voucher nos. 7373 to 7381).

Phytolith Analysis

About five to ten plants remaining intact after taxonomic descriptions and dry preservation for hebarium specimens, were dismembered into underground (root) and above ground (culm, leaf and synflorescence) parts. The material was homogenized (part wise) into lots. Some of the material from each lot was preserved in 70% ethanol at 4°C for *in situ* location of phytoliths. The rest of the material in each lot was washed to clear dust and adhering soil particles, sundried and stored in plastic jars for dry ashing and further analysis.

Methodology of the present study followed a logical and systematic sequence from *in situ* visualization of the phytoliths in the leaf epidermis to dry ashing of plant parts for disarticulation of individual morphotypes for recording qualitative (morphotypic) data and collection of quantitative (micromorphometric) data on phytoliths among the species and their parts. Quantitative assessment also included frequency distribution of various morphotypes. After data collection at the level of light microscopy (LM), scanning electron microscopy (SEM) of morphotypes was carried out to record their surface ornamentations and three dimensional structures. Transmission electron microscopy (TEM) was employed to study variations in texture, interplanar spacing, and crystallinity of various morphotypes. EDX analysis was employed to study elemental composition of phytolith morphotypes and the rhizospheric soil. XRD analysis revealed the physical phases of silica and other minerals in the phytoliths. Similarly, FTIR analysis was carried out to know the functional groups of phytoliths from different plant parts.

In Situ Location

A study of *in situ* location and epidermal patterning of phytoliths on both adaxial and abaxial surfaces of the leaf was carried out according to the method of Clarke (1959) with some modifications. The leaf segments from mature leaves were boiled in tubes for 5–10 min in distilled water. After cooling down the tubes, leaf segments were put in ethanol (absolute) and heated gently (80°C) in a water bath till they were decolorized. Thereafter, the segments were immersed in a solution of lactic acid and chloral hydrate (3:1 v/v) and boiled again for 20–30 min in a water bath. After clearing, they were placed on clean ceramic tiles with the adaxial surface upwards and the epidermis was peeled off the middle part of mature leaf blades. Similarly, peelings from abaxial surface of leaf segments were obtained. Epidermal peelings were stained in Gentian Violet and passed through a dehydration series of ethanol (30% through 50, 70, 90% and absolute ethanol) and mounted in DPX for light microscopy and microphotography with a Micro Image Projection System (MIPS-USB 0262) mounted on an Olympus Binocular and connected to a computer for imaging.

Dry Ashing Method

The standard protocol of Carnelli et al. (2001) with some modifications was employed for dry ashing of the plant material. The dried and stored material of individual parts was taken from the plastic jars, further dried in an oven, weighed and transferred to porcelain crucibles. The material was incinerated at 550°C for 4–6 h to ashes. The crucibles were taken out of the furnace, allowed to cool and ash contents were transferred to test tubes. A sufficient amount of hydrogen peroxide (30%) was added to submerge the ash and the test tubes were kept at 80°C for 1 h in a water bath. The mixture was decanted and rinsed twice in distilled water. Hydrochloric acid (10%) was added to the pellet and incubated at 80°C for 1 h. Thereafter, the mixture was washed in distilled water and centrifuged for 15 min at 7,500 rpm. The supernatant was decanted off and the pellet was washed twice in distilled water. The process was repeated till the pellet was clear. Finally, the pellet was oven dried for 24 h at 60°C to a powder form and weighed. The silica content (%) was calculated by the formula: final ash content/dry mass × 100.

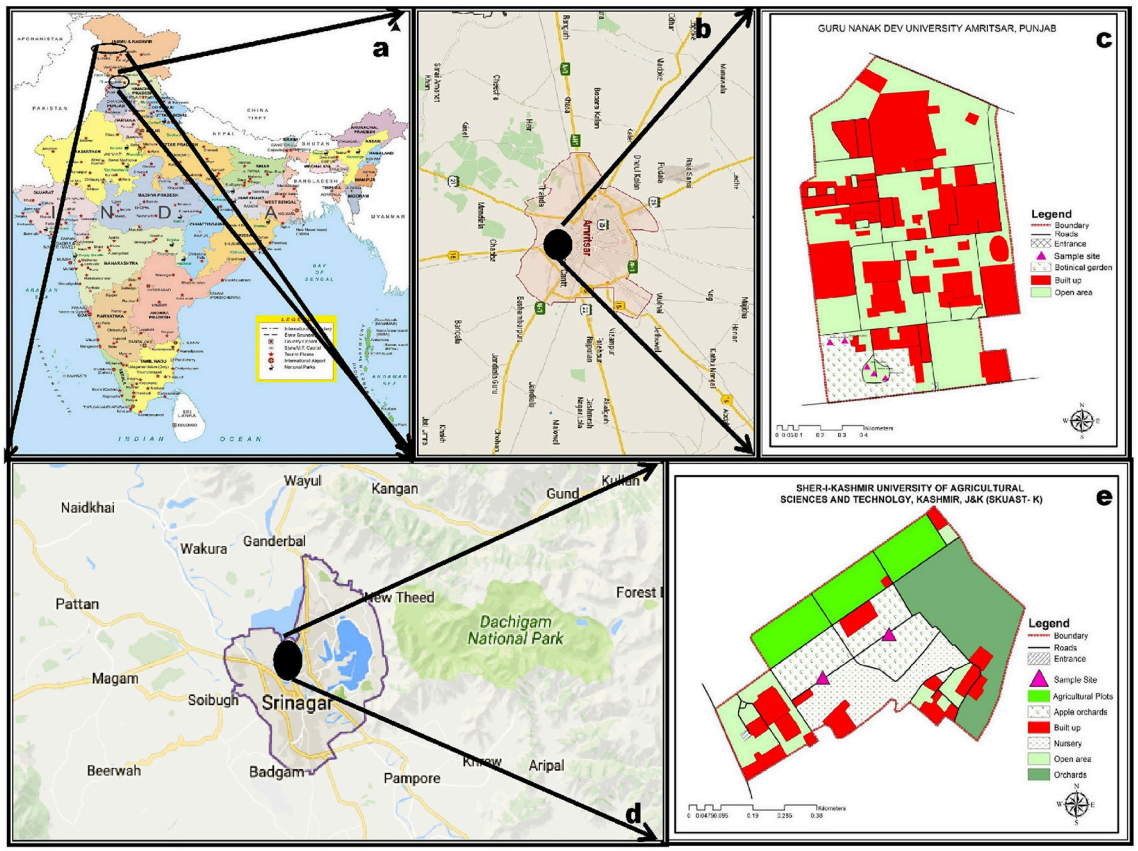

FIGURE 1 | Distribution of sampling sites in India **(a–e)**: *Setaria pumila* (Poir.) Roem. & Schult. and *Setaria verticillata* (L.) P. Beauv. **(b,c)** and *Setaria viridis* (L.) P. Beauv. & Schult. **(d,e)**.

A small amount (ca. 0.1 mg) of dried ash was dipped in 10 ml of Gentian Violet in a watch glass and stirred. A drop of this mixture was put on a glass slide and covered with a cover slip. The slides were heated gently and excess stain drained off with a filter paper. Ten slides were prepared for each sample. Morphotypes of phytoliths were photographed by Olympus Micro Image Projection System (MIPS-USB 0262) at a uniform magnification (40X). The phytoliths isolated by the dry ashing method from underground (root) and aerial (culm, leaf, and synflorescence) parts showed considerable diversity of phytolith morphotypes in terms of their shapes and were classified according to the International Code of Phytolith Nomenclature (ICPN 1.0; Madella et al., 2005). Some of the morphotypes whose description was not available in the ICPN nomenclature were classified as per the schemes presented in **Table 1**.

Morphometry

Morphometric measurements of phytolith morphotypes were made using Image J software (version 1.46r.). A total of 5 morphometric parameters of size and shape descriptors were recorded on a minimum sample size calculated as per recommendations of the International Committee for Phytolith Morphometrics (ICPM, Ball et al., 2016) by the formula:

$$N_{\min} = Z^2_{\alpha/2} \times S^2/(ME)^2$$

Where: $\mathbf{N}_{\min}$ = the minimum adequate sample size; $\mathbf{Z}^2_{\alpha/2} = 1.64$, which is the square of the two tailed Z value for level of significance (α) = 0.10; $\mathbf{S}^2$ = the variance, and $\mathbf{(ME)}^2$ = the square of the permissible margin of error (in this case 0.05) × the sample mean. This calculation estimates the minimum adequate sample size required for 95% confidence that the sample means are within 5% deviation from actual population means.

Scanning Electron Microscopy (SEM)

For SEM, dry ash was spread evenly over the stubs with the help of double-sided adhesive tape under the stereoscope. Silver paint was applied on edges of the stub and the samples dried overnight at 40°C. The next day, stubs were coated with graphite using a vacuum evaporator and later coated with gold by a sputter coater (QUORUM) and imaged under SEM (CARL ZEISS EVO 40) at an accelerating voltage of 40 KV.

Transmission Electron Microscopy

TEM micrographs were obtained using a JEOL JEM-2100 operating at 200 keV. Samples were prepared by suspending a

TABLE 1 | Description of different phytolith morphotypes and their diagnostic potential in *Setaria* spp. of the present study.

S.No	Phytolith Morphotypes	Acronym	Morphotype description (as per ICPN 1.0)			*Setaria pumila* (Poir.) Roem. & Schult.[SP]				*Setaria verticillata* (L.) P. Beauv. [SVC]				*Setaria viridis* (L.) P. Beauv. [SV]				Diagnostic for	Ubiquity	Reference (s)
			First descriptor	Second descriptor	Third descriptor	Rt	Cl	Lf	Synflo	Rt	Cl	Lf	Synflo	Rt	Cl	Lf	Synflo			
1.	Acicular	ACL	Acicular	—————	————	−	−	−	−	−	−	−	+	−	−	−	+	SVC & SV	0.66 (0.17)	Madella et al., 2005
2.	Bilobate class I	BCI	Bilobate class I	—————	————	+	−	−	+	−	−	−	−	−	−	−	−	SP	0.33 (0.17)	Gallego and Distel, 2004
3.	Bilobate class II	BCII	Bilobate class II	—————	————	−	−	−	−	−	−	−	−	−	−	+	+	SV	0.33 (0.17)	Gallego and Distel, 2004
4.	Bilobate class III	BCIII	Bilobate class III	—————	————	−	−	+	−	−	−	+	−	−	−	−	−	SP & SVC	0.66 (0.17)	Gallego and Distel, 2004
5.	Bilobate class IV	BCIV	Bilobate class IV	—————	————	−	−	−	−	−	−	+	−	−	−	+	−	SVC & SV	0.66 (0.17)	Gallego and Distel, 2004
6.	Bilobate class V	BCV	Bilobate class V	—————	————	+	−	+	−	+	−	−	−	−	−	+	−	−−	0.66 (0.33)	Gallego and Distel, 2004
7.	Bilobate class VI	BCVI	Bilobate class VI	—————	————	+	−	+	−	−	−	−	−	−	−	+	−	SP & SV	0.66 (0.25)	Gallego and Distel, 2004
8.	Bilobate class VII	BCVII	Bilobate class VII	—————	————	−	−	−	−	−	−	+	−	−	−	+	−	SVC & SV	0.66 (0.17)	Gallego and Distel, 2004
9.	Bilobate class VIII	BCVIII	Bilobate class VIII	—————	————	−	−	−	−	−	−	−	−	−	−	+	−	SV	0.33 (0.08)	Blinnikov, 2005
10.	Blocky crenate	BC	Blocky	Crenate	————	−	−	−	−	−	+	−	−	−	−	−	−	SVC	0.33 (0.08)	Barboni et al., 2010
11.	Blocky irregular	BIR	Blocky	Irregular	————	+	−	+	+	+	+	+	+	+	+	+	+	−−	1.0 (0.91)	Barboni et al., 2010

(Continued)

TABLE 1 | Continued

S.No	Phytolith Morphotypes	Acronym	Morphotype description (as per ICPN 1.0)			*Setaria pumila* (Poir.) Roem. & Schult.[SP]				*Setaria verticillata* (L.) P. Beauv. [SVC]				*Setaria viridis* (L.) P. Beauv. [SV]				Diagnostic for	Ubiquity	Reference (s)
			First descriptor	Second descriptor	Third descriptor	Rt	Cl	Lf	Synflo	Rt	Cl	Lf	Synflo	Rt	Cl	Lf	Synflo			
12.	Blocky polyhedral	BPH	Blocky	Polyhedral	—————	−	+	+	+	+	+	+	−	+	+	+	−	−−	1.0 (0.75)	Blinnikov, 2005
13.	Carinate	CRN	Carinate	—————	—————	−	−	−	−	−	−	−	−	−	+	−	+	SV	0.33 (0.17)	Madella et al., 2005
14.	Clavate	CLV	Clavate	—————	—————	−	−	+	+	−	−	+	−	−	+	+	−	−−	1.0 (0.40)	Madella et al., 2005
15.	Columellate elongate	CE	Columellate	Elongates		−	−	−	+	−	−	−	+	−	−	−	−	SP & SVC	0.66 (0.17)	Madella et al., 2005
16.	Crescent moon	CM	Crescent moon	—————	—————	−	−	−	−	+	−	−	−	−	−	−	−	SVC	0.33 (0.08)	Fernandez Honaine et al., 2006
17.	Cross	CRS	Cross	—————	—————	−	−	+	−	−	−	+	+	−	−	−	−	SP & SVC	0.66 (0.25)	Madella et al., 2005
18.	Cuboid	CUB	Cuboid	—————	—————	−	−	+	−	+	+	−	−	+	+	+	−	−−	1.0 (0.50)	Ellis, 1979
19.	Cuneiform bulliform	CB	Cuneiform	—————	Bulliform	+	+	−	+	+	−	+	+	−	+	−	+	−−	1.0 (0.66)	Madella et al., 2005
20.	Cylindrical	CYD	Cylindrical		—————	−	−	+	−	+	−	−	−	−	−	−	+	−−	1.0 (0.25)	Madella et al., 2005
21..	Echinate elongate	EE	Elongate	Echinate	—————	−	+	−	+	−	−	−	+	−	−	+	−	−−	1.0 (0.25)	Madella et al., 2005
22.	Elongate irregular	EIR	Elongate	Irregular	—————	−	−	+	+	−	+	+	−	−	+	−	−	−−	1.0 (0.41)	Gallego and Distel, 2004
23.	Elongate with concave ends	ECE	Elongate	Concave ends	—————	−	−	−	−	+	−	−	−	−	−	−	−	SVC	0.33 (0.08)	Gallego and Distel, 2004
24.	Epidermal element	EPE	—————	—————	Epidermal element	−	−	−	+	−	−	−	−	−	−	−	+	SP & SV	0.66 (0.17)	Gallego and Distel, 2004

(Continued)

TABLE 1 | Continued

S.No	Phytolith Morphotypes	Acronym	Morphotype description (as per ICPN 1.0)			*Setaria pumila* (Poir.) Roem. & Schult.[SP]				*Setaria verticillata* (L.) P. Beauv. [SVC]				*Setaria viridis* (L.) P. Beauv. [SV]				Diagnostic for	Ubiquity	Reference (s)
			First descriptor	Second descriptor	Third descriptor	Rt	Cl	Lf	Synflo	Rt	Cl	Lf	Synflo	Rt	Cl	Lf	Synflo			
25.	Epidermal element with columellate extensions	EECE	—————	Columellate extensions	Epidermal element	−	−	−	−	−	−	−	+	−	−	−	−	SVC	0.33 (0.08)	Madella et al., 2005
26.	Epidermal element with short silica cells and stomata	EESSCS	—————	—————	Epidermal element with short silica cells and stomata	−	−	−	−	−	−	−	−	−	−	−	+	SV	0.33 (0.17)	Madella et al., 2005
27.	Epidermal element with undulated ridges	EEUR	—————	Undulated ridges	Epidermal element	−	−	−	+	−	−	−	−	−	+	−	−	SP & SV	.66 (0.17)	Gallego and Distel, 2004
28.	Epidermal papillate	EP	—————	Papillate	Epidermal	−	−	−	−	−	−	−	−	−	−	−	+	SV	0.33 (0.08)	Gallego and Distel, 2004
29.	Facetate elongate	FE	Elongate	Facetate	—————	−	−	−	+	−	−	−	−	−	−	−	−	SP	0.33 (0.08)	Madella et al., 2005
30.	Globular echinate	GE	Globular	Echinate	—————	−	−	−	−	+	−	−	−	−	+	+	−	SVC & SV	0.66 (0.25)	Madella et al., 2005
31	Globular granulate	GG	Globular	Granulate	—————	+	−	+	+	−	−	+	−	+	−	+	−	−−	1.0 (0.50)	Madella et al., 2005
32.	Globular polyhedral	GPH	Globular	Polyhedral	—————	+	+	+	+	+	−	+	+	−	+	+	+	−−	1.0 (0.83)	Tsartsidou et al., 2007
33.	Globular psilate	GPI	Globular	Psilate	—————	−	−	−	−	+	+	−	−	+	+	−	+	SVC & SV	0.66 (0.41)	Madella et al., 2005
34.	Half moon	HM	Half moon	—————	—————	−	−	−	−	−	+	−	−	−	−	−	−	SVC	0.33 (0.08)	Morris et al., 2009
35.	Horned tower	HT	Horned tower	—————	—————	−	−	−	+	−	−	+	−	−	−	−	−	SP & SVC	0.66 (0.17)	Twiss et al., 1969
36.	Macrohairs	MH	—————	—————	Macrohairs	−	−	−	+	−	−	+	−	−	−	+	−	−−	1.00 (0.25)	Madella et al., 2005

(Continued)

TABLE 1 | Continued

S.No	Phytolith Morphotypes	Acronym	Morphotype description (as per ICPN 1.0)			*Setaria pumila* (Poir.) Roem. & Schult.[SP]				*Setaria verticillata* (L.) P. Beauv. [SVC]				*Setaria viridis* (L.) P. Beauv. [SV]				Diagnostic for	Ubiquity	Reference (s)
			First descriptor	Second descriptor	Third descriptor	Rt	Cl	Lf	Synflo	Rt	Cl	Lf	Synflo	Rt	Cl	Lf	Synflo			
37.	Nodular bilobate	NBL	Nodular bilobate	—————	—————	+	−	+	−	−	−	+	−	−	−	+	−	−−	1.0 (0.33)	Fahmy, 2008
38.	Oblong	OBL	Oblong	—————	—————	+	−	−	−	−	−	−	−	+	−	−	+	SP & SVC	0.66 (0.25)	Madella et al., 2005
39.	Ovate	OVT	Ovate	—————	—————	−	−	+	−	−	+	_	−	−	−	+	−	−−	1.0 (0.25)	Madella et al., 2005
40.	Parallelepipedal bulliform cell	PBFC	Parallelepipedal	—————	Bulliform cell	−	−	+	−	+	−	−	−	+	−	−	+	−−	1.0 (0.33)	Madella et al., 2005
41.	Plates	PLT	Plates	—————	—————	−	−	−	+	−	−	−	−	−	+	+	−	SP & SV	0.66 (0.25)	Blinnikov, 2005
42.	Polylobate	PL	Polylobate	—————	—————	+	−	−	−	−	−	−	−	−	−	−	−	SP	0.33 (0.08)	Fahmy, 2008
43.	Polylobate irregular	PLIR	Polylobate	Irregular	—————	−	−	−	−	−	−	−	+	−	−	−	−	SVC	0.33 (0.08)	Fahmy, 2008
44.	Prickle hair	PH	—————	—————	Prickle hair	−	−	+	+	−	−	+	−	−	−	+	−	−−	1.0 (0.33)	Madella et al., 2005
45.	Prickly elongate	PE	Elongate	Prickly	—————	−	−	−	−	−	−	−	−	−	−	−	+	SV	0.33 (0.08)	Ellis, 1979
46.	Rectangular	RT	Rectangular	—————	—————	+	−	+	−	+	−	+	+	+	+	−	−	−−	1.0 (0.58)	Madella et al., 2005
47.	Rondel	RD	Rondel	—————	—————	−	−	−	−	−	−	−	+	−	+	−	−	SVC & SV	0.66 (0.17)	Madella et al., 2005
48.	Scutiform	STF	Scutiform	—————	—————	+	−	+	−	−	+	+	+	+	−	+	+	−−	1.0 (0.66)	Madella et al., 2005
49.	Sinuate elongate	SnE	Elongate	Sinuate	—————	−	+	−	+	−	+	−	−	−	−	+	−	−−	1.0 (0.33)	Madella et al., 2005
50.	Sinuate elongate with convex ends	SnECE	—————	Sinuate with convex ends	—————	−	+	−	−	−	−	−	−	−	−	−	−	SP	0.33 (0.08)	Gallego and Distel, 2004

(Continued)

TABLE 1 | Continued

S.No	Phytolith Morphotypes	Acronym	Morphotype description (as per ICPN 1.0)			*Setaria pumila* (Poir.) Roem. & Schult.[SP]				*Setaria verticillata* (L.) P. Beauv. [SVC]				*Setaria viridis* (L.) P. Beauv. [SV]				Diagnostic for	Ubiquity	Reference (s)
			First descriptor	Second descriptor	Third descriptor	Rt	Cl	Lf	Synflo	Rt	Cl	Lf	Synflo	Rt	Cl	Lf	Synflo			
51.	Smooth elongate	SmE	Elongate	Smooth	———— —	–	+	+	+	+	+	–	+	–	+	+	+	––	1.0 (0.75)	Madella et al., 2005
52.	Stomata	STM	—————	—————	Stomata	–	–	–	+	–	–	–	–	–	–	–	–	SV	0.33 (0.08)	Gallego and Distel, 2004
53.	Tabular simple	TBS	Simple tabular	—————	———— —	–	–	+	–	+	–	–	–	–	–	–	–	SP & SVC	0.66 (0.17)	Madella et al., 2005
54.	Tabular irregular	TIR	Tabular	Irregular	———— —	+	+	–	–	–	–	+	–	–	–	+	–	––	1.0 (0.33)	Barboni et al., 2010
55.	Tabular polyhedral	TPH	Tabular	Polyhedral	———— —	–	–	–	–	–	–	–	–	–	+	+	–	SV	0.33 (0.17)	Barboni et al., 2010
56.	Tracheid	TRCHD	—————	—————	Tracheid	–	–	–	+	–	–	–	–	–	–	–	–	SP	0.33 (0.08)	Madella et al., 2005
57.	Trapezoid	TZ	Trapezoid	—————	———— —	+	+	+	+	+	+	+	+	+	+	+	+	––	1.0 (1.00)	Madella et al., 2005
58.	Triangular	TRN	Triangular	—————	———— —	–	–	–	–	+	–	–	–	+	+	–	+	SVC & SV	0.66 (0.33)	Gallego and Distel, 2004

Rt, Root; Cl. Culm; Lf, Leaf; Syn, Synflorescence; (+), Presence; (–), Absence of particular phytolith morphotype; SP, Setaria pumila (Poir.) Roem. & Schult.; SVC, Setaria verticillata (L.) P. Beauv.; SV, Setaria viridis (L.) P. Beauv.

small quantity of powder (crushed in pestle and motar) in double distilled water (DDW). The samples were sonicated for 30 min and a drop of material was placed on a carbon coated copper grid. The grids were dried on filter paper using an electric lamp and were subsequently analyzed. Structural details as well as the chemistry of the samples were worked out by High Resolution Transmission Electron Microscopy (HRTEM) and Selected Area Electron Diffraction (SAED) of various phytolith types.

Biochemical Architecture

Elemental analysis of phytolith morphotypes and soil samples were carried out with Scanning Electron Microscope-Energy Dispersive X-ray analysis (SEM-EDX). Infrared spectra of silica powder were obtained on a Fourier Transform Infrared (FTIR) Spectrophotometer (System92035, Perkin-Elmer, England) at room temperature using the standard KBr method. The functional group spectra were recorded over a wavelength range of 500–4,000 cm^{-1}. X-ray Diffraction (XRD) studies were performed on powder XRD system (Bruker D8 Advance) using Cu Kα radiation (k = 1.5418 Å) in the 2θ (Bragg's angle) at a range of 20–70. The data were analyzed for presence of different polymorphic structures of silica and other compounds using the origin pro 8 software and following the notation of the Joint Committee on Powder Diffraction.

Elemental composition of rhizospheric soil samples was carried out with SEM-EDX. Soil samples (ca. 5 g) from the rhizospheric region of the specimens taken for phytolith analysis were collected and ground into fine powder. Small bits of the powder were spread uniformly on the stubs and were scanned using Energy Dispersive X-ray analyzer coupled with the SEM through *Inca software*.

Statistical Analysis

Descriptive statistics of morphometric and elemental composition data was carried out with the help of paleontological statistics (PAST) software (Hammer et al., 2001). Cluster analysis of presence/absence data of bilobate classes of phytoliths and Principal component analysis (PCA) of morphometric and elemental composition data was carried out using C2 data analysis software (Juggins, 2003). This software has also been used for plotting the stratigraphic diagram of the frequency data of phytoliths. Pearson's coefficient of association of phytolith morphotypes of the three species were also calculated employing computer programs developed for the purpose.

RESULTS AND DISCUSSION

Taxonomic descriptions of grasses include several (vegetative and reproductive) characteristics that help to characterize and classify taxa from subfamily down to the species and infra specific levels. Morphological and morphometrical characters that diagnose *Setaria pumila*, *S. verticillata,* and *S. viridis* from one another are presented in Supplementary Table 1. Whereas qualitative characteristics provide a clear cut account of similarities and dissimilarities in paired comparisons, quantitative characteristics show overlapping ranges and cryptic distinctions requiring additional evidence for taxonomic resolution. In the present context, phytolith analysis was employed to supplement and substantiate taxonomic demarcation among the three species of the genus *Setaria* P. Beauv.

Epidermal Patterns

Leaf epidermal characteristics play an important role in taxonomic demarcation of grass taxa due to the unique arrangement of epidermal long and short cells in the costal and intercostal regions (Prat, 1936, 1948; Metcalfe, 1960; Ellis, 1979; Hilu, 1984; Rudall et al., 2014).

The present study has revealed two distinct distribution patterns of silica cells and associated epidermal cells. The first one comprises long-short cell alternation in the intercostal region of the epidermis and the second one includes axial rows of closely spaced short silica cells in the costal region. These costal rows of silica bodies are separated from each other by a single short intervening cell known as the cork cell and are considered highly diagnostic in grasses (Prasad et al., 2011). The intervening cells are relatively thin walled, but resemble silica bodies in size and shape.

The underlying causes for the concentration of the silica bodies over the veins remain unknown though there is an apparent positive correlation between silica deposition and proximity to lignified tissues of the vascular bundles. Indirect support for this association between lignin and silica deposition comes from studies indicating a correlation between silica deposition and lignin metabolism in grasses (Schoelynck et al., 2010).

Supplementary Table 2 summarizes epidermal patterning and the distribution of silica cells and other associated epidermal cells on the adaxial and abaxial leaf surfaces of grass species under investigation. *S. pumila* revealed one to three axially oriented rows of bilobate phytoliths with each bilobate phytolith flanked by silica cork cell in the coastal region on the adaxial surface of cleared leaf segments (**Figures 2Aa–e**). It also showed the presence of nodular bilobate phytoliths (**Figure 2Aa**). The costal rows of silica cells showed the presence of prickle hairs (**Figure 2Ae**). The intercostal region on adaxial surfaces completely lacked silica cells except for occasional prickle hairs (**Figure 2Af**) with those on the margin having the length of base greater than the barb (**Figure 2Ag**). The abaxial surface of cleared leaf segments of *S. pumila* presented a different scenario. The costal region showed 1–3 bilobate to cross shaped silica cells with each bilobate/cross pair of silica cells separated by silica cork cells (**Figures 2Ah–j**). The intercostal region of the abaxial surface in *S. pumila* showed prickle hairs between each pair of epidermal long cells in alternating axial rows (**Figures 2Ak,l**). The margins on abaxial surfaces showed prickle hairs with a much higher base to barb length ratio than those on the margins of adaxial surfaces.

We have classified bilobate phytolith morphotypes into eight subtypes based upon the length of their shank (the interconnecting segment between two lobes) and the shape of the outer margin of their lobes as proposed by Lu and Liu (2003) (Supplementary Tables 2, 3 and **Figure 2B**). The bilobate shape is highly conserved and has been employed in identification of grass species (Lu and Liu, 2003; Gallego and Distel, 2004; Fahmy, 2008). The costal region on adaxial surface of *S. pumila* showed

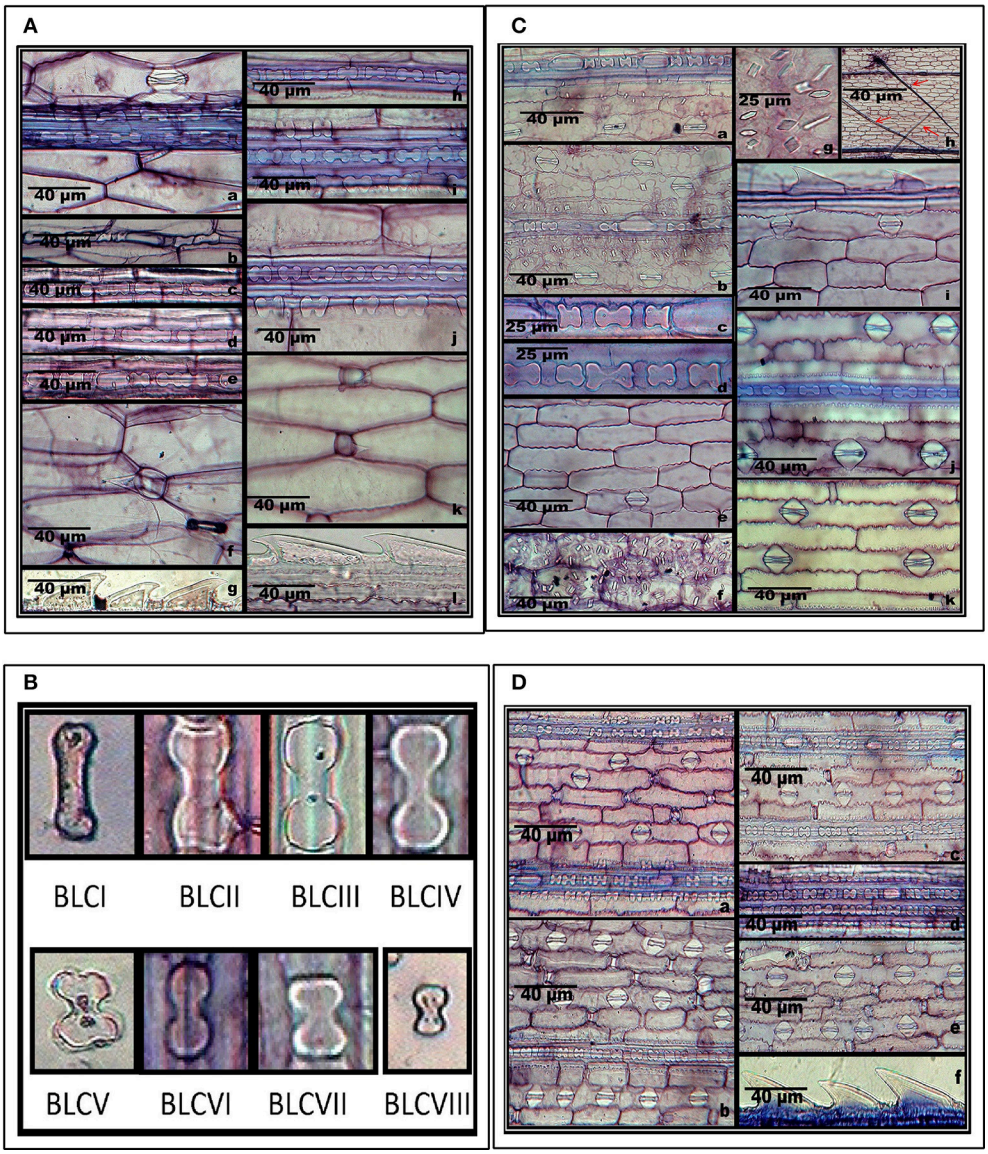

FIGURE 2 | (A) *In-situ* location of phytoliths in leaf epidermis of *Setaria pumila* (Poir.) Roem. & Schult. Adaxial surface **(a–g)** and abaxial surface **(h–l). (B)** Morphological classification of bilobate phytolith morphotypes (data in Supplementary Table 4). **(C)** *In-situ* location of phytoliths in leaf epidermis of *Setaria verticillata* (L.) P. Beauv. Adaxial surface **(a–i)** and abaxial surface **(j–k). (D)** *In-situ* location of phytoliths in leaf epidermis of *Setaria viridis* (L.) P. Beauv. & Schult. Adaxial surface **(a,b)** and abaxial surface **(c–f)**.

three structural variants of the bilobate phytoliths, (III, V, and VI) out of a total eight variants of bilobates recorded from different parts of *Setaria* species (Supplementary Table 3 and **Figure 2B**). The bilobate and nodular bilobate type of phytoliths with each lobate pair separated by silica cork cells have been reported in the costal region of *S. pumila* (Sharma and Kaur, 1983; Ishtiaq et al., 2001; Shaheen et al., 2011). However, these authors did not report structural variations within the bilobates as recorded in the present investigations.

S. verticillata showed an axial row of phytoliths comprising of 3–6 bilobates, a cross and a nodular bilobate flanked by prickle hairs, with each phytolith pair separated by silica cork cells in the costal region (**Figures 2Ca–d**). The costal region on adaxial surfaces of *S. verticillata* had only two structural variants of bilobate phytoliths (VII and IV as compared to three variants in *S. pumila* (Supplementary Table 3). Shaheen et al. (2011) reported bilobates on adaxial surfaces of the costal region of *S. verticillata*. However, this work made no mention of the presence of the nodular bilobate type of phytolith in the costal region on adaxial surfaces. The intercostal regions lacked silica cells and prickle hairs but showed the presence of long hairs (**Figures 2Ce,h**) in contrast to *S. pumila* in which prickle hairs were present and long hairs were completely absent. The presence of cystoliths (calcium oxalate crystals) on the adaxial epidermal surface of *S. verticillata*

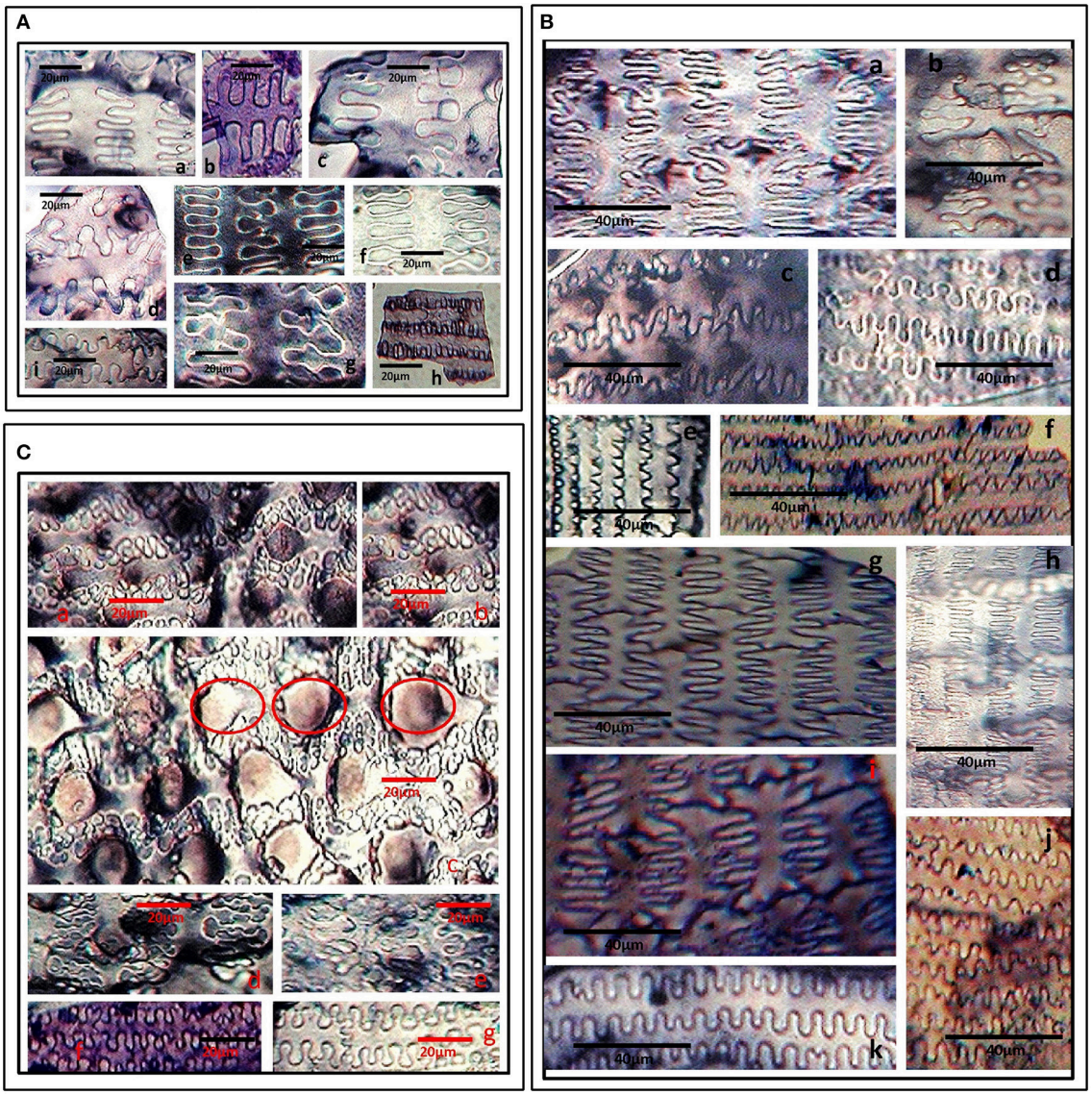

FIGURE 3 | (A) Undulated patterns and ornamentations on the epidermal long cells of *Setaria pumila* (Poir.) Roem. & Schult. synflorescence. Columellate extensions **(a–c)**; η-I type **(d–g)**; granulate **(h)** and n-I type **(i)** type of epidermal undulation patterns. **(B)** Undulated patterns and ornamentations on the epidermal long cells of *Setaria verticillata* (L.) P. Beauv. synflorescence. η-I **(a–c)**; Ω-I **(d)**, Λ-I **(e,f)** Λ-II **(g,h)**, Λ-III **(i)** and n-I **(j),** and n-II **(k)** type of epidermal undulation patterns. **(C)** Undulated patterns and ornamentations on the epidermal long cells of *Setaria viridis* (L.) P. Beauv. synflorescence. Ω-I **(a,b,g)**, Ω –II with papillate structures (encircled) **(c–e)** and granulate epidermal extensions **(f)**.

leaf as quadrihedrons and hexahedrons has emerged as the most important diagnostic feature of the species. The cystoliths showed greater concentration in costal rather than the intercostal regions (**Figures 2Cf,g**). Even though cystoliths have been reported from leaf epidermis in several other grass species (Benecke, 1903; Sato, 1968; Dayanandan et al., 1977; Sato and Shibata, 1981; Lerseten, 1983; Prasad et al., 2005), the present study is the first report of cystoliths for the genus *Setaria*. The abaxial surface in the costal regions showed a single axial row of bilobate and nodular bilobate types of phytoliths (**Figure 2Cj**). The bilobate class revealed two structural variants (III and IV). The intercostal region showed 1–2 stomatal files of high domed stomata (**Figure 2Ck**). The margins on abaxial surface showed the presence of prickle hairs with base lengths greater than the barb (**Figure 2Ci**).

S. viridis showed, on the adaxial surfaces 1-4 axial rows of bilobate and nodular bilobate type of phytoliths in the costal region with each phytolith pair flanked by silica cork cells (**Figures 2Da,b**). Three variants of bilobate phytoliths were present in *S. viridis* (II, IV, and V). These phytoliths are flanked by a pair of prickle hairs in the costal region. The intercostal region showed prickle hairs between each epidermal long cell pair. In contrast to *S. pumila* and *S. verticillata*, the intercostal regions of *S. viridis* occasionally showed a single row of phytoliths.

S. viridis abaxial leaf surface had 1–3 rows of bilobate phytoliths with occasional nodular bilobate types in the costal region (**Figures 2Dc,d**). The bilobate class included two structural variants (V and VI). The species had small one celled prickle hairs in the intercostal regions in addition to prickle hairs with bases smaller than the barb on the leaf margins (**Figures 2De,f**).

Epidermal Ornamentation and Undulation Patterns

The ornamentation and undulation patterns of epidermal long cells of synfloresence bracts have been put into three categories *viz.,* Ω-undulated, η-undulated, and n-undulated ornamentations (Lu et al., 2009). We propose another undulated ornamentation which can be represented by the symbol 'Λ' (Greek-Lamda) and further categorize it into three subtypes: Λ-I, Λ- II, and Λ- III. The Λ-type of undulations were classified on the width of the base and the length of the lateral extensions. If the width of the base and its length was nearly equal, it was put as Λ-I type and if the length was three times the base of lateral extensions, it was recognized as Λ-II type. Similarly, if the length of the lateral extension is more than thrice the width of the base of the extension, it was put as Λ-III. The Ω and η-undulated ornamentations are generally present on the lemmas and palea and have been further put into subtypes based on the degree of undulations as Ω-I, Ω -II & Ω-III and η-I, η-II, η-III respectively (Lu et al., 2009). n-undulated ornamentations were reported on the margins of lemmas and paleas (Zhang et al., 2011).

S. pumila showed columellate extensions of epidermal cells (**Figures 3Aa–c**) whereas they were absent in the other two species. In addition to columellate extensions, *S. pumila* showed the presence of η-I (**Figures 3Ad–g**), granulate (**Figures 3Ah**), and n-I (**Figures 3Ai**) type of undulated ornamentations. These types of ornamentations have been reported in some other species of *Setaria* including *S. italica*, (Lu et al., 2009; Zhang et al., 2011). In our sample, *S. verticillata* showed the presence of η-I (**Figures 3Ba–c**) Ω-I (**Figures 3Bd**), Λ-I (**Figures 3Be,f**) Λ –II (**Figures 3Bg,h**), Λ –III (**Figure 3Bi**) and n-I (**Figure 3Bj**) and n-II (**Figure 3Bk**). *S. viridis* showed Ω-I (**Figures 3C a,b,g**), Ω –II (**Figures 3Cc–e**) and granulate (**Figures 3Cf,g**). The epidermal elements also showed the presence of papillae on the surface of lemmas. Kealhofer et al. (2015) also reported the similar (Ω –II) type of epidermal undulated ornamentations in *S. viridis*.

Phytolith Morphotypes

In the present study, a cumulative total of 58 phytolith morphotypes were identified with an individual distribution of 38 in *S. pumila*, 39 in *S. verticillata,* and 41 in *S. viridis*. These morphotypes were grouped into nine broad categories namely, bulliform cells, epidermal elements, hairs, long cells, short cells, tabular types, globular types, blocky types, and tracheids (**Table 1** and **Figures 4–6**, **7A–C**). The first seven categories are known to have their origin in the epidermis, blocky types in the endodermis and the last one in the vascular tissue system (Twiss et al., 1969; Lu and Liu, 2003).

Except for the blocky and globular types, phytolith morphotypes have been well reported in family Poaceae (Twiss et al., 1969; Bonnett, 1972; Prychid et al., 2004). Both

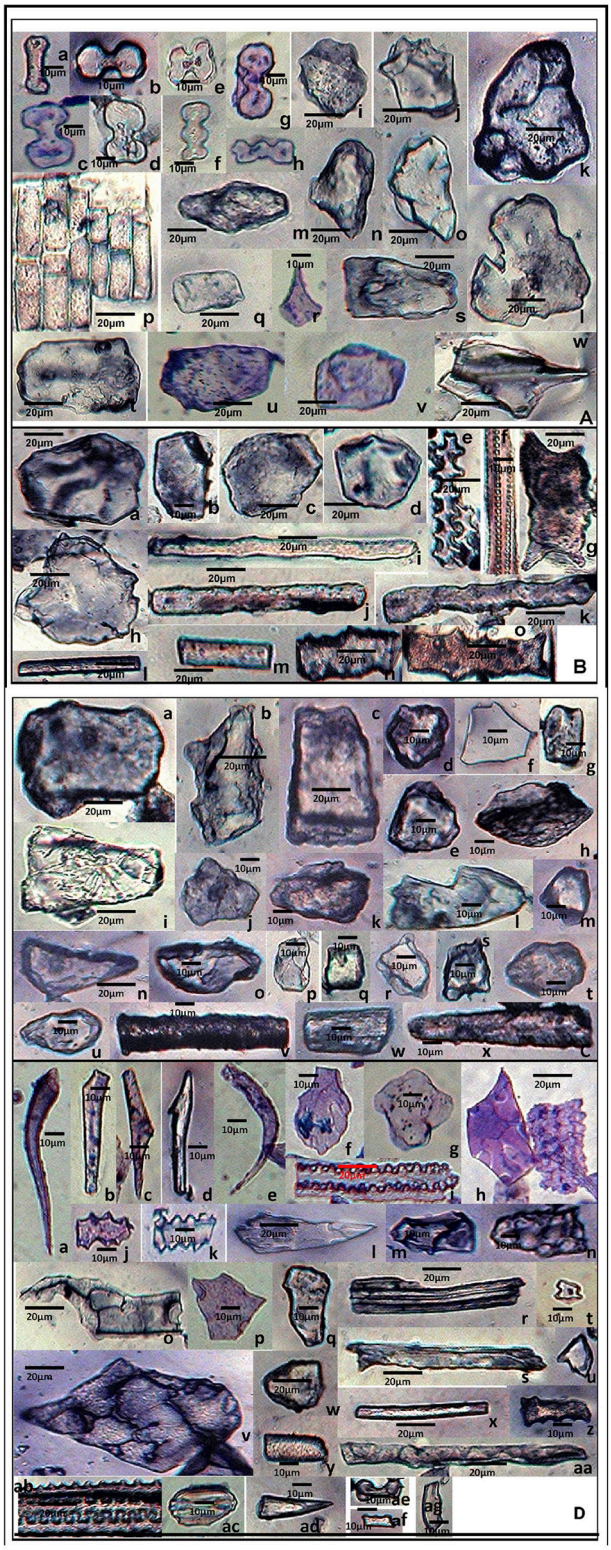

FIGURE 4 | Phytolith morphotypes from various parts of *Setaria pumila* (Poir.) Roem. & Schult. **(A)** (Root): Bilobate class I **(a)**; Bilobate class VI **(b,c)**; Bilobate class V **(d,e)**; Polylobate **(f)**; Nodular bilobate **(g,h)**; Globular

(Continued)

FIGURE 4 | polyhedral **(i,j)**, Blocky irregular **(k,l)**; Oblong **(m)**; Trapezoid **(n,o)**; Rectangular **(p,q)**; Cuneiform bulliform **(r)**; Tabular irregular **(s–v)**; Scutiform **(w)**. **(B)** (Culm): Blocky polyhedral **(a,b)**; Trapezoid **(c)**; Globular polyhedral **(d)**; Echinate elongate **(e,f)**; Sinuate elongate with concave ends **(g)**; Tabular irregular **(h)**; Sinuate elongate **(i–k)**; Smooth elongate **(l,m)**; Elongate irregular **(n,o)**. **(C)** (Leaf): Tabular simple **(a)**; Blocky irregular **(b)**; Rectangular **(c)**; Globular granulate **(d,e)**; Blocky polyhedral **(f)**; Parrellepedal bulliform cells **(g)**; Trapezoid **(h–l)**; Globular polyhedral **(m)**; Clavate **(n,o)**; Cuboid **(p,q)**; Scutiform **(r,s)**; Ovate **(t,u)**; Cylindrical **(v,w)**; Smooth elongate **(x)**. **(D)** (synflorescence): Macrohairs **(a–e)**; Cuneiform bulliform **(f)**; Globular polyhedral **(g)**; Epidermal elements **(h)**; Echinate elongate **(i–k)**; Clavate **(i)**; Trapezoid **(m,n)**, Tracheid **(o)**, Blocky polyhedral **(p,q)**; Elongate irregular **(r,s)**; Horned tower **(t,u)**; Blocky irregular **(v)**; Globular granulate **(w)**; Smooth elongate **(x,y)**; Facetate elongate **(z)**; Sinuate elongate **(aa)**; Columellate elongate **(ab)**; Stomata **(ac)**; Prickle hair **(ad)**; Bilobate class I **(ae)**; Plates **(af,ag)**.

blocky and globular (spherical) morphotypes are considered to be characteristic of forest trees (Runge, 1999). Even within monocots, spinulose to tabular spheres are typically associated with the arborescent (palm) family, Arecaceae (Kealhofer and Piperno, 1998) wherein these types are produced in great abundance (Albert et al., 2007). While the blocky morphotype has been reported in some grasses (Wang and Lu, 1993; Carnelli et al., 2004), we have not come across any report of the globular type in the family. However, in view of the reports of the globular type from the commelinid families, Zingiberaceae, Marantaceae, and Strelitziaceae (Tomlinson, 1956, 1961; Kealhofer and Piperno, 1998; Brilhante de Albuquerque et al., 2013) and the non-commelinid family Orchidaceae (Sandoval-Zapotitla et al., 2010), the recovery of the globular morphotype in Poaceae during the present studies was not entirely unexpected.

The present study marks a significant addition to information on phytolith profiles particularly from underground (root) parts of three species of genus *Setaria*. Most of the previous studies in grasses have documented phytoliths from above ground parts, mainly the leaf (Tomlinson, 1969; Twiss et al., 1969; Bonnett, 1972; Krishnan et al., 2000; Lu and Liu, 2003; Prychid et al., 2004; Fahmy, 2008; Barboni and Bremond, 2009; Rudall et al., 2014; Shakoor et al., 2014; Jattisha and Sabu, 2015). Only a limited number of reports are available on phytolith analysis of roots of plant species (Ezell-Chandler et al., 2006; Das et al., 2014; Soukup et al., 2014; Shakoor et al., 2016).

A comparison among the three congeneric species of *Setaria* revealed that some of the phytolith morphotypes were shared by all the three species while some others were restricted to only one or two of the three species in the present study (**Table 1**). At one extreme were some morphotypes which had a ubiquity value of unity, i.e. they occur in at least one plant part in all the three species. For example, bilobate class V, blocky irregular and blocky polyhedral were present at least in one plant part in all the three species and hence carried a ubiquity value of unity (**Table 1**). Such morphotypes have the lowest diagnostic value. Similarly, phytolith morphotypes with a ubiquity value of 0.66 indicates their presence in two out of the three species. These types could be utilized for taxonomic diagnosis and demarcation of pairs of species in the present sample from the one lacking these morphotypes (**Table 1**). For example, bilobate class III,

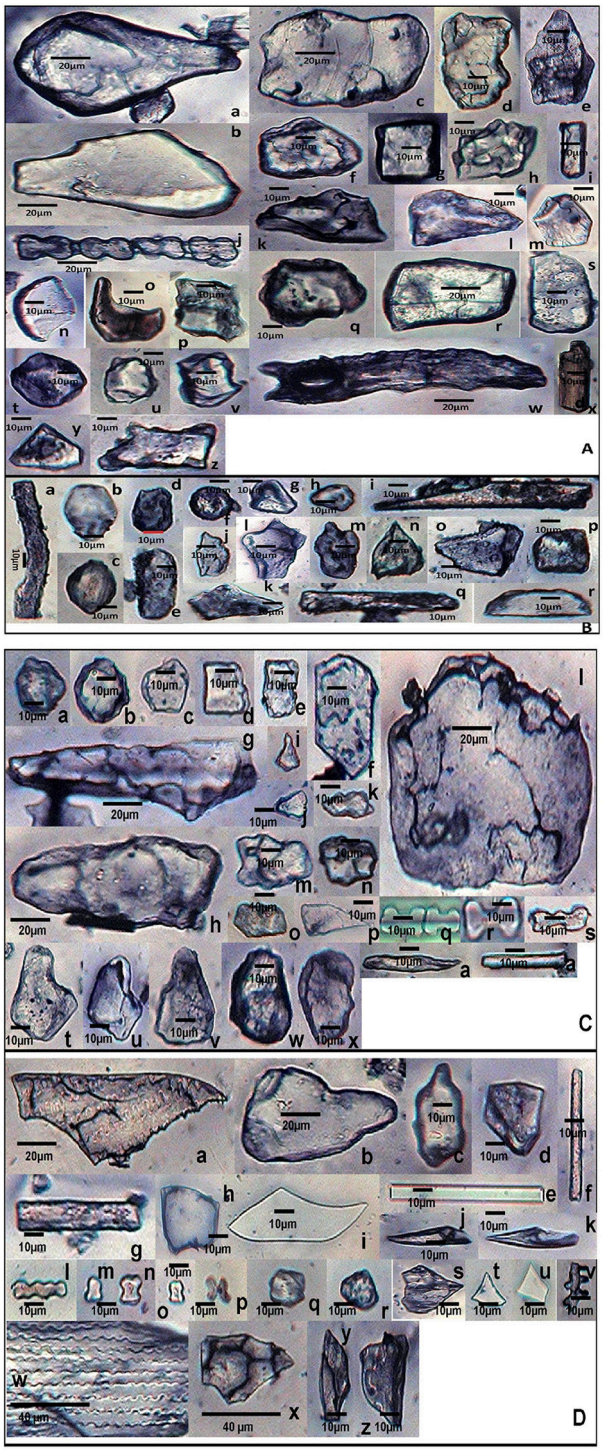

FIGURE 5 | Phytolith morphotypes from various parts of *Setaria verticillata* (L.) P.Beauv. **(A)** (Root): Cuneiform bulliform **(a,b)**; Tabular simple **(c)**; Blocky irregular **(d–f)**; Cuboid **(g)**; Globular echinate **(h)**; Smooth elongate **(i)**; Bilobate class VII **(j)**; Blocky polyhedral **(k–m)**; Crescent moon **(n,o)**; Parrellepedal bulliform cells **(p,q)**; Rectangular **(r,s)**; Globular polyhedral **(t–v)**; Elongate with concave ends **(w)**; Cylindrical **(x)**; Triangular **(y)**; Trapezoid **(z)**. **(B)** (Culm): Sinuate elongate **(a)**; Ovate **(b,c)**; Blocky crenate **(d,e)**; Globular psilate **(f)**; *(Continued)*

FIGURE 5 | Trapezoid **(g,h)**; Clavate **(i)**; Scutiform **(j,k)**; Blocky irregular **(l–n)**; Blocky polyhedral **(o)**; Cuboid **(p)**; Smooth elongate **(q)**; Half-moon **(r)**. **(C)** (Leaf): Globular granulate **(a,b)**; Globular polyhedral **(c)**; Rectangular **(d,e)**; Blocky polyhedral **(f)**; Elongate irregular **(g,h)**; Horned tower **(i–k)**; Tabular irregular **(l)**; Trapezoid **(m–o)**; Scutiform **(p)**; Bilobate class IV **(q)**; Bilobate class VII **(r)**; Nodular bilobate **(s)**; Cuneiform bulliform **(t–v)**; Blocky irregular **(w,x)**. **(D)** (Synflorescence): Epidermal element with columellate extensions **(a)**; Cuneiform bulliform **(b,c)**; Blocky polyhedral **(d)** Smooth elongate **(e,f)**; Rectangular **(g)**; Cuboid **(h)**; Clavate **(i)**; Acicular **(j,k)**; Polylobate irregular **(l)**; Rondel **(m–o)**; Cross **(p)**; Globular polyhedral **(q,r)**; Scutiform **(s–u)**; Columellate elongate **(v)**; Echinate elongate **(w)**; Trapezoid **(x–z)**.

columellate elongate, cross, horned tower, oblong and tabular simple demarcate *S. pumila* and *S. verticillata* from *S. viridis* in the present sample. Similar is the case with other morphotypes with ubiquity value of 0.66 between other pairs of species within the three congenerics (**Table 1**).

Phytolith morphotypes with ubiquity value of 0.33 indicates their presence in only one of the three studied species. Within the limited context of the present work, these phytoliths marked the individual species from the other two and helped in their taxonomic demarcation. For example, bilobate class I (**Figures 4Aa**,**Da,e**) from roots and synflorescences, polylobate (**Figure 4Af**) from roots, sinuate elongate with concave ends (**Figure 4Bg**) from culms, stomatas (**Figures 4Dac**) facetate elongate (**Figure 4Dz**), and tracheids (**Figure 4Do**) from synflorescences have ubiquity values of 0.33 and diagnose *S. pumila* from the other pair of species (**Table 1**). The "marker" phytolith morphotypes yielded by various parts of *S. verticillata* included blocky crenate (**Figures 5Bd,e**) from culms, crescent moon (**Figures 5An,o**) and elongate with concave ends (**Figure 5Aw**) from roots, half-moon (**Figure 5Br**), epidermal element with columellate extensions (**Figure 5Da**) and polylobate irregular (**Figure 5Dl**) from the synflorescences (**Table 1**). Similarly, the "marker" morphotypes from *S. viridis* included bilobate class II (**Figures 6D-h-j**), epidermal element with short silica cells and stomata, epidermal papillate, and prickly elongate (**Figures 7Cw,y,ad,ac**) from synflorescences, bilobate class VIII (**Figure 6Bv**) from culms, tabular polyhedral from the culms and leaves (**Figures 6Ce, 7Cl**) and carinate (**Figures 6Bt,u, 7Cx**) from the culms and the synflorescences (**Table 1**). What adds to the diagnostic significance of these morphotypes is that these were recovered from all the plant parts ranging from roots to synflorescences. Hence, the present study reiterates the necessity and significance of analysis of phytoliths from all the underground and aerial plant parts before utilizing them for taxonomic diagnosis as suggested in some earlier studies as well (Kealhofer et al., 2015; Shakoor et al., 2016). Here, it may be emphasized that these morphotypes "mark" the individual species only from the other two in the present study. An unqualified use of the term marker phytolith for the types recovered from species in the present sample would be an overstatement implying that these types diagnose these species individually from rest of the species of the foxtail grass genus *Setaria*. The full potential of phytolith types for interspecific diagnosis can only be realized after phytolith analysis of the entire

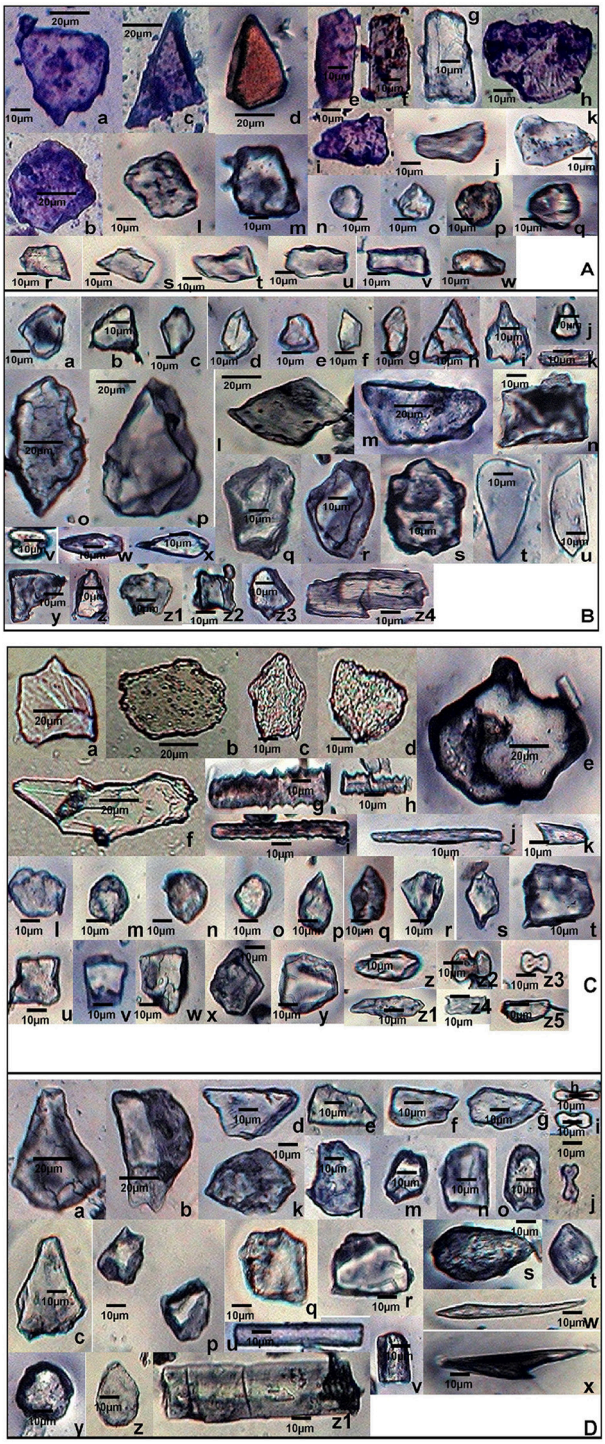

FIGURE 6 | Phytolith morphotypes from various parts of *Setaria viridis* (L.) P. Beauv. **(A)** (Root): Blocky polyhedral **(a,b)**; Triangular **(c,d)**; Rectangular **(e–g)**; Blocky irregular **(h)**; Trapezoid **(i–k)**; cuboid **(l,m)**; Globular psilate **(n)**; Globular granulate **(o–q)**; Scutiform **(r,s)**; Parrellepedal bulliform cells **(t–v)**; Oblong **(w)**. **(B)** (Culm): Globular polyhedral **(a–e)**; plates **(f,g)**; Triangular **(h)**; Cuneiform bulliform **(i)**; Rondel **(j)**; Smooth elongate **(k)**; Rectangular **(l–n)**; Blocky irregular **(o,p)**; Blocky polyhedral **(q,r)**; Globular echinate **(s)**; Carinate **(t,u)**; *(Continued)*

FIGURE 6 | Bilobate class VIII **(v)**; Clavate **(w,x)**; Trapezoid **(y–z1)**; Cuboid **(z2, z3)**; Elongate irregular **(z4)**. **(C)** (Leaf): Blocky irregular **(a–d)**; Tabular polyhedral **(e)**; Clavate **(f)**; Echinate elongate **(g,h)**; Sinuate elongate **(i)**; Smooth elongate **(j)**; Pickle hair **(k)**; Globular granulate **(l–o)**; Scutiform **(p–s)**; Cuboid **(t–v)**; Trapezoid **(w–y)**; Ovate **(z,z1)**; Bilobates class VII **(z2)** Bilobates class VIII **(z3)**; Plates **(z4,z5)**. **(D)** (Synflorescence): Cuneiform bulliform **(a–c)**; Blocky polyhedral **(d–g)**; Bilobate class II **(h–j)**; Blocky irregular **(k,l)**; Parrellepedal bulliform cells **(m–o)**; Globular polyhedral **(p–r)**; Ovate **(s,t)**; Smooth elongate **(u,v)**; Acicular **(w)**; Prickle hair **(x)**; Globular psilate **(y,z)**; Cylindrical **(z1)**.

genus. Similarly, "marker" types for the genus and suprageneric levels can only be identified by profiling all the taxa included in these ranks.

SEM of phytoliths of the three congenerics of *Setaria* revealed subtle differences in topography of phytolith morphotypes which was not clear in light microscopy (**Figures 7A–C**). SEM has helped to distinguish and segregate particular phytolith morphotypes into sub-types. For example, the globular morphotype was further resolved into globular crenate (**Figure 7Cr**) globular granulate (**Figures 7Aa,d,Bi**), globular echinate (**Figures 7Al,Co,p**), globular polyhedral (**Figures 7Aq,r,Bh,Ca,h,z**), and globular psilate (**Figures 7Be,Ck**) morphotypes based on the type and degree of surface ornamentations. Similarly, the tabular morphotype was segregated into tabular polyhedral (**Figure 7Cl**), tabular irregular (**Figure 7Cq**) and tabular polyhedral (**Figure 7Ct**). Earlier studies grouped all broad and multisided structures into trapezoid category (Piperno, 1988, 2001; Pearsall, 2000). But recent studies have distinguished two more categories within the trapezoid morphotype *viz.,* blocky polyhedral and blocky irregular morphotypes (Traoré et al., 2014). We have also recognized blocky irregular (**Figures 7Ab,o,Bj,r,Cb**) and blocky polyhedral (**Figures 7Af,k,Ba,b,Cc,d,n,ab**) morphotypes. Additionally, SEM has revealed the interlocking patterns between epidermal elements (**Figures 7Cv,w,y**). It has also revealed the presence of silica short cells embedded with the epidermal elements (**Figure 7Cw**).Thus, SEM has been employed as an effective tool in elucidation of ultrastructural features of phytolith morphotypes and their classification into subtypes that have further helped in demarcation of the grass species under reference.

The coefficient of association of phytolith morphotypes based on Pearson's association revealed highest association among overground parts (Supplementary Table 4). The strongest association was found among the leaf and synflorescence of *S. pumila* and *S. viridis* whereas *S. verticillata* showed significantly lower values of association (Supplementary Table 4). The highest values of coefficient of association between leaf and synflorescence could be attributed to the anatomical similarities of leaf and synflorescence bracts that produce phytoliths. Similarly, insignificant association between the underground and overground parts could be explained by the anatomical, histological and physiological differences among these plant parts and hence the phytolith morphotypes produced by them.

Clustering of species on the presence/ absence data of bilobate classes, using Jaccard's similarity index was carried out. *S. pumila* belongs to one clade of *Setaria* whereas the other two species belong to the other clade (Doust and Kellogg, 2002). A similar trend was observed in clusters from the totality of morphotypes (**Figure 8**). *S. pumila* stood apart from the other two species as it has 33% similarity of phytolith profile with *S. verticillata* and 28.57% with *S. viridis*. However, *S. verticillata* and *S. viridis* showed 42.85% similarity and were grouped together (**Figure 8**).

Frequency Distributions and Morphometric Measurements

Several studies in the past have utilized data on morphotypes for taxonomic characterization and identification of plant species (Twiss et al., 1969; Lau et al., 1978; Hodson and Sangster, 1988; Ollendorf et al., 1988; Whang et al., 1998; Krishnan et al., 2000; Ponzi and Pizzolongo, 2003; Piperno, 2006). However, recent studies have enlarged the scope of phytolith research by including data on morphometric measurements and frequency distributions of phytolith morphotypes for taxonomic demarcation of species down the taxonomic hierarchy from family, genus, and species levels (Strömberg, 2009; Jattisha and Sabu, 2012; Tripathi et al., 2013; Szabo et al., 2014; Shakoor et al., 2016; Ball et al., 2017; Out and Madella, 2017).

Setaria spp. showed considerable differences in the frequency distribution of various phytolith morphotypes (**Figure 9**). The most frequent in all the three species were the trapezoids. However, they differ significantly within and between the species with 19.47% frequency in *S. pumila*, 14.38% in *S. verticillata* and 7.91% in *S. viridis* ($p \leq 0.05$; χ^2-test). Acicular morphotypes present in both *S. verticillata* and *S. viridis* differed many fold in terms of their percentage frequency with 15.17% in the former and 2.18% in the later species. Bilobate classes also differ significantly with respect to frequency distributions. For example, bilobate class III were present in the leaves of *S. pumila* and *S. verticillata* with highly variable percentage frequency values of 9.44% and 3.10% respectively ($p \leq 0.05$; χ^2-test). Similarly, bilobate class IV occurred in the leaves of *S. verticillata* and *S. viridis* with a percentage frequency of 8.10 and 4.39% respectively ($p \leq 0.05$; χ^2-test). Similarly, other phytolith morphotypes revealed significant differences in percentage frequency providing a definite clue that frequency of occurrence of phytolith morphotypes provides an additional evidence for taxonomic characterization apart from qualitative differences in phytolith types (**Figure 9**).

Apart from frequency distributions, morphometric data on size dimensions and shape descriptors of morphotypes also revealed significant differences between the species (Supplementary Tables 5A–C). In the present analysis, we included data on size parameters (length, width, area and perimeter) and one shape descriptor, the aspect ratio. Further, length and width of the shank of bilobate types have been employed as additional characteristics to classify the bilobates into various subtypes in order to further supplement taxonomic diagnosis of species (Supplementary Table 3). The use of multivariate statistical approaches like principal component

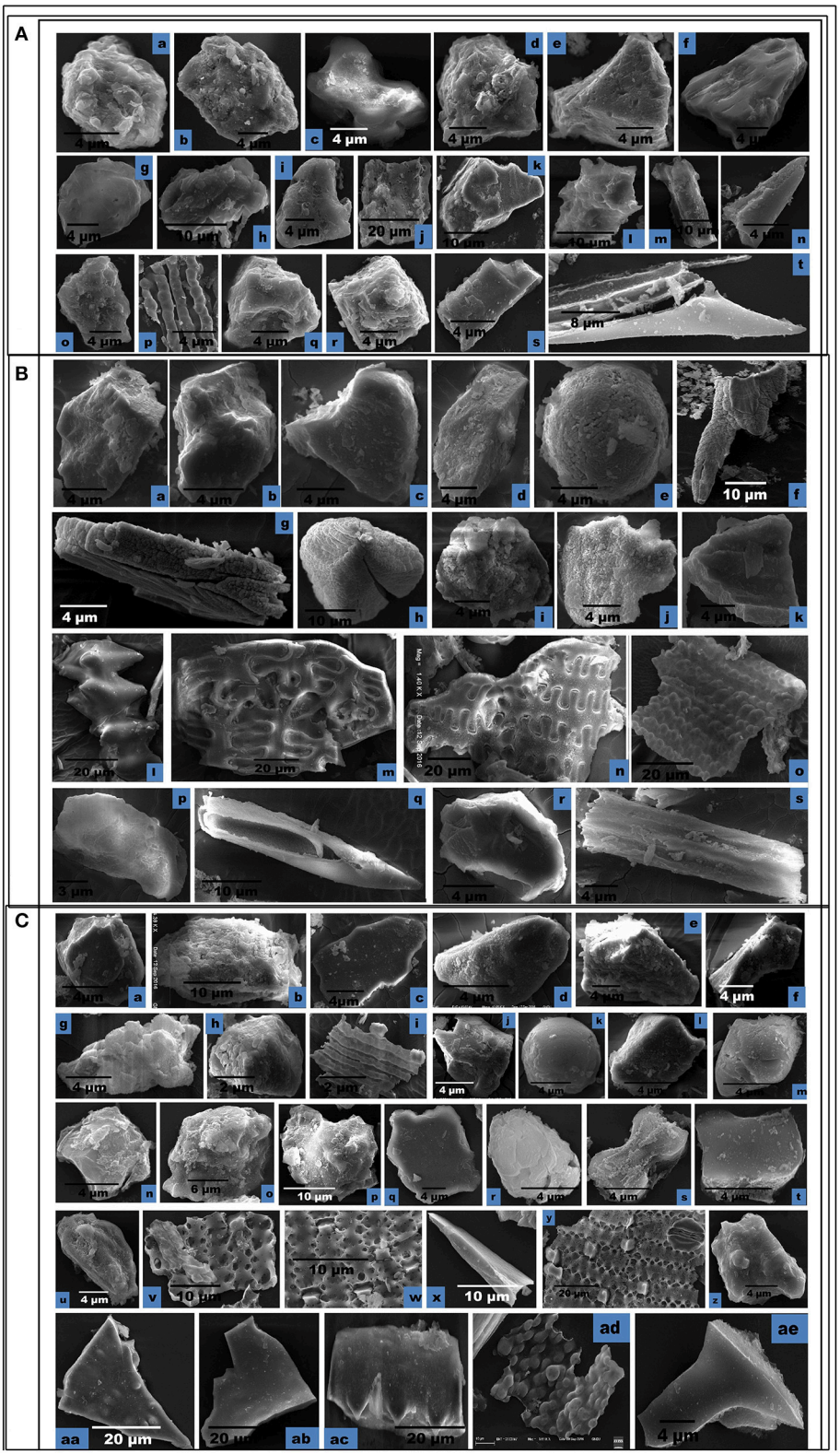

FIGURE 7 | Scanning Electron Micrographs (SEM) of phytolith morphotypes from various parts of: **(A)** *Setaria pumila* (Poir.) Roem. & Schult. Root: Globular granulate **(a)** Blocky irregular **(b)**; Bilobate class V **(c)**. Culm: Globular granulate **(d)** Cuneiform bulliform **(e)**. Blocky polyhedral **(f)**; Trapezoid **(g)**; Leaf: Trapezoid **(h,i)**;

(Continued)

FIGURE 7 | Blocky irregular **(j)**; Blocky polyhedral **(k)**; Globular echinate **(l)**; Elonagate irregular **(m)**. Synflorescence: Prickle hair **(n)**; Blocky irregular **(o)**; Epidermal element with undulated ridges **(p)**; Globular polyhedral **(q,r)**; Trapezoid **(s)**; Prickle hair **(t)**. **(B)** *Setaria verticillata* (L.) P.Beauv. Root: Blocky polyhedral **(a,b)**; Cuneiform bulliform **(c)**; Trapezoid **(d)**; Globular psilate **(e)**. Culm: Scutiform **(f)**; Elongate irregular **(g)**. Leaf: Globular polyhedral **(h)**; Globular granulate **(i)**; Blocky irregular **(j)**; Blocky polyhedral **(k)**. Synflorescence: Echinate elongate **(l)**; Crenate elongate **(m)**; Columellate elongate **(n)**; Blocky papillate **(o)**; Trapezoid **(p)**; Acicular **(q)**; Blocky irregular **(r)**; Rugose elongate **(s)**. **(C)** *Setaria viridis* (L.) P. Beauv. Root: Globular polyhedral **(a)**; Blocky irregular **(b)**; Blocky polyhedral **(c,d)**; Trapezoid **(e,f)**. Culm**:** Trapezoid **(g)**. Globular polyhedral **(h)**; Epidermal element with undulated ridge (i); Blocky irregular **(j)**; Globular psilate **(k)**; Tabular polyhedral **(l)**. Leaf: Trapezoid **(m)**; Blocky polyhedral **(n)**; Globular echinate **(o,p)**; Tabular irregular **(q)**; Globular crenate **(r)**; Bilobate class V **(s)**; Tabular polyhedral **(t)**. Synflorescence: Trapezoid **(u)**; Epidermal element **(v)**; Epidermal element with silica short cells & stomata **(w,y)**; Carinate **(x)**; Globular polyhedral **(z)**; Triangular **(aa)**; Blocky polyhedral **(ab)**; Prickly elongate **(ac)**; Epidermal papillate **(ad)**; Scutiform **(ae)**.

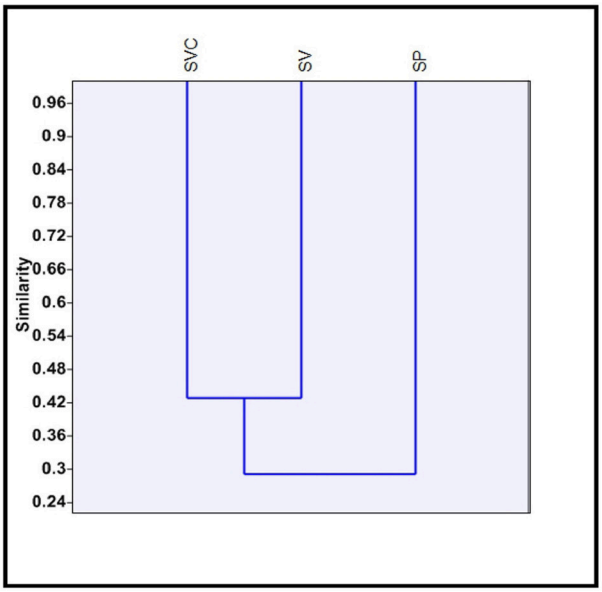

FIGURE 8 | Clustering of three species of *Setaria* P. Beauv. based on presence/absence data of bilobate phytolith morphotypes. [SP, *Setaria pumila* (Poir.) Roem. & Schult.; SVC, *Setaria verticillata* (L.) P. Beauv.; SV, *Setaria viridis* (L.) P. Beauv.].

analysis has been recommended and employed in earlier studies for taxonomic demarcation of species (Benvenuto et al., 2015; Pearsall, 2015; Ball et al., 2016).

Joint PCA analysis of morphometric parameters of phytoliths from different parts of the three species led to overcrowding of the data and did not help in diagnosis of species. However, PCA analysis of morphometric parameters of phytoliths from different parts individually proved useful in taxonomic demarcation of the species. PCA analysis of root phytoliths clearly separated the three species on the basis of surface areas of different morphotypes (Supplementary Figures 1a,b). *S. pumila* was demarcated on the basis of surface areas of blocky irregular and tabular irregular, *S. verticillata* by blocky polyhedral and *S. viridis* by area of trapezoid morphotypes as revealed by PCA results of component 1 and 2 (Supplementary Figure 1a). However, the PCA plot between component 1 and 3 revealed more clear demarcation than obtained from components 1 and 2 (Supplementary Figures 1b). PCA analysis of phytolith morphotypes of culm of the three species brought about the taxonomic demarcation of species on the basis of the area of smooth elongates for *S. verticillata*, and tabular irregular for *S. pumila* (Supplementary Figure 2). Similarly, PCA analysis of leaf and synflorescence phytolith morphotypes of the three species lent further support to taxonomic analysis of the three species of *Setaria* (Supplementary Figures 3, 4).

Transmission Electron Microscopy

TEM allows visualization and microstructural examination through a combination of high magnification and resolution. It helped to distinguish various physical states including amorphous from the crystalline and helped to study their atomic planes, (columns of atoms in crystals). TEM images of phytolith morphotypes from leaves and synflorescences of *S. pumila* and *S. verticillata* showed macroscopic clusters and agglomerates of silica that were not distinguished into particles at nanoscale regime (**Figures 10Aa–d,Ba–d,Ca–c,Da,b**). However, phytoliths from leaves and synflorescences of *S. viridis* revealed silica particles of spherical and cubic morphologies of nanoscale regime and were clustered (**Figures 10Ea,b,Fa,b**). The presence of spherical and cubic nanoparticle clusters in the latter species clearly demarcates it from the other two congenerics. Gonzalez-Espindola et al. (2014) reported clusters and agglomerates of phytoliths as well as spherical particles of nanoscale regime from the leaves of the grass species *Stenotaphrum secundatum*. Palanivelu et al. (2014) reported agglomerated particles of silica nanoparticles from rice hulls collected from different geographical locations.

High resolution transmission electron microscopy (HRTEM) revealed the presence of ordered interplanar atomic layers of Si–O, Si–O–Si bonds in all the species except in the leaf phytoliths of *S. verticillata* (**Figures 10Ae,Be,Dc,Ec,Fc**), which did not possess regular ordering of local clusters of Si–O and the silica bodies were completely amorphous (**Figures 10Bd,e**). HRTEM analysis of phytoliths from leaves of *S. pumila* and *S. viridis* revealed microcrystalline structures with an interplanar distance (d-spacing) of 0.1 nm which was indicative of the presence of tetragonal cristobalite polymorph of silica (**Figures 10Ae,Fc**). Similarly, silica from the synflorescences of all the three species revealed microcrystalline structures with a difference of interplanar distance which was 0.08 nm for *S. pumila* and *S. viridis* and 0.083 nm for *S. verticillata*. These distances correspond to tetragonal stishovite polymorphs (**Figures 10Be,Dc,Fc**) whose formation was favored by the presence of localized crystallization centers such as extraneous cations dispersed throughout

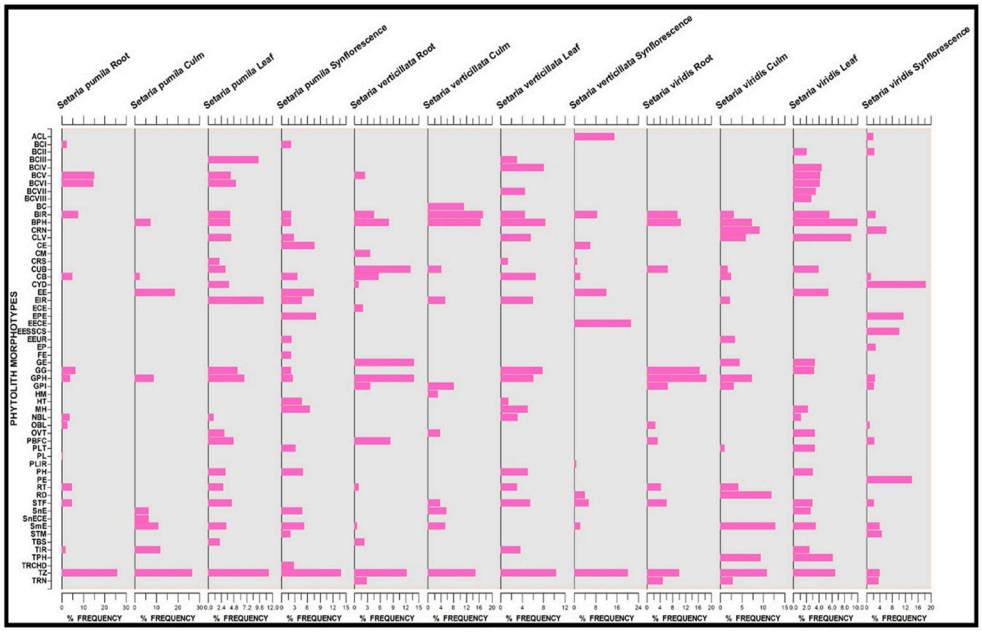

FIGURE 9 | Stratigraphic diagram showing percentage frequency of different phytolith morphotypes. (Description of phytolith morphotypes from **Table 1**).

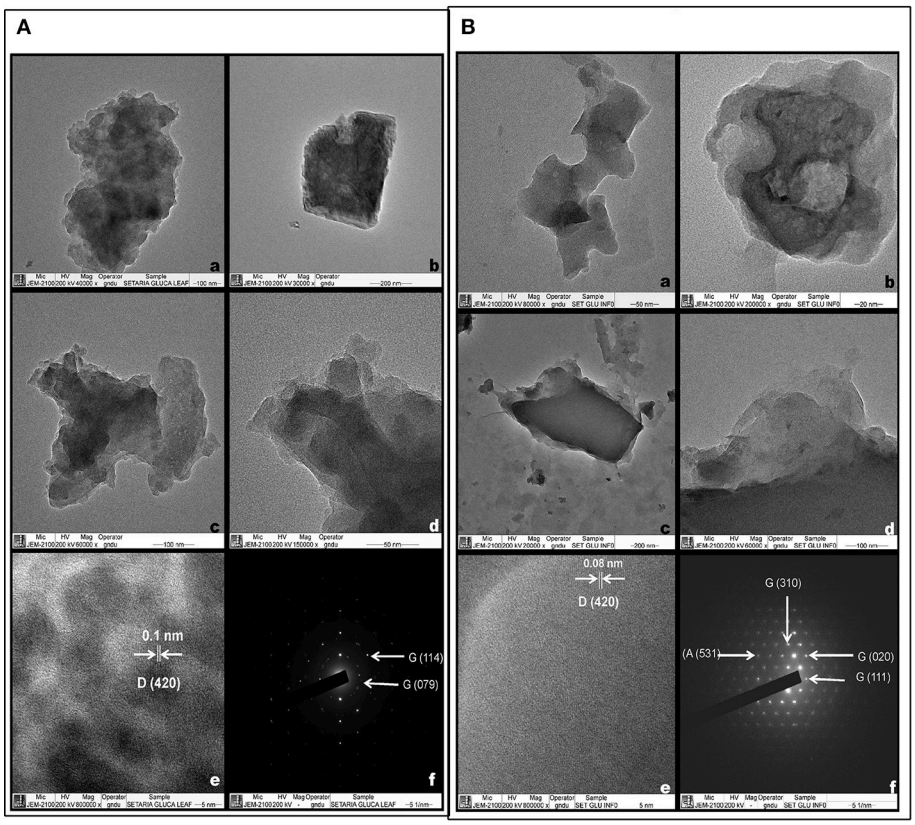

FIGURE 10 | Continued.

the siliceous phytoliths (Mann and Perry, 1986). The link got substantiated and explained by the presence of cations like Al^{2+}, Ba^{2+}, Fe^{2+},Ca^{2+},Cu^{2+}, Mg^{2+}, Na^{+}, and K^{+} as revealed by SEM-EDX analysis of phytoliths (Supplementary Table 6).

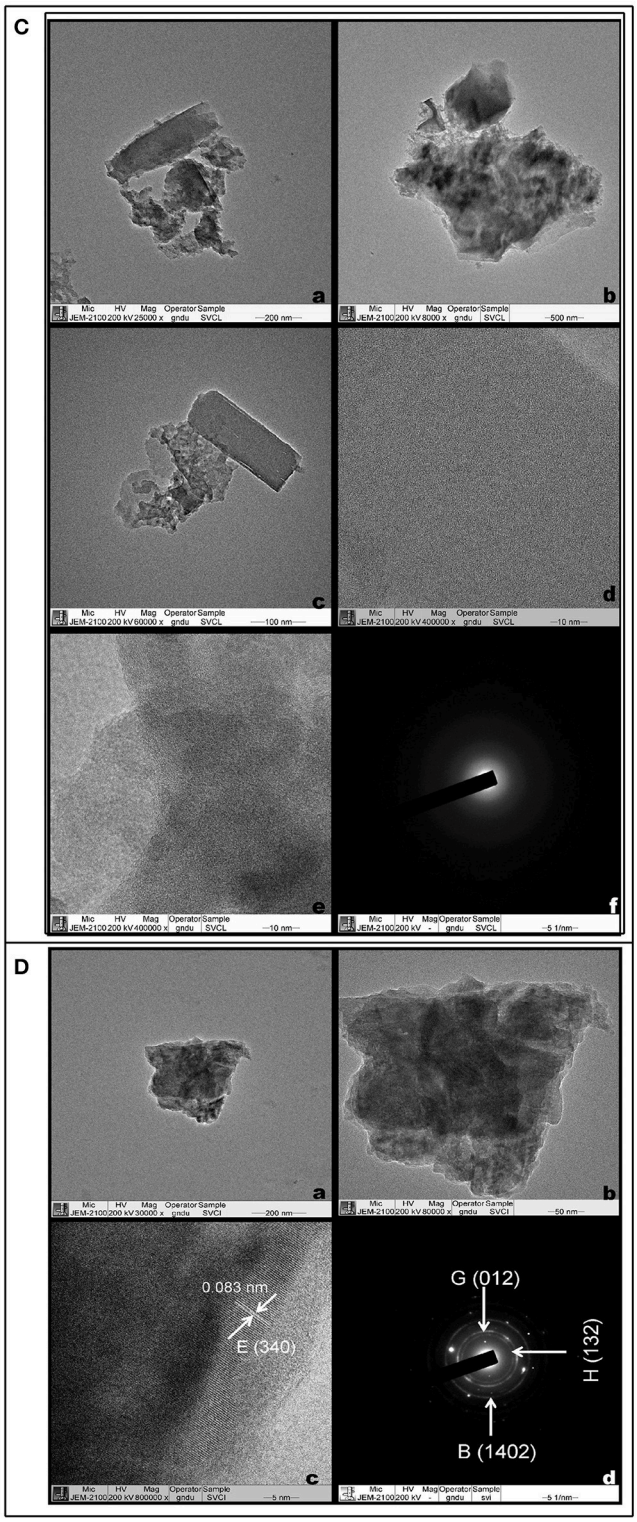

FIGURE 10 | Continued.

Selected area electron diffraction (SAED) reveals the chemical composition of different mineral phases by their different patterns generated by the impact of X-rays and fast moving electrons. Phytoliths from the leaves of *S. pumila* and *S. viridis* revealed well defined single crystalline lattices that could be resolved to hexagonal and orthorhombic lattices of SiO_2. (**Figures 10Af,Ed**) that were continuous and unbroken in the former but lacked grain boundaries in the latter (cf. Reid et al., 2011). The amorphous structure of phytoliths was revealed by an absence of SAED patterns (**Figure 10C**). Similarly, phytoliths from synflorescences of *S. pumila* revealed single crystal lattices corresponding to SiO_2 (with cubic, tetragonal and orthorhombic morphologies) and zeolites with a cubic lattice system (**Figure 10B**). The SAED pattern of synflorescences of *S. verticillata* and *S. viridis* showed well defined rings confirming their polycrystalline nature (**Figures 10Dd,Fd**). The SAED patterns of phytoliths from *S. verticillata* correspond to orthorhombic ferrierite and tridymite and anorthic SiO_2 polymorphs. Similarly, SAED patterns of silica from *S. viridis* correspond to orthorhombic ferrierite and tridymite (**Figure 10Fd**). Apart from taxonomic resolution, the formation of nanoscale silica particles during dry ashing of the plant material has applications in nanotechnology, particularly synthesis of metal silicates (Neethirajan et al., 2009; Qadri et al., 2015).

Biosilica Content

Grasses deposit silica in varied amounts in different plant parts ranging from 1 to 11% (Jones and Handreck, 1967). In the present study, the three species of *Setaria* revealed considerable differences in terms of ash and silica content in their parts (Supplementary Figure 5). The species showed higher values of ash and silica in their foliar parts with 21.06% ash and 11.62% silica in *S. pumila*, 19.87% ash and 9.23% silica in *S. verticillata* and 16.43% ash and 6.24% silica in *S. viridis*. The ash and silica content in other parts were in the order of, synflorescences>roots>culms. Higher amounts of silica in the leaves and synflorescences of grasses are well reported (Lanning and Eleuterius, 1981, 1987, 1989). The differential amounts of silica within and between different parts of the plant body have been correlated to the differences in the targeted cellular sites of silicification. For example, in roots endodermal cells have been proved to be the usual targets of silicification while in the aerial parts of the plant body different epidermal cells and associated structures as well as the cells of vascular bundles, and the spaces between the cortical cells are believed to be the targeted sites of silicification (Kumar et al., 2017; Kumar and Elbaum, 2018).

Our results indicated significantly higher silica content in the leaves of the presently studied *Setaria* species as compared to some other species of the genus. For example a much lower amount (6.06%) was reported in *S. magna* Griseb. (Hodson et al. (1982)) and other members of tribe Paniceae (1.04% for *Panicum reptans* L., 3.7% for *Digitaria macroblephara* (Hack.) Paoli) and related tribes (1.34% for *Imperata cylindrical* (L.) Raeusch. and

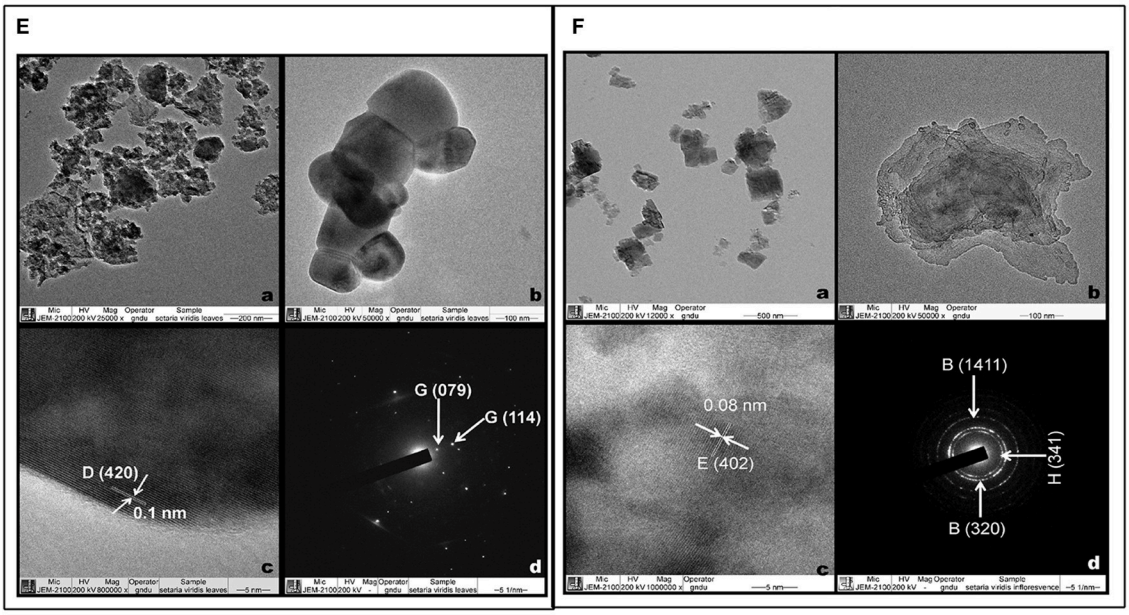

FIGURE 10 | Transmission electron microscopy of Phytoliths **(A,B)**: *Setaria pumila* (Poir.) Roem. & Schult. Leaf **(A) (a–d)** Clusters and agglomerates of silica **(e)** HRTEM **(f)** SAED patterns (Figures in parenthesis indicate hkl values and for description of alphabets refer Supplementary Table 8) and Synflorescence **(B) (a–d)** (Clusters and agglomerates of silica **(e)** HRTEM **(f)** SAED patterns (Figures in parenthesis indicate hkl values and for description of alphabets refer Supplementary Table 8). **(C,D)** *Setaria verticillata* (L.) P. Beauv. Leaf **(C) (a–c)** Clusters and agglomerates of silica **(d–e)** HRTEM **(f)** SAED patterns and Synflorescence **(D) (a–b)** Clusters and agglomerates of silica **(c)** HRTEM **(d)** SAED patterns (Figures in parenthesis indicate hkl values and and for description of alphabets refer Supplementary Table 8). **(E,F)** *Setaria viridis* (L.) P. Beauv. Leaf **(E) (a,b)** Spherical silica particles **(c)** HRTEM **(d)** SAED patterns (Figures in parenthesis indicate hkl values and for description of alphabets refer Supplementary Table 8) and Synflorescence **(F) (a,b)** Cubic and agglomerated silica **(c)** HRTEM **(d)** SAED patterns (Figures in parenthesis indicate hkl values and for description of alphabets refer Supplementary Table 8).

2.7% for *Themeda triandra* Forssk.) of the subfamily Panicoideae (Lanning and Eleuterius, 1989; Quigley and Anderson, 2014).

The variation in silicification rates in underground and aerial parts (particularly leaf and synflorescence bracts) are known to be controlled by a multitude of extrinsic (availability of silica and water in the soil) and intrinsic factors including the extent and nature of silicon transporters and channels, sink strength and the functional anatomy of various plant parts (Motomura et al., 2002; Ma and Yamaji, 2006; Honaine and Osterrieth, 2011). Besides these factors of control, higher levels of silicification in leaf laminae and the synflorescence bracts of aerial plant parts have been correlated with higher evapotranspiration rates in these parts. Once absorbed, silica is transported *via* xylem to various plant parts through the transpiration stream. As water evaporates during transpiration, silicic acid solutes are progressively concentrated resulting in super-saturated concentrations of $Si(OH)_4$ and deposition in tissues as amorphous silica in the form of phytoliths; the extent of supersaturation being controlled by the concentration of silicic acid in soil water (Jones and Handreck, 1965; Rosen and Weiner, 1994; Raven, 2003; Exley, 2015).

Elemental Composition

Though mainly siliceous in nature, phytoliths deposit many other elements in addition to silicon and oxygen in varying proportions during the course of their development (Shakoor et al., 2016). The elemental composition of phytolith morphotypes is reported to be controlled by species characteristics, geochemistry and prevailing environmental conditions (Bujan, 2013; Kamenik et al., 2013; Hodson, 2016). However, the elemental composition of phytoliths in association with their morphology has proved useful for taxonomic diagnosis of species. Elemental composition has been shown to be stable enough to serve as definitive evidence of palaeo-environments by providing clues to the type of the soil in which a given species grew (Kamenik et al., 2013; Hodson, 2016).

The presence of different elements in phytolith morphotypes of the present samples reflect the availability of elements in the soil (Supplementary Table 7). However, the present study revealed some species-specific elements as well. The elemental composition of rhizospheric soil samples from the three sampling sites (**Figure 1**) revealed a cumulative number of fourteen (14) elements (aluminum (Al), carbon (C), calcium (Ca), copper (Cu), iron (Fe), magnesium (Mg), sodium (Na), phosphorous (P), potassium (K), oxygen (O), silicon (Si), sulfur (S), titanium (Ti), and zinc (Zn). Species wise characterization of the soil revealed 11 elements (Al, Ca, C, Fe, Mg, O, K, Si, Na, Ti, and Zn excluding Cu, P, and S from the cumulative list) from sampling sites of *S. pumila*, 10 elements (excluding Cu, P, S, and Zn) from the soil supporting *S. verticillata* whereas the rhizospheric soil samples from the *S. viridis* sampling site revealed 12 elements (excluding Na and Zn from the cumulative list).

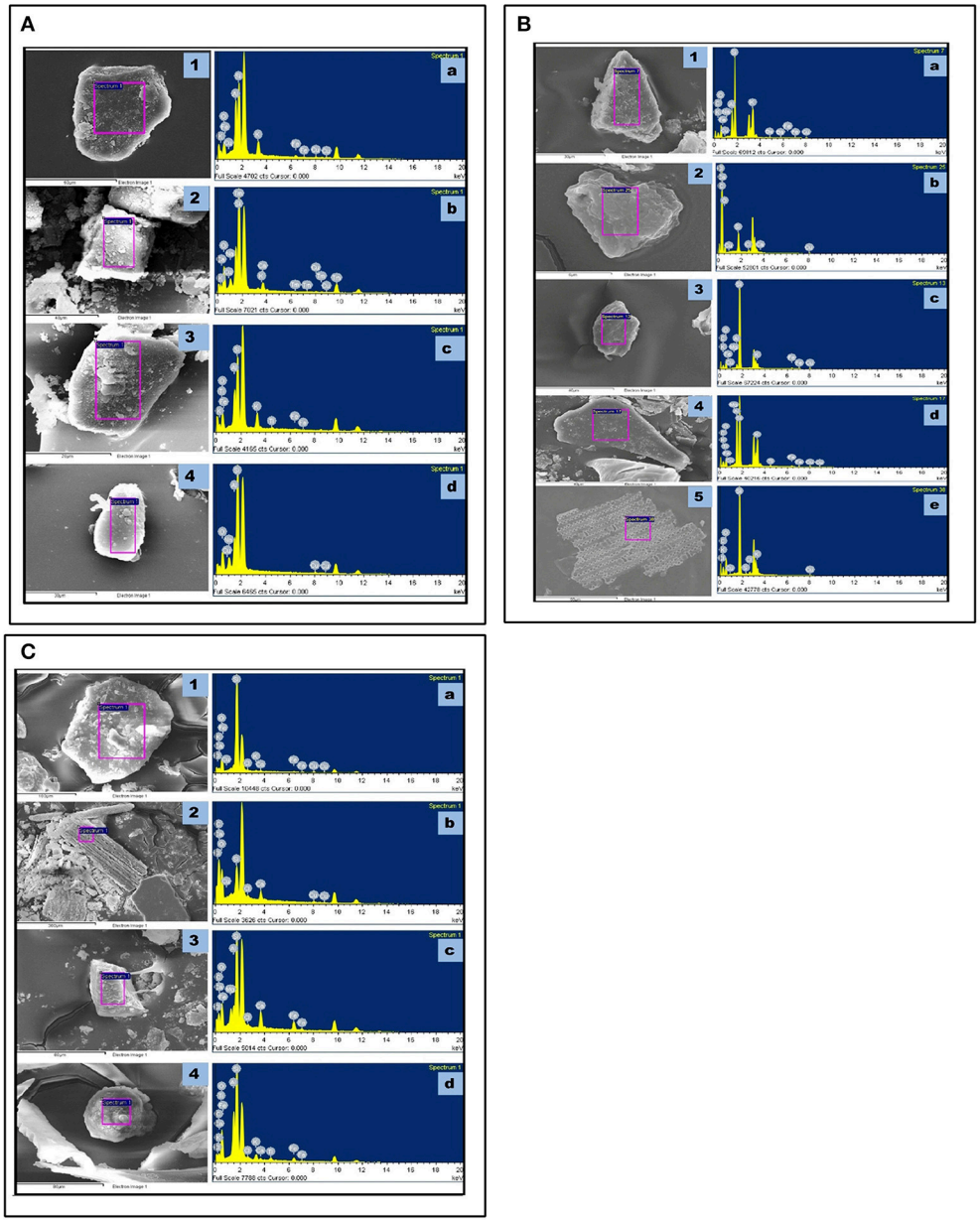

FIGURE 11 | SEM-EDX spectra of phytoliths isolated from different parts: **(A)** *Setaria viridis* (L.) P. Beauv. Root **(1-a)**; Culm **(2-b)**; Leaf **(3-c)**; and Synflorescence **(4-d)**. **(B)** *Setaria verticillata* (L.) P.Beauv. Root **(1-a)**; Culm **(2-b)**; Leaf **(3-c,4-d)**, and Synflorescence **(5-e)**. **(C)** *Setaria pumila* (Poir. Roem. & Schult. Root **(1-a)**; Culm **(2-b)**; Leaf **(3-c)**; and Synflorescence **(4-d)**.

SEM-EDX analysis of the phytolith morphotypes from different parts of the three species revealed a cumulative total of 16 elements with 12 in *S. pumila* 14 in *S. verticillata* and 11 in *S. viridis* (**Figures 11A–C** and Supplementary Table 6). A comparison of elemental composition data of soil samples and phytolith morphotypes revealed that soil geochemistry controls the composition of phytoliths. However, some elements were present in phytolith samples in traces but were not detected in soil samples. For example chlorine (Cl) was detected in phytoliths from all parts of *S. pumila* and *S. verticillata*. Similarly barium (Ba), copper (Cu), and sulfur (S) were detected in the latter named species and rubidium (Rb) and sodium (Na) in *S. viridis*. This unexpected difference in elemental composition of soil samples and phytoliths could be attributed to some sort of "accumulation" of these elements in the living cells producing phytoliths. Most importantly, some elements were unique to one or the other species: barium (Ba), phosphorous (S), and sulfur (S) were detected in *S. verticillata* and rubidium (Rb) in *S. viridis* Principal Component Analysis (PCA) of elemental composition data from different parts of the three congeneric

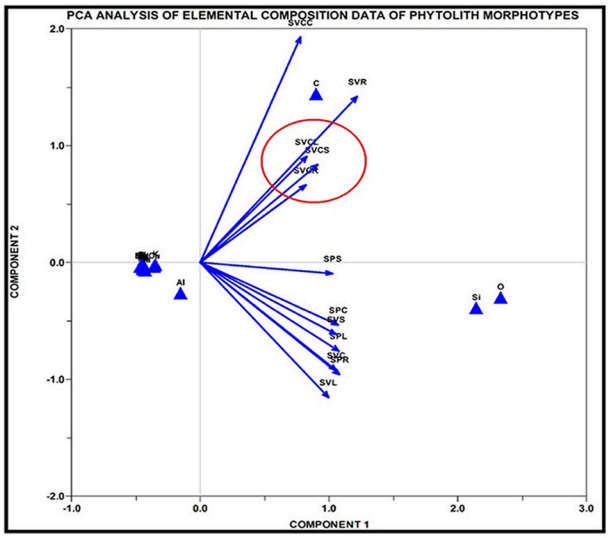

FIGURE 12 | PC analysis of elemental composition of data of phytolith morphotypes of *Setaria* spp. SPR, Setaria pumila root; SPC, *Setaria pumila* culm; SPL, *Setaria pumila* leaf; SPS, *Setaria pumila* synflorescence; SVCR, *Setaria verticillata* root; SVCC, *Setaria verticillata* culm; SVCL, *Setaria verticillata* leaf; SVCS, *Setaria verticillata* synflorescence; SVR, *Setaria viridis* root; SVC, *Setaria viridis* culm; SVL, *Setaria viridis* leaf; SVS, *Setaria viridis* synflorescence.

species led to demarcation of *S.'verticillata* from the other two congenerics with the first two components explaining 97.12% (85.12% component 1 + 15% component 2) variation in the data set (**Figure 12**). The present study has revealed higher atomic and weight percentage values for carbon (C), oxygen (O), and silicon (Si) in phytoliths whereas other elements were present in considerably lesser amounts. The occlusion of carbon in phytoliths has been compared to its sequestration in cellulose and lignin (Parr and Sullivan, 2005). However, EDX analysis revealed the element form of carbon in phytoliths rather than the organic form.

Biomineralization of silica in plants is known to ameliorate metal (Al, Cu, Fe) and salinity stress (Okuda and Takahashi, 1962; Matoh et al., 1986; Cocker et al., 1998; Yeo et al., 1999). The deposition of metals like Al, Cu, Fe in phytoliths possibly alleviates the toxicity associated with these elements. Similarly, salinity stress seemed to be ameliorated by the bioaccumulation of silicophytoliths as revealed by K, Ca, and Mg in phytoliths (Anala and Nambisan, 2015). The segregation and compartmentalization of phytoliths embodying Si and other minerals has made isolation of these elements possible (Raven, 1983). Thus, deposition and immobilization of these toxic elements in the silicification process may be a strategy of plant species to get rid of these materials via their transport along the transpirational route and final occlusion in phytoliths.

X-Ray Diffraction Analysis

Silica exists in diverse polymorphs and sub-morphs; crystalline forms include alpha and beta-quartz, cristobalite, tridymite, coesite, keatite, and stishovite. Amorphous silica has the same composition as SiO_2 but has a random structure of the crystal lattice. The presence of both types in our specimens can be attributed to the transformation of amorphous silica into different crystalline polymorphs during dry ashing of the material (Holm et al., 1967).

Powder diffractograms of phytoliths isolated from underground and aerial parts of *Setaria* showed peaks characteristic of different crystalline polymorphic phases (**Figures 13A–C**). The most frequent phases were silicon dioxide (SiO_2) from all the parts of the species (except the leaf of *S.* verticillata) and quartz (except in leaves and synflorescences of *S. verticillata.* The other phases present in all the three species (at least in one of the parts) included zeolites, tridymite, stishovite, ferririte, coesite and cristobalite (**Figures 13A–C** and Supplementary Table 8). However, stishovite was diagnostic of roots and leaves of *S. pumila* whereas ferririte was restricted only to the roots of *S. viridis*, suggesting a role in taxonomic diagnosis as already reported for some of the grass species (Gonzalez-Espindola et al., 2010, 2014; Shakoor et al., 2016).

The polymorphic phases have been known to have an identical chemical composition (SiO_2) but different physical properties and lattice symmetries. They show distinct lattice systems ranging from anorthic (triclinic), through monoclinic, orthorhombic, hexagonal, cubic, and tetragonal. The present studies lend further credence to the existence of polymorphic silica in plants (Ollendorf et al., 1988; Piperno, 1988, 2006; Lu and Liu, 2003; Lu et al., 2009; Zhang et al., 2011; Szabo et al., 2015; Ge et al., 2016). The diffractogram of phytoliths of *S. viridis* (root) and *S. pumila* (root and culm) showed a unique peak corresponding to ferrierite and zeolite respectively. (**Figures 13A,C**). Ferrierite is a zeolite (aluminosilicate mineral) that binds a number of cations viz., Na^+, K^+, Ca^{2+}, Mg^{2+} etc. The presence of these phases can be explained by elemental composition data.

Further, the FTIR analysis revealed a peak of Aluminosilicate minerals in these species, thus supporting our XRD results (**Figures 14A,C**). Earlier, Kow et al. (2014) confirmed the shift from amorphous to crystalline phases of silica in cogon grass (*Imperata cylindrica* (L.) P. Beauv.) in the presence of potassium (K). Similarly, the presence of other minerals like, Na, Ca, Mg, K etc. in phytoliths from the different parts of these congeneric species could afford a possible explanation (acting as a controlling factor) for the presence of different crystalline polymorphic phases of silica. Such an association is further indicated by the presence of only amorphous silica in the phytoliths from the culms of *S. verticillata* that harbor a smaller number of elements (only 4 besides C & H) as compared to phytoliths from other parts of the plant body (**Figure 13B** and Supplementary Table 7).

FT-IR Spectroscopy

FTIR spectroscopy of silica from different parts of *Setaria* spp. revealed several peaks that could be assigned to different structural units of silica with varied vibrational degrees of freedom (**Figures 14A–C** and Supplementary Table 9). The peaks between 445.67–472.00 cm^{-1}, 637.48–699.54 cm^{-1}, 712.70–801.08 cm^{-1}, 1080.06–1094.44 cm^{-1}, 1602.17-1616.24 cm^{-1},

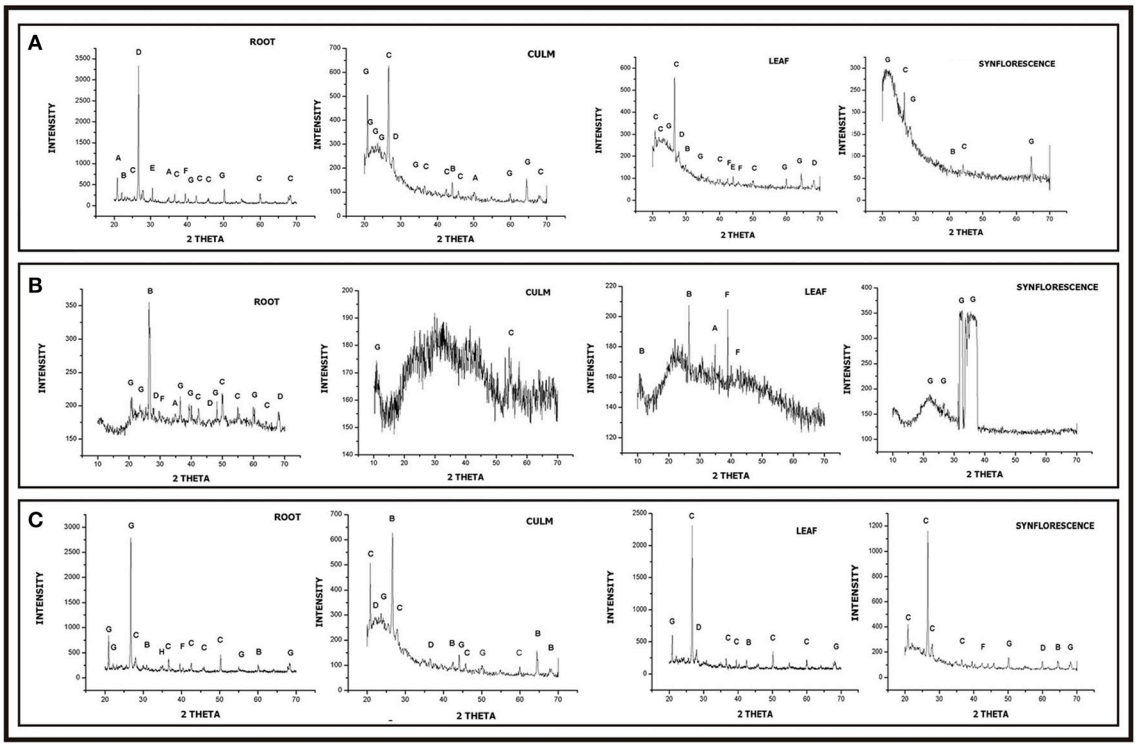

FIGURE 13 | XRD diffraction spectra of phytoliths isolated from different parts of *Setaria* spp. **(A)** *Setraia pumila* **(B)** *Setaria verticillata* **(C)** *Setaria viridis* (for description of peak points, refer to Supplementary Table 8).

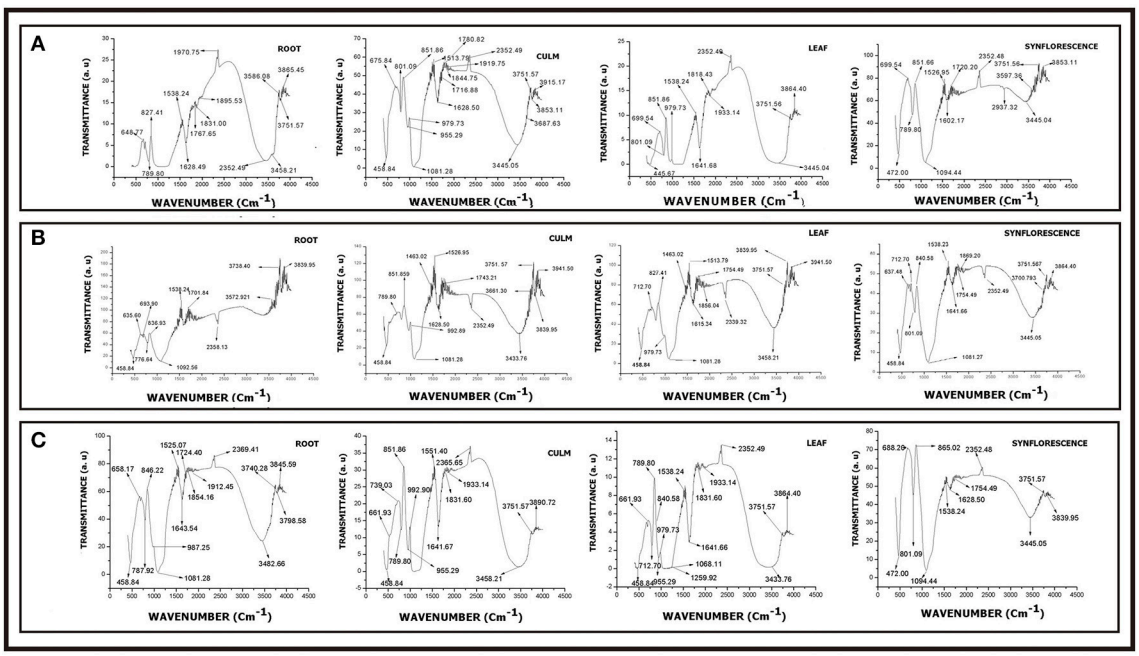

FIGURE 14 | FTIR spectra of phytoliths from different parts of *Setaria sps.* **(A)** *Setaria pumila* **(B)** *Setaria verticillata* **(C)** *Setaria viridis* (for description of peak points, refer to Supplementary Table 9).

1628.50–1641.66 cm^{-1}, 2339.32–2366.49 cm^{-1}, and 3346.27–3597.36 cm^{-1} present in all the three species (**Figures 14A–C** and Supplementary Table 9) have earlier been variously ascribed to deformation vibration of O–Si–O group (Bertoluzza et al., 1982), symmetrical vibration of Si–O–Si (Gopal et al., 2004), symmetric vibration of Si–O (Brinker et al., 1990), asymmetric vibration of Si–O–Si (Karunakaran et al., 2013; Mourhly et al., 2015), inplane stretching vibration of C-C (Ou and Seddon, 1997), deformation vibration of H–O–H (Socrates, 2001), inplane stretching vibration of Si–C (Socrates, 2001) and O–H/Si–OH bonds (Brinker et al., 1990) bonds. Peaks between 530.39–563.18, 1164.92, 1218.93, 1323.08–1332.72, 1743.21–1933.14, 2825.52, and 3006.82–3271.05 cm^{-1} characteristic of *S. verticillata* (L.) P. Beauv. (**Figure 14B** and Supplementary Table 9) could be ascribed to stretching vibration of O–Si (SiO_2 defect) (Brinker et al., 1990), asymmetric vibration of Si–O–Si (Duran et al., 1986), inplane stretching of free Si–O (Chmel et al., 2005), symmetric deformation vibration of Si–R (Socrates, 2001), deformation vibration of R (alkyl group), symmetric vibration of C–H (Gunzler and Gremlich, 2002), and stretching vibration of O–H bonds (Brinker et al., 1990). Similarly, peaks at 1463.02 and 1701.84 cm^{-1} characteristic of *S. viridis* (**Figures 14C** and Table 10) could be ascribed to asymmetric and symmetric deformation vibrations of hydrocarbons (–CH_3-CH_2)– (Watling et al., 2011) and inplane stretching vibrations of Si–C bonds.

CONCLUSIONS

Within the context, scope and parameters of reference samples used in the present work, the three congenerics of *Setaria* revealed a degree of similarity in phytolith profiles but each was found to be well demarcated from the other in the group by "unique" morphotypes and their characteristic assemblages and structures. The bilobate morphotypes aptly illustrate phytolith-assisted taxonomic demarcation of the three species. In the present study, eight variants of the bilobate morphotype were recognized on the basis of the length of the shanks (the interconnecting segment between the lobes) and the shape of the outer margin of the lobes. *S. pumila* showed three of the eight structural variants of the bilobate phytoliths (III, V, and VI) in the costal region on the adaxial surfaces. In the same location, *S. viridis* also showed three of these variants (II, IV, and V) whereas *S. verticillata* had only two of them (VII and IV). Thus bilobate classes were found to be highly conserved and useful for identification of grass species. Quadrihedral and hexahedral cystoliths (calcium oxalate crystals) on the adaxial epidermal surfaces of *S. verticillata* emerged as another diagnostic feature of the species (a first report for the foxtail grass genus *Setaria*)*S. verticillata* was also marked out by the presence of a new undulation type, (the Λ-lambda with three variants *viz.* Λ-I, Λ-II, and Λ-III) in the long epidermal cells.

Besides qualitative differences, the present samples of the three species also revealed interspecific variations in frequency distribution and morphometric measurements of various morphotypes. For example, the frequency of trapezoids was significantly different in these species: 19.47% in *S. pumila*, 14.38% in *S. verticillata,* and 7.91% in *S. viridis* ($p \leq 0.05$; χ^2-test). Acicular morphotypes were present in both *S. verticillata* and *S. viridis* but differed many fold in their percentage frequency (15.17 and 2.18% respectively).

Principal Component Analysis of morphometric parameters of phytoliths from different parts of the plant body proved useful in taxonomic demarcation of the species. PCA of root phytoliths clearly separated the three species on the basis of the surface area of different morphotypes. *S. pumila* was demarcated on the basis of the surface area of blocky irregular and tabular irregular, *S. verticillata* by the surface area of blocky polyhedral and *S. viridis* by the area of trapezoid morphotype.

TEM revealed three valuable distinguishing parameters of phytoliths namely, micro-structural details, degree of amorpho-crystalline nature and inter-atomic planer distances in crystalline samples. Secondly, ultramicroscopy has proved useful in comparing and collating phytolith profiles from different parts of the plant body to develop phytolith signatures for each species. SAED patterns revealed by TEM showed the polycrystalline nature of silica in the synflorescences of *S. verticillata* and *S. viridis* whereas single crystal systems were reported in other parts of the three species. Thirdly, indexing of SAED patterns revealed silica polymorphism. The polymorphs of silica revealed by TEM were further confirmed by XRD patterns, particularly the ferrierite in *S. viridis* (root) and zeolite in *S. pumila* (root and culm).

The elemental composition of phytolith morphotypes from different parts of the present samples of the three species has revealed a cumulative total of 16 elements with 12 in *S. pumila* 14 in *S. verticillata* and 11 in *S. viridis*. A comparison of elemental composition of soil samples and phytolith morphotypes revealed that soil geochemistry controls the composition of phytoliths. Powder diffractograms of phytoliths revealed a number of polymorphic phases of silica. Stishovite was diagnostic of roots and leaves of *S. pumila* whereas ferririte was restricted only to the roots of *S. viridis*, thus strengthening a case for their role in taxonomic diagnosis as already reported for some other grass species.

FTIR analysis has revealed diversity of functional groups and their modes of vibrations with some groups being exclusively species specific. *S. verticillata* showed stretching vibration of O–Si (SiO_2 defect), asymmetric vibration of Si–O–Si, inplane stretching of free Si–O bond, symmetric deformation vibration of Si–R, deformation vibration of R (alkyl group), symmetric vibration of C–H and stretching vibration of O–H bonds. Similarly, groups characteristic of *S. viridis* include asymmetric and symmetric deformation vibrations of hydrocarbons (–CH_3-CH_2) – and inplane stretching vibrations of Si–C bonds.

The multiproxy approach employed in the present work has led to anatomical and physico-chemical characterization of the phytoliths produced by the present samples of three related species of the foxtail genus *Setaria* Phytolith analysis seems to confirm the comparatively isolated position of *S. pumila*

in the present triumvirate of species. *S. pumila* was marked by two unique bilobate types compared to only one each in the other two species, the absence of polycrystalline silica in the synflorescences and the presence of the polymorphic silica as stishovite in the roots and the leaves. Clustering of species using Jaccard's similarity index for presence/absence data of the entire data set of phytolith morphotypes also revealed that *S. pumila* had a low similarity (33%) of phytolith profiles with *S. verticillata* and *S. viridis* (28.57%). However, *S. verticillata* and *S. viridis* showed much higher similarity (42.85%) and were grouped together (**Figures 8**). A plausible explanation may lie in the difference in the centers of origin of *S. pumila* (Africa) and the other two species (Asia).

Even though the full potential of phytoliths in understanding the taxonomy and phylogeny of the foxtail grass genus (*Setaria*) must come through future research involving an assessment of inter-population and intra-population variations and construction of representative master profiles for each species, the paper has made an initial contribution. We have made plant collections from single locations and homogenized the material part-wise but this limitation has been partly made good by following a multiproxy and multi-organ approach in carrying out the present work. In the larger context of plant systematics, concerted and coordinated efforts of a multidisciplinary nature are required to develop integrated and robust phytolith profiles of different groups of plants and their application in the characterization and diagnosis of plant taxa.

AUTHOR CONTRIBUTIONS

MB collected the material, conducted leaf epidermal studies, and wrote the initial draft of the manuscript. SS and PB carried out experimental work. AS designed the work, guided the conduct of experiments and checked the final manuscript.

ACKNOWLEDGMENTS

The authors are grateful to Professor Incharge, Emerging Life Sciences Laboratory, Guru Nanak Dev University, Amritsar, Punjab (India) and Director Indian Institute of Integrative Medicine, Jammu (Jammu and Kashmir) for SEM The help received from Mr. Musaib Ahmad Wani (Guru Ram Das School of Planning, Guru Nanak Dev University, Amritsar) in designing the map of the study area is gratefully acknowledged. The first author is thankful to the University Grants Commission, New Delhi for financial assistance under a major UGC project on phytolith studies on the grasses of the North West Himalayan region. The authors wish to thank the two reviewers whose comments and suggestions have vastly improved the quality of presentation and contributed to the logical coherence of the paper.

SUPPLEMENTARY MATERIAL

The Supplementary Material for this article can be found online at: https://www.frontiersin.org/articles/10.3389/fpls.2018.00864/full#supplementary-material

REFERENCES

Albert, R. M., Bar-Yosef, O., and Weiner, S. (2007). "Use of plant material in Kebara cave: phytoliths and mineralogical analyses," in *The Middle and Upper Paleolithic Archaeology Cambridge,* eds O. Bar-Yosef and L. Meignen (Israel, MA: Peabody Museum of Archaeology and Ethnology Harvard University), 147–162.

Albert, R. M., and Henry, D. O. (2004). Herding and agricultural activities at the early Neolithic site of Ayn Abu Nukhayla (Wady Rum, Jordan). The results of phytolith and spherulite analyses. *Paléorient* 30, 81–92. doi: 10.3406/paleo.2004.1012

Alexandre, A., Basile-Doelsch, I., Delhaye, T., Borshneck, D., Mazur, J. C., Reyerson, P., et al. (2015). New highlights of phytolith structure and occluded carbon location: 3-D X-ray microscopy and Nano SIMS results. *Biogeosciences* 12, 863–873. doi: 10.5194/bg-12-863-2015

Aliscioni, S. S., Gómiz, N. E., Torretta, J. P., and Pensiero, J. F. (2011). Reproductive biology of *Setaria magna* Griseb. (Poaceae: Panicoideae: Paniceae). *Plant Syst. Evol.* 293, 111–118. doi: 10.1007/s00606-011-0428-0

Aliscioni, S. S., Ospina, J. C., and Gomiz, N. E. (2016). Morphology and leaf anatomy of *Setaria* sl (Poaceae: Panicoideae: Paniceae) and its taxonomic significance. *Plant Syst. Evol.* 302, 173–185. doi: 10.1007/s00606-015-1251-9

Anala, R., and Nambisan, P. (2015). Study of morphology and chemical composition of phytoliths on the surface of paddy straw. *Paddy Water Environ.* 13, 521–527. doi: 10.1007/s10333-014-0468-5

Astudillo, F. (2017). *Environmental Historical Archaeology of the Galápagos Islands: Paleoethnobotany of Hacienda El Progreso, 1870-1904.* Doctoral dissertation, Environment, Department of Archaeology.

Baker, G. (1959a). A contrast in the opal phytolith assemblages of two Victorian soils. *Aust. J. Bot.* 7, 88–96. doi: 10.1071/BT9590088

Baker, G. (1959b). Fossil opal-phytoliths and phytolith nomenclature. *Aust. J. Sci.* 21, 305-306. doi: 10.1093/oxfordjournals

Ball, T. B., Davis, A., Evett, R. R., Ladwig, J. L., Tromp, M., Out, W. A., et al. (2016). Morphometric analysis of phytoliths: recommendations towards standardization from the International Committee for Phytolith Morphometrics. *J. Archaeol. Sci.* 68, 106–111. doi: 10.1016/j.jas.2015.03.023

Ball, T., Vrydaghs, L., Mercer, T., Pearce, M., Snyder, S., Lisztes-Szab,ó, Z., et al. (2017). A morphometric study of variance in articulated dendritic phytolith wave lobes within selected species of Triticeae and Aveneae. *Veg. Hist. Archaeobot.* 26, 85–97. doi: 10.1007/s00334-015-0551-x

Barboni, D., Ashley, G. M., Dominguez-Rodrigo, M., Bunn, H. T., Mabulla, A. Z., and Baquedano, E. (2010). Phytoliths infer locally dense and heterogeneous paleovegetation at FLK North and surrounding localities during upper Bed I time, *Olduvai Gorge, Tanzania. Quat. Res.* 74, 344–354. doi: 10.1016/j.yqres.2010.09.005

Barboni, D., and Bremond, L. (2009). Phytoliths of East African grasses: an assessment of their environmental and taxonomic significance based on floristic data. *Rev. Palaeobot. Palynol.* 158, 29–41. doi: 10.1016/j.revpalbo.2009.07.002

Benecke, W. (1903). Ueber Oxalsaurebildung in grunen Pflanzen. *Botanisches Zeitung* 61, 79–110.

Benvenuto, M. L., Honaine, M. F., Osterrieth, M. L., and Morel, E. (2015). Differentiation of globular phytoliths in Arecaceae and other monocotyledons: morphological description for paleobotanical application. *Turk. J. Bot.* 39, 341–353. doi: 10.3906/bot-1312-72

Bertoluzza, A., Fagnano, C., Morelli, M. A., Gottardi, V., and Guglielmi, M. (1982). Raman and infrared spectra on silica gel evolving toward glass. *J. Non-Cryst. Solids* 48, l7–128. doi: 10.1016/0022-3093(82)90250-2

Blinnikov, M. S. (2005). Phytoliths in plants and soils of the interior Pacific Northwest USA. *Rev. Palaeobot. Palynol.* 135, 71–98. doi: 10.1016/j.revpalbo.2005.02.006

Bombin, M. (1984). *On Information Evolutionary Theory, Phytoliths, and the Late Quaternary Ecology of Beringia.* Doctoral dissertation, Ph.D. diss., Department of Anthropology, University of Alberta, Edmonton.

Bonnett, O. T. (1972). *Silicificd Cells of Grasses: A Major Source of Plant Opal in Illinois Soils*. New York, NY: University of lllinois at Urbana-Champaign, College of Agriculture.

Bor, N. L. (1960). *Grasses of Burma, Ceylon, India and Pakistan*. Oxford: Pergamon Press.

Borrelli, N., Alvarez, M. F., Osterrieth, M. L., and Marcovecchio, J. E. (2010). Silica content in soil solution and its relation with phytolith weathering and silica biogeochemical cycle in typical argiudolls of the Pampean Plain, Argentina—a preliminary study. *J. Soils Sediments* 10, 983–994. doi: 10.1007/s11368-010-0205-7

Bozarth, S. R. (1987). Diagnostic opal phytoliths from rinds of selected *Cucurbita* species. *Am. Antiq.* 52, 607–615. doi: 10.2307/281602

Brilhante de Albuquerque, E. S., Alvarenga Braga, J. M., and Cardoso Vieira, R. (2013). Morphological characterisation of silica phytoliths in Neotropical Marantaceae leaves. *Plant Syst. Evol.* 299, 1659–1670. doi: 10.1007/s00606-013-0823-9

Brinker, C. J., and Scherer, G., W (1990). *Sol-Gel Science: The Chemistry and Physics of Sol-Gel Processing.* London: Academic Press

Bujan, E. (2013). Elemental composition of phytoliths in modern plants (Ericaceae). *Quat. Int*. 287, 114–120. doi: 10.1016/j.quaint.2012.02.046

Carbone, V. A. (1977). Phytoliths as paleoecological indicators. *Ann. N. Y. Acad. Sci.* 288, 194–205. doi: 10.1111/j.1749-6632.1977.tb33615.x

Carnelli, A. L., Madella, M., and Theurillat, J. P. (2001). Biogenic silica production inselected alpine plant species and plant communities. *Ann. Bot.* 87, 425–434. doi: 10.1006/anbo.2000.1355

Carnelli, A. L., Theurillat, J. P., and Madella, M. (2004). Phytolith types and type-frequencies in subalpine–alpine plant species of the European Alps. *Rev. Palaeobot. Palynol.* 129, 39–65. doi: 10.1016/j.revpalbo.2003.11.002

Chauhan, D. K., Tripathi, D. K., Rai, N. K., and Rai, A. K. (2011). Detection of biogenic silica in leaf blade, leaf sheath, and stem of Bermuda grass (*Cynodon Dactylon*) using libs and phytolith analysis. *Food Biophys.* 6, 416–423. doi: 10.1007/s11483-011-9219-y

Chen, Y., Yin, Q., Ji, X., Zhang, S., Chen, H., Zheng, Y., et al. (2012). Manganese oxide-based multifunctional izedmesoporous silica nanoparticles for pH-responsive MRI, ultra sonography and circumvention of MDR in cancer cells. *Biomaterials* 33, 7126–7137. doi: 10.1016/j.biomaterials.2012.06.059

Chmel, A., Smirnov, V. N., and Astakhov, M. P. (2005). The Arctic sea-ice cover: fractal space–time domain. *Physica. A Stat. Mech. Appl.* 357, 556–564. doi: 10.1016/j.physa.2005.04.009

Clarke, J. (1959). Preparation of leaf epidermis for topographic study. *Stain Technol.* 35, 35–39. doi: 10.3109/10520296009114713

Clayton, W. D., and Renvoize, S. A. (1986). *Genera Graminum: Grasses of the World.* London: *Kew Bull.*

Clayton, W. D., Vorontsova, M. S., Harman, K. T., and Williamson, H. (2016). GrassBase—*The online World grass flora: The Board of Trustees, Royal Botanic Gardens [online].* Available online at http://www.kew.org/data/grasses-db.html

Cocker, K. M., Evans, D. E., and Hodson, M. J. (1998). The amelioration of aluminium toxicity by silicon in higher plants: solution chemistry or an in planta mechanism? *Physiol. Plant.* 104, 608–614. doi: 10.1034/j.1399-3054.1998.1040413.x

Conley, D. J. (2002). Terrestrial ecosystems and the global biogeochemical silica cycle. *Global Biogeochem. Cycles* 16:1121. doi: 10.1029/2002GB001894

Cope, T. A. (1982). "Poaceae," in *Flora of Pakistan. Karachi, Islamabad*, eds E. Nasir and S. I. Ali (Karachi: Pakistan Agricultural Research Council), 40–678.

Coughenour, M. B. (1985). Graminoid responses to grazing by large herbivores: adaptations, exaptations, and interacting processes. *Ann. Mo. Bot. Gard.* 72, 852–863. doi: 10.2307/2399227

Crawford, G. W. (2009). Agricultural origins in North China pushed back to the Pleistocene–Holocene boundary. *Proc. Natl. Acad. Sci. U.S.A* 106, 7271–7272. doi: 10.1073/pnas.0903375106

Das, S., Ghosh, R., Paruya, D. K., Yao, Y. F., Li, C. S., and Bera, S. (2014). Phytolith spectra in respiratory aerial roots of some mangrove plants of the Indian Sunderbans and its efficacy in ancient deltaic environment reconstruction. *Quat. Int.* 325, 179–196. doi: 10.1016/j.quaint.2013.11.025

Dayanandan, P., Hebard, F. V., Baldwin, V. D., and Kaufman, P. B. (1977). Structure of gravity-sensitive sheath and internodal pulvini in grass shoots. *Am. J. Bot.* 64, 1189–1199.

Doust, A. N., and Kellogg, E. A. (2002). Inflorescence diversification in the panicoid 'bristle grass' clade (Paniceae, Poaceae): evidence from molecular phylogenies and developmental morphology. *Am. J. Bot.* 89, 1203–1222. doi: 10.3732/ajb.89.8.1203.

Duran, A., Serna, C., Fornes, V., and Navarro, J. F. (1986). Structural considerations about SiO_2 glasses prepared by sol-gel. *J. Non-Cryst. Solids* 82, 69–77. doi: 10.1016/0022-3093(86)90112-2

Ellis, R. P. (1979). A procedure for standardizing comparative leaf anatomy in the Poaceae: II. The epidermis as seen in surface view. *Bothalia* 12, 641–671. doi: 10.4102/abc.v12i4.1441

Ellis, R. P. (1984). Eragrostis walteri—a first record of non-Kranz leaf anatomy in the sub-family Chloridoideae (Poaceae). *S. Afr. J. Bot.* 3, 380–386.

Epstein, E. (1994). The anomaly of silicon in plant biology. *Proc. Natl. Acad. Sci. U.S.A.* 91, 11–17. doi: 10.1073/pnas.91.1.11

Epstein, E. (1999). Silicon. *Annu. Rev. Plant Physiol. Plant Mol. Biol.* 50, 641–664. doi: 10.1146/annurev.arplant.50.1.641

Exley, C. (2015). A possible mechanism of biological silicification in plants. *Front. Plant Sci.* 6:853. doi: 10.3389/fpls.2015.00853

Ezell-Chandler, K., Pearsall, D. M., and Zeidler, J. A. (2006). Root and tuber phytoliths and starch grains document manioc *(Manihot Esculenta)*, arrowroot *(Maranta Arundinacea)*, and Llerén *(Calathea* sp.*)* at the real alto site, ecuador. *Econ. Bot.* 60, 103–120. doi: 10.1663/0013-0001(2006)60[103:RATPAS]2.0.CO;2

Fahmy, A. G. (2008). Diversity of lobate phytoliths in grass leaves from the Sahel region, West Tropical Africa: Tribe Paniceae. *Pl. Syst. Evol.* 270, 1–23. doi: 10.1007/s00606-007-0597-z

Fernandez Honaine, M., Zucol, A. F., and Osterrieth, M. L. (2006). Phytolith assemblages and systematic associations in grassland species of the South-Eastern Pampean Plains, Argentina. *Ann. Bot.* 98, 1155–1165. doi: 10.1093/aob/mcl207

Fisher, R. F., Bourn, C. N., and Fisher, W. F. (1995). Opal phytoliths as an indicator of the floristics of prehistoric grasslands. *Geoderma* 68, 243–255. doi: 10.1016/0016-7061(95)00044-9

Fox, C. L., Juan, J., and Albert, R. M. (1996). Phytolith analysis on dental calculus, enamel surface, and burial soil: information about diet and paleoenvironment. *Am. J. Phys. Anthropol.* 10, 101–113. doi: 10.1002/(SICI)1096-8644(199609)101:1<101::AID-AJPA7>3.0.CO;2-Y

Fredlund, G. G., Johnson, W. C., and Dort, J. W. (1985). "A preliminary analysis of opal phytoliths from the Eustis ash pit, Frontier County, Nebraska," in Institute for *Tertiary-Quaternary Studies-TER-QUA Symposium Series* (Nebraska), 147–162.

Fuller, D. Q., Qin, L., and Harvey, E. (2007). A critical assessment of early agriculture in East Asia, with emphasis on Lower Yangzte rice *domestication.Pragdhara* 18, 17–52.

Gallego, L., and Distel, R. A. (2004). Phytolith assemblages in grasses native to Central Argentina. *Ann. Bot.* 94, 865–874. doi: 10.1093/aob/mch214

Gao, G., Jie, D., Wang, Y., Liu, L., Liu, H., Li, D., et al. (2018). Do soil phytoliths accurately represent plant communities in a temperate region? A case study of Northeast China. *Veg. Hist. Archaeobot.* 28, 1–13. doi: 10.1007/s00334-018-0670-2

García-Granero, J. J., Lancelotti, C., Madella, M., Ajithprasad, P., Crowther, A., Korisettar, R., et al. (2016). Millets and herders: the origins of plant cultivation in semiarid North Gujarat (India). *Curr. Anthropol.* 57, 149–173. doi: 10.1086/685775

Ge, Y., Lu, H., Zhang, J., Wang, C., He, K., and Huan, X. (2016). *Phytolith analysis for the identification of barnyard millet (Echinochloa sp.) and its implications. Archaeol. Anthropol. Sci.* 10, 61–73. doi: 10.1007/s12520-016-0341-0

Gerard, F., Mayer, K. U., Hodson, M. J., and Ranger, J. (2008). Modelling the biogeochemical cycle of silicon in soils: application to

a temperate forest ecosystem. *Geochim. Cosmochim. Acta* 72, 741–758. doi: 10.1016/j.gca.2007.11.010

Gonzalez-Espindola, A., Harnendez-Martinez, A. L., Chaves-Angeles, C., Catano, M. V., and Santos-Velasco, C. (2010). Novel crystalline SiO2 nanoparticles via annelids bioprocessing of agro-industrial wastes. *Nanoscale Res. Lett.* 5, 1408–1417. doi: 10.1007/s11671-010-9654-6

Gonzalez-Espindola, A., Ramirez-Fuentes, R., Harnendez-Martinez, L. A., Catano, M. V., and Santos- Velasco, C. (2014). Structural characterization of silica particles extracted from grass *Stenotaphrum secundatum*: biotransformation viaannelids. *Adv. Mater. Sci. Eng.* 2014:956945. doi: 10.1155/2014/956945

Gopal, N. O., Narasimhulu, K. V., and Rao, J. L. (2004). EPR, optical, infrared and Raman spectral studies of Actinolite mineral. *Spectrochim. Acta Part A* 60, 2441–2448. doi: 10.1016/j.saa.2003.12.021

Gould, F. W. (1968). *Grass Systematics*. New York, NY:McGraw-Hill.

Gould, F. W., and Shaw, R. B. (1983). Grass systematics. *Brittonia* 35, 310–310. doi: 10.1007/BF02831478

GPWG (Grass Phylogeny Working Group). (2001). Phylogeny and subfamilial classification of the grasses (Poaceae). *Ann. Mo. Bot. Gard.* 88, 373–457. doi: 10.2307/3298585

GPWG (Grass Phylogeny Working Group II). (2011). New grass phylogeny resolves deep evolutionary relationships and discovers C4 origins. *New Phytol.* 193, 304–312. doi: 10.1111/j.1469-8137.2011.03972.x

Gross, E. R. (1973). *Buried Soils of the Drainage ways in the Driftless Area of the Upper Mississippi River Valley,* Unpublished Ph.D. *dissertation, University of Minnesota* 195.

Gunzler, H., and Gremlich, H. U. (2002). *Absorption and Molecular Design. IR Spectroscopy, an Introduction. Weinheim: Wiley-VCH.*

Hammer, O., Harper, D. A. T., and Ryan, P. D. (2001). PAST: Paleontological Statistic software package for education and data analysis. *Paleontol. Eletron.* 4 , 1–9.

Hattori, T., Inanaga, S., Araki, H., An, P., Morita, S., Luxova, M., et al. (2005). Application of silicon enhanced drought tolerance in *Sorghum* bicolor. *Physiol. Plant.* 123, 459–466. doi: 10.1111/j.1399-3054.2005.00481.x

Hilu, W. K. (1984). Leaf epidermes of *Andropogon* sect. *Leptopogon (Poaceae) in North America. Syst. Bot.* 9, 247–257. doi: 10.2307/2418830

Hodson, M. G., Sangster, A. G., and Parry, D. W. (1985). An ultrastructural study on the developmental phases and silicification of the glumes of *Phalaris canariensis* L. *Ann. Bot.* 55, 649–665. doi: 10.1093/oxfordjournals.aob.a086944

Hodson, M. J. (2016). The development of phytoliths in plants and its influence on their chemistry and isotopic composition. implications for palaeoecology and archaeology. *J. Archaeol. Sci* 68, 62–69. doi: 10.1016/j.jas.2015.09.002

Hodson, M. J., and Evans, D. E. (1995). Aluminium/silicon interactions in higher plants. *J. Exp. Bot.* 46, 161–171. doi: 10.1093/jxb/46.2.161

Hodson, M. J., and Sangster, A. G. (1988). Observation on the distribution of mineral elements in the leaf of wheat (*Triticum aestivum* L.) with particular reference to silicon. *Ann. Bot.* 62, 463–471. doi: 10.1093/oxfordjournals.aob.a087681

Hodson, M. J., Sangster, A. G., and Parry, D. W. (1982). Silicon deposition in the inflorescence bristles and macrohairs of *Setaria italica* (L.) beauv. *Ann. Bot.* 50, 843–850. doi: 10.1093/oxfordjournals.aob.a086427

Holm, J. L., Kleppa, O. J., Westrum, J.r., and Edgar, F. (1967). Thermodynamics of polymorphic transformations in silica: thermal properties from 5 to 1070 K and pressure-temperature stability fields for coesite and stishovite. *Geochim. Cosmochim. Acta* 31, 2289–2307. doi: 10.1016/0016-7037(67)90003-8

Honaine, M. F., and Osterrieth, M. L. (2011). Silicification of the adaxial epidermis of leaves of a panicoid grass in relation to leaf position and section and environmental conditions. *Plant Biol.* 14, 596–604. doi: 10.1111/j.1438-8677.2011.00530.x

Hongyan, L., Dongmei, J., Lidan, L., Zhuo, G., Guizai, G., Lianxuan, S., et al. (2018). the research on phytoliths size variation characteristics in phragmites communis under warming conditions. *Silicon* 10, 445–454. doi: 10.1007/s12633-016-9472-2

Hunt, H. V., Vander Linden, M., Liu, X., Motuzaite-Matuzeviciute, G., Colledge, S., and Jones, M. K. (2008). Millets across Eurasia: chronology and context of early records of the genera *Panicum* and *Setaria* from archaeological sites in the old world. *Veget. Hist. Archaeobot.* 17, 5–18. doi: 10.1007/s00334-008-0187-1

Ingram, A. L. (2010). Evolution of leaf blade anatomy in *Eragrostis* (Poaceae). *Syst. Bot.* 35, 755–765. doi: 10.1600/036364410X539844

Ishtiaq, C. A., Mumtaz, S., and Khan, M. A. (2001). Leaf epidermal anatomy of medicinal grasses of Islamabad, Attock and Mirpur. *Pak. J. Biol. Sci.* 4, 1466–1469. doi: 10.3923/pjbs.2001.1466.1469

Itzstein-Davey, F., Taylor, D., Dodson, J., Atahan, P., and Zheng, H. (2007). Wild and domesticated forms of rice (*Oryza* sp.) in early agriculture at Qingpu, lower Yangtze, China: evidence from phytoliths. *J. Archaeol. Sci.* 34, 2101–2108. doi: 10.1016/j.jas.2007.02.018

Jattisha, P. I., and Sabu, M. (2012). Phytoliths as a tool for the identification of some chloridoideae grasses in Kerala. *ISRN Bot.* 2012:246057. doi: 10.5402/2012/246057

Jattisha, P. I., and Sabu, M. (2015). Foliar phytoliths as an aid to the identification of *Paniceae* (Panicoideae: poaceae) grasses in South India. *J. Plant Taxo. Geogra.* 70, 115–131. doi: 10.1080/00837792.2015.1005908

Jones, L. H. E., and Handreck, K. A. (1965). Studies of silica in the oat plant, III: uptake ofsilica from soils by the plant. *Plant Soil.* 23, 79–96. doi: 10.1007/BF01349120

Jones, L. H. P., and Handreck, K. A. (1967). Silica in soils, plants, and animals. *Adv. Agron.* 19, 107–147. doi: 10.1016/S0065-2113(08)60734-8

Jones, R. L. (1964). Note on occurrence of opal phytoliths in some Cenozoic sedimentary rocks. *J. Paleontol.* 30, 773–775.

Jones, R. L., and Beavers, A. H. (1964). Aspects of catenary and depth distribution of opal phytoliths in illinois soils[1]. *Soil Sci. Soc. Am. J.* 28, 413–416. doi: 10.2136/sssaj1964.03615995002800030033x

Juggins, S., (2003). *C2 User guide. Software for Ecological and Palaeoecological Analysis and Visualisation*. Newcastle upon Tyne: University of Newcastle.

Kamenik, J., Mizera, J., and Randa, Z. (2013). Chemical composition of plant silica phytoliths. *Environ. Chem. Lett.* 11, 189–195. doi: 10.1007/s10311-012-0396-9

Karunakaran, G., Suriyaprabha, R., Manivasakan, P., Yuvakkumar, R., Rajendran, V., Prabu, P., et al. (2013). Effect of nanosilica and silicon sources on plant growth promoting rhizobacteria, soil nutrients and maize seed germination. *IET Nanobiotechnol.* 7, 70–77. doi: 10.1049/iet-nbt.2012.0048

Kealhofer, L., Huang, F., DeVincenzi, M., and Morris, M. K. (2015). Phytoliths in Chinese foxtail millet (*Setaria italica*). *Rev. Palaeobot. Palynol.* 223, 116–127. doi: 10.1016/j.revpalbo.2015.09.004

Kealhofer, L., and Piperno, D. R. (1998). "Opal Phytoliths in Southeast Asian Flora," in *Smithsonian Contributions to Botany*, *Vol. 88*, eds D. Piperno and L. Kealhofer (Washington, DC: Smithsonian Institution Press), 1–39.

Kellogg, E. A. (2015). "Flowering plants, monocots, Poaceae," in *The Families and Genera of Vascular Plants*, ed K. Kubitski (Cham; Heidelberg: Springer), 1–416.

Kellogg, E. A., Aliscioni, S. S., Morrone, O., Pensiero, J., and Zuloaga, F. (2009). A phylogeny of Setaria (Poaceae, Panicoideae, Paniceae) and related genera based on the chloroplast gene ndhF. *Int. J. Plant Sci.* 170, 117–131. doi: 10.1086/593043

Kow, K. W., Yusoff, R., Aziz-Abdul, A. R., and Abdullah, E. C. (2014). Characterisation of bio-silica synthesized from cogon grass. *Powder Technol.* 254, 206–2013. doi: 10.1016/j.powtec.2014.01.018

Krishnan, S., Samson, N. P., Ravichandran, P., Narasimhan, D., and Dayanandan, P. (2000). Phytoliths of Indian grasses and their potential use in identification. *Bot. J. Linn. Soc.* 132, 241–252. doi: 10.1111/j.1095-8339.2000.tb01529.x

Kumar, A. (2014). *Exploration and Systematics of the grass flora of Punjab*. Ph.D. thesis, Guru Nanak Dev University, Amritsar (Punjab) India.

Kumar, S., and Elbaum, R. (2018). Interplay between silica deposition and viability during the life span of sorghum silica cells. *New Phytol.* 217, 1137–1145. doi: 10.1111/nph.14867

Kumar, S., Soukup, M., and Elbaum, R. (2017). Silicification in grasses: variation between different cell types. *Front. Plant Sci.* 8:438. doi: 10.3389/fpls.2017.00438

Lanning, F. C., and Eleuterius, L. N. (1981). Silica and ash in several marsh plants. *Gulf Caribb. Res.* 7, 47–52.

Lanning, F. C., and Eleuterius, L. N. (1987). Silica and ash in native plants of the central and southeastern regions of the United States. *Ann. Bot.* 60, 361–375. doi: 10.1093/oxfordjournals.aob.a087456

Lanning, F. C., and Eleuterius, L. N. (1989). Silica deposition in some C3 and C4 species of grasses, sedges and composites in the USA. *Ann. Bot.* 64, 395–410. doi: 10.1093/oxfordjournals.aob.a087858

La Roche, J. (1977). La silice et les plantes superieures. *Revue Cytol. Biol. Veg.* 40, 15–46.

Lau, E., Goldoftas, M., Baldwin, V. D., Dayanandan, P., Srinivasan, J., and Kaufman, P. B. (1978). Structure and localization of silica in the leaf and internodal epidermal system of the marsh grass *Phragmites australis*. *Can. J. Bot*. 56, 1696–1701. doi: 10.1139/b78-199

Layton, D. J., and Kellogg, E. A. (2014). Morphological, phylogenetic, and ecological diversity of the new model species *Setaria viridis* (Poaceae: Paniceae) and its close relatives. *Can. J. Bot.* 101, 539–557. doi: 10.3732/ajb.1300428

Lerseten, N. (1983). Crystals of calcium compound in Gramineae. *New Phytol.* 93, 633–637. doi: 10.1111/j.1469-8137.1983.tb02713.x

Lu, H., and Liu, K. (2003). Phytoliths of common grasses in the coastal environments of southeastern USA. *Estuar. Coast. Shelf Sci.* 58, 587–600. doi: 10.1016/S0272-7714(03)00137-9

Lu, H., Zhang, J., Wu, N., Liu, K. B., Xu, D., and Li, Q. (2009). Phytoliths analysis for the discrimination of foxtail millet *(Setaria italica*) and common millet (*Panicum miliaceum*). *PLoS ONE* 4:e4448. doi: 10.1371/journal.pone.0004448

Lux, A., Luxova, M., Abe, J., Tanimoto, E., Hattori, T., and Inanaga, S. (2003). The dynamics of silicon deposition in the Sorghum root endodermis. *New Phytol.* 158, 437–441. doi: 10.1046/j.1469-8137.2003.00764.x

Ma, J. F., and Yamaji, N. (2006). Silicon uptake and accumulation in higher plants. *Trends Plant Sci*. 11, 39–397. doi: 10.1016/j.tplants.2006.06.007

Ma, J. F., and Yamaji, N. (2015). A cooperative system of silicon transport in plants. *Trends Plant Sci.* 20, 435–442. doi: 10.1016/j.tplants.2015.04.007

Ma, J. F., Yamaji, N., and Mitani-Ueno, N. (2011). Transport of silicon from roots to panicles in plants. *Proc. Jpn. Acad. Ser. B Phys. Biol. Sci.* 87, 377–385. doi: 10.2183/pjab.87.377

Madella, M., Alexandr,é, A., and Ball, T. (2005). International code for phytolith nomenclature 1.0. *Ann. Bot*. 96, 253–260. doi: 10.1093/aob/mci172

Madella, M., García-Granero, J. J., Out, W. A., Ryan, P., and Usai, D. (2014). Microbotanical evidence of domestic cereals in Africa 7000 years ago. *PLoS ONE* 9:e110177. doi: 10.1371/journal.pone.0110177

Madella, M., and Lancelotti, C. (2012). Taphonomy and phytoliths: a usermanual. *Quat. Int*. 275, 76–83. doi: 10.1016/j.quaint.2011.09.008

Madella, M., Lancelotti, C., and García-Granero, J. J. (2016). Millet microremains-an alternative approach to understand cultivation and use of critical crops in Prehistory. *Archaeol. Anthropol. Sci.* 8, 17–28. doi: 10.1007/s12520-013-0130-y

Mann, S., and Perry, C. C. (1986). Structural aspects of biogenic silica. In Silicon Biochemistry. *Ciba Found. Symp.* 121:40e58.

Marinoni, L. D. R., Zabala, J. M., Exner, E. D. L., and Pensiero, J. F. (2013). Germinative behavior and forage potential of *Setaria magna* (Poaceae). *Bol. Soc. Argent. Bot.* 48, 261–270.

Matoh, T., Kairusmee, P., and Takahashi, E. (1986). Salt-induced damage to rice plants and alleviation effect of silicate. *Soil. Sci. Plant Nutr***.** 32, 295–304. doi: 10.1080/00380768.1986.10557506

Mazumdar, J. (2011). Phytoliths of pteridophytes. *S. Afr. J. Bot.* 77, 10–19. doi: 10.1016/j.sajb.2010.07.020

Metcalfe, C. R. (1960). *Anatomy of the Monocotyledons: I. Gramineae.* London: Oxford University Press.

Morris, L. R., Baker, F. A., Morris, C., and Ryel, R. J. (2009). Phytolith types and type-frequencies in native and introduced species of the sagebrush steppe and pinyon-juniper woodlands of the Great Basin, USA. *Rev. Palaeobot. Palynol.* 157, 339–357. doi: 10.1016/j.revpalbo.2009.06.007

Morrone, O., Aagesen, L., Scataglini, M. A., Salariato, D. L., Denham, S. S., Chemisquy, M. A., et al. (2012). Phylogeny of the Paniceae (Poaceae: Panicoideae): integrating plastid DNA sequences and morphology into a new classification. *Cladistics* 28, 333–356. doi: 10.1111/j.1096-0031.2011.00384.x

Morrone, O., Aliscioni, S. S., Veldkamp, J. F., Pensiero, J. F., Zuloaga, F. O., and Kellogg, E. A. (2014). Revision of the Old World species of *Setaria* (Poaceae: Panicoideae: Paniceae). *Syst. Bot. Monogr.* 96, 1–161.

Motomura, H., Mita, N., and Suzuki, M. (2002). Silica accumulation in long-lived leaves of *Sasa veitchii* (Carrie're) rehder (Poaceae, bambusoideae). *Ann. Bot.* 90, 149–152. doi: 10.1093/aob/mcf148

Mourhly, A., Khachani, M., Hamidi, E. A., Kacimi, M., Halim, M., and Arsalane, S. (2015). The synthesis and characterization of low-cost mesoporous silica SiO2 from local pumice rock. *Nanomater. Nanotechno.* 5, 1–7. doi: 10.5772/62033

Mulholland, S. C. (1989). Phytolith shape frequencies in North Dakota grasses: a comparison to general patterns. *J. Archaeol. Sci.* 16, 489–511. doi: 10.1016/0305-4403(89)90070-8

Neethirajan, S., Gordon, R., and Wang, L. (2009). Potential of silica bodies (phytoliths) for nanotechnology. *Trends Biotechnol*. 27, 461–467. doi: 10.1016/j.tibtech.2009.05.002

Netolitsky, F. (1929). Die Kieselkorper. Linsbauer'sHandb. Der Pflanzenanatomie. Berlin: Gebrude

Okuda, A., and Takahashi, E. (1962). Studies on the physiological role of silicon in crop plant. Part 8 Some examination on the specific behavior of low land rice in silicon uptake. *Jap. J. Soil Sci. Manr.* 33, 217–221.

Ollendorf, A. L., Mulholland, S. C., and Rapp, G. Jr. (1988). Phytolith analysis as a means of plant identification: *Arundo donax* and *Phragmites communis*. *Ann. Bot.* 61, 209–214. doi: 10.1093/oxfordjournals.aob.a087544

Ou, D. L., and Seddon, A. B. (1997). Near- and mid-infrared spectroscopy of sol–gel derived ormosils: vinyl and phenyl silicates. *J. Non-Cryst. Solids* 210, 187–203. doi: 10.1016/S0022-3093(96)00585-6

Out, W. A., Grau, J. F. P., and Madella, M. (2014). A new method for morphometric analysis of opal phytoliths from plants. *Microsc. Microanal.* 20, 1876–1887. doi: 10.1017/S1431927614013270

Out, W. A., and Madella, M. (2016). Morphometric distinction between bilobate phytoliths from *Panicum miliaceum* and *Setaria italica* leaves. *Archaeol. Anthropol. Sci.* 8, 505–521. doi: 10.1007/s12520-015-0235-6

Out, W. A., and Madella, M. (2017). Towards improved detection and identification of crop by-products: morphometric analysis of bilobate leaf phytoliths of *Pennisetum glaucum* and *Sorghum bicolor*. *Quat. Int*. 434, 1–4 doi: 10.1016/j.quaint.2015.07.017

Palanivelu, R., Padmanaban, P., Sutha, S., and Rajendran, V. (2014). Inexpensive approach for production of high-surface-area silica nanoparticles from rice hulls biomass. *IET Nanobiotechnol.* 8, 290–294. doi: 10.1049/iet-nbt.2013.0057

Parr, J. F., and Sullivan, L. A. (2005). Soil carbon sequestration in phytoliths. *Soil Biol. Biochem*. 37, 117–124. doi: 10.1016/j.soilbio.2004.06.013

Parr, J. F., and Sullivan, L. A. (2014). Comparison of two methods for the isolation of phytolith occluded carbon from plant material. *Plant Soil* 374, 45–53. doi: 10.1007/s11104-013-1847-1

Parry, D. W., Hodson, M. J., and Sangster, A. G. (1984). Some recent advances in studies of silicon in higher plants. *Phil. Trans. R. Soc. Lond. B* 304, 537–549. doi: 10.1098/rstb.1984.0045

Parry, D. W., and Smithson, F. (1958a). Silicification of bulliform cells in grasses. *Nature* 181, 1549–1550. doi: 10.1038/1811549b0

Parry, D. W., and Smithson, F. (1958b). Silicification of branched cells in the leaves of *Nardus stricta* L. *Nature* 182, 1460–1461. doi: 10.1038/1821460b0

Pearsall, D., Chandler-Ezell, K., and Chandler-Ezell, A. (2003). Identifying maize in neotropicalsediments and soils using cob phytoliths. *J. Archaeol. Sci.* 30, 611–627. doi: 10.1016/S0305-4403(02)00237-6

Pearsall, D. M. (1978). Phytolith analysis of archeological soils: evidence for maize cultivation in formative Ecuador. *Science* 199, 177–178. doi: 10.1126/science.199.4325.177

Pearsall, D. M. (2000). *Paleoethnobotany: A Handbook of Procedures, 2nd Edn,* San Diego, CA: Academic Press.

Pearsall, D. M. (2015). *Paleoethnobotany: A Handbook of Procedures*. New York, NY: Left Coast Press.

Pearsall, D. M., and Trimble, M. K. (1984). Identifying past agricultural activity through soil phytolith analysis: a case study from the Hawaiian Islands. *J. Archaeol. Sci.* 11, 119–133. doi: 10.1016/0305-4403(84)90047-5

Pearsall, D., Piperno, D., Dinan, E.h., Umlauf, M., Zhao, Z., and Benfer, R. A. (1995). Distinguishing rice (*Oryza Sativa* Poaceae) from wild *Oryza* species through phytolith analysis: results of preliminary research. *Econ. Bot.* 49, 183–196. doi: 10.1007/BF02862923

Pease, D. S., and Anderson, J. U. (1969). Opal phytoliths in *Bouteloua eriopoda* torr. roots and soils[1]. *Soil Sci. Soc. Am. J.* 33, 321–322. doi: 10.2136/sssaj1969.03615995003300020043x

Pensiero, J. F. (1999). Las especies sudamericanas del género Setaria (Poaceae, Paniceae). *Darwiniana*, 37–151.

Piperno, D. (1998). Palaeoethnobotany in the neotropics from microfossils: new insights into ancient plant use and agricultural origins in the tropical forest. *J. W. Prehistory* 12, 393–449. doi: 10.1023/A:1022812132194

Piperno, D., and Pearsall, D. (1993). Phytoliths in the reproductive structures of maize and teosinte: implications for the study of maize evolution. *J. Archaeol. Sci.* 20, 337–362. doi: 10.1006/jasc.1993.1021

Piperno, D. R. (1984). A comparison and differentiation of phytoliths from maize and wild grasses: use of morphological criteria. *Am. Antiq.* 49, 361–383. doi: 10.2307/280024

Piperno, D. R. (1985). Phytolith analysis and tropical paleo-ecology: production and taxonomic significance of siliceous forms in new world plant domesticates and wild species. *Rev. Palaeobot. Palynol.* 45, 185–228. doi: 10.1016/0034-6667(85)90002-8

Piperno, D. R. (1988). *Phytolith Analysis: An Archaeological and Geological Perspective*. San Diego, CA: Academic Press.

Piperno, D. R. (2001). "Phytoliths," in *Tracking Environmental Change Using Lake Sediments, Terrestrial, Algal, and Siliceous Indicators*, eds J. P. Smol, H. J. B. Birks, and W. M. Last (Dordrecht: Kluwer Academic), 235–251.

Piperno, D. R. (2006). *Phytoliths: A Comprehensive Guide for Archaeologists and Paleoecologists.* New York, NY: Alta Mira Press.

Piperno, D. R. (2009). Identifying crop plants with phytoliths (and starch grains) in Central and South America: a review and an update of the evidence. *Quat. Int.* 193, 146–159. doi: 10.1016/j.quaint.2007.11.011

Piperno, D. R., Andres, T. C., and Stothert, K. E. (2000). Phytoliths in *Cucurbita* and other neotropical cucurbitaceae and their occurrence in early archaeological sites from the lowland american tropics. *J. Archeol. Sci.* 27, 193–208. doi: 10.1006/jasc.1999.0443

Piperno, D. R., and Pearsall, D. (1998). *The Silica Bodies of Tropical American Grasses: Morphology, Taxonomy, and Implications for Grass Systematics and Fossil Phytolith Identification.* Washington, DC: Smithsonian Institution Press.

Ponzi, R., and Pizzolongo, P. (2003). Morphology and distribution of epidermal phytoliths in *Triticum aestivum* L. *Plant Biosyst.* 137, 3–10. doi: 10.1080/11263500312331351271

Prasad, V., Stromberg, C. A., Alimohammadian, H., and Sahni, A. (2005). Dinosaur coprolites and the early evolution of grasses and grazers. *Science* 310, 1177–1180. doi: 10.1126/science.1118806

Prasad, V., Strömberg, C. A. E., Leaché, A. D., Samant, B., Patnaik, R., Tang, L., et al. (2011). Late Cretaceous origin of the rice tribe provides evidence for early diversification in Poaceae. *Nat. Commun.* 2:480. doi: 10.1038/ncomms1482

Prat, H. (1936). La systematique des graminees. *Ann. Sci. Bot.* 18, 165–258.

Prat, H. (1948). General features of the epidermis in Zea mays. *Ann. Missouri Bot. Garden* 35, 341–351. doi: 10.2307/2394699

Prychid, C. J., Rudall, P. J., and Gregory, M. (2004). Systematics and biology of silica bodies in monocotyledons. *Bot. Rev.* 69, 377–440. doi: 10.1663/0006-8101(2004)069[0377:SABOSB]2.0.CO;2

Qadri, S. B., Gorzkowski, E., Rath, B. B., Feng, J., Qadri, S. N., Kim, H., et al. (2015). Nanoparticles and nanorods of silicon carbide from the residues of corn. *J. Appl. Phys.* 117:044306. doi: 10.1063/1.4906974

Quigley, K. M., and Anderson, T. M. (2014). Leaf silica concentration in Serengeti grasses increases with watering but not clipping: insights from a common garden study and literature review. *Front. Plant Sci.* 5:568. doi: 10.3389/fpls.2014.00568

Rajendiran, S., Coumar, M. V., Kundu, S., Dotaniya, A. M., and Rao, A. S. (2012). Role of phytolith occluded carbon of crop plants for enhancing soil carbon sequestration in agro-ecosystems. *Curr. Sci.* 103, 911–920.

Raven, J. A. (1983). The transport and function of silicon in plants. *Biol. Rev.* 58, 179–207. doi: 10.1111/j.1469-185X.1983.tb00385.x

Raven, J. A. (2003). Cycling silicon-the role of accumulation in plants. *New Phytol.* 158, 419–430. doi: 10.1046/j.1469-8137.2003.00778.x

Reid, C. S., Patrick, D. A., He, S., Fotie, J., Premalatha, K., Tidwell, R. R., et al. (2011). Synthesis and antitrypanosomal evaluation of derivatives of N-benzyl-1, 2-dihydroquinolin-6-ols: effect of core substitutions and salt formation. *Bioorganic Med. Chem.* 19, 513–523. doi: 10.1016/j.bmc.2010.11.003

Rominger, J. M. D., Setaria, P., Beauv. In: Barkworth, M. E., Capels, K. M., Long, S., and Piep, M. B. (2003) (eds). *Flora of North America North of Mexico, Magnoliophyta: Commelinidae (in part): Poaceae, part 1, Vol. 25.* New York, NY: Oxford University Press.

Rosen, A. M., and Weiner, S. (1994). Identifying ancient irrigation: a new method using opaline phytoliths from Emmer wheat. *J. Archaeol. Sci.* 21, 125–132. doi: 10.1006/jasc.1994.1013

Rovner, I. (1971). Potential of opal phytoliths for use in palaeoecological reconstruction. *Quat. Res.* 1, 345–359. doi: 10.1016/0033-5894(71)90070-6

Rovner, I. (1983). Plant opal phytolith analysis: major advances in archaeobotanical research. *Adv. Archaeol. Method Theory* 6, 225–266. doi: 10.1016/B978-0-12-003106-1.50011-0

Ru, N., Yang, X., Song, Z., Liu, H., Hao, Q., Liu, X., et al. (2018). Phytoliths and phytolith carbon occlusion in aboveground vegetation of sandy grasslands in eastern Inner Mongolia, China. *Sci. Total Env.* 625, 1283–1289. doi: 10.1016/j.scitotenv.2018.01.055

Rudall, J. P., Prychid, J. C., and Gregory, T. (2014). Epidermal patterning and silica phytoliths in grasses: an evolutionary history. *Bot. Rev.* 80, 59–71. doi: 10.1007/s12229-014-9133-3

Runge, F. (1999). The opal phytolith inventory of soils in central Africa—quantities, shapes, classification, and spectra. *Rev. Palaeobot. Palynol.* 107, 23–53. doi: 10.1016/S0034-6667(99)00018-4

Ryan, P. (2011). Plants as material culture in the Near Eastern Neolithic: Perspectives from the silica skeleton artifactual remains at Çatalhöyük. *J. Anthropol. Archaeol.* 30, 292–305. doi: 10.1016/j.jaa.2011.06.002

Sandoval-Zapotitla, E., Terrazas, T., and Villaseñor, J. L. (2010). Diversidad de inclusiones minerales en la subtribu Oncidiinae (Orchidaceae). *Rev. Biol. Trop.* 58, 733–755. doi: 10.15517/rbt.v58i2.5242

Sangster, A. G., and Parry, D. W. (1971). Silica deposition in the grass leaf in relation to transpiration and the effect of dinitrophenol. *Ann. Bot.* 35, 667–677. doi: 10.1093/oxfordjournals.aob.a084511

Sato, K. (1968). The existence of calcium oxalate crystals in pulvinus of rice plants. *Proc. Crop. Sci. Soc. Jpn* 37, 458–459. doi: 10.1626/jcs.37.458

Sato, K., and Shibata, S. (1981). Crystal statolith at palvinus of rice leaf (in Japanese). *Jpn. J .Crop Sci.* 50, 77–78. doi: 10.1626/jcs.50.77

Schellenberg, H. C. (1908). "Wheat and Barley from the North Kurgan, Anau,". in *Explorations in Turkestan*, ed R. Pumpelly (Washington, DC*: Carnegie Institution*), 471–473.

Schoelynck, J., Bal, K., Backx, H., Okruszko, T., Meire, P., and Struyf, E. (2010). Silica uptake in aquatic and wetland macrophytes: a strategic choice between silica, lignin and cellulose? *New Phytol.* 186, 385–391. doi: 10.1111/j.1469-8137.2009.03176.x

Shaheen, S., Mushtaq, A., Farah, K., Muhammad, Z., Mir, A. K., Shazia, S., et al. (2011). Systematic application of palyno-anatomical characterization of *Setaria* species based in scanning electron microscopy (SEM) and light microscope (LM) analysis. *J. Med. Plants Res.* 5, 5803–5809.

Shakoor, S. A., Bhat, M. A., Mir, S. H., and Soodan, A. S. (2014). Investigations into phytoliths as diagnostic markers for the grasses (Poaceae) of Punjab. *Univers. J. Plant. Sci.* 2, 107–122. doi: 10.13189/ujps.2014.020602

Shakoor, S. A., Bhat, M. A., and Soodan, A. S. (2016). Taxonomic demarcation of *Arundo donax* L. and *Phragmites karka* (Retz.) Trin. ex Steud.(Arundinoideae, Poaceae) from phytolith signatures. *Flora-Morphol. Dist. Funct. Eco. Plants* 224, 130–153. doi: 10.1016/j.flora.2016.07.011

Sharma, M. L., and Kaur, S. (1983). Leaf epidermal studies in Gramineae. *Res. Bull.* 34, 77.

Sharma, M. L., and Khosla, P. K. (1989). *Grasses of Punjab and Chandigarh*. Lahore: Publication Bureau, Punjab University.

Shi, Y., Wang, T., Li, Y., and Darmency, H. (2008). Impact of transgene inheritance on the mitigation of gene flow between crops and their wild relatives: the example of foxtail millet. *Genetics* 180, 969–975. doi: 10.1534/genetics.108.092809

Shillito, L. M. (2013). Grains of truth or transparent blindfolds*? A review of current debates in archaeological phytolith analysis. Veg. Hist. Archaeobot.* 22, 71–82. doi: 10.1007/s00334-011-0341-z

Socrates, G. (2001). *Infrared and Raman Characteristic Group Frequencies: Tables and Charts*. Chichester: John Wiley and Sons.

Soreng, J. R., Paul, M. P., Konstantin, R., Gerrit, D., Jordan, K. T., Lynn, G. C., et al. (2017). A worldwide phylogenetic classification of the Poaceae (Gramineae) II: an update and a comparison of two 2015 classifications. *J. Syst. Evol.* 55, 259–290. doi: 10.1111/jse.12262

Soukup, M., Martinka, M., Cigán, M., Ravaszová, F., and Lux, A. (2014). New method for visualization of silica phytoliths in *Sorghum bicolor* roots by fluorescence microscopy revealed silicate concentration-dependent phytolith formation. *Planta* 240, 1365–1372. doi: 10.1007/s00425-014-2179-y

Stapf, O., and Hubbard, C. E. (1934). *Flora of tropical Africa.* Ashford: Kent, L. Reeve and Co., Ltd.

Stebbins, G. L. (1972). "The Evolution of the Grass Family," in *The Biology and Utilization of Grasses*, eds Younger and C. M. Mc Kell (New York, NY: Academic Press), 1–17.

Stebbins, G. L. (1981). Coevolution of grasses and herbivores. *Ann. Mo. Bot. Gard.* 68, 75–86. doi: 10.2307/2398811

Strömberg, C. A. (2009). Methodological concerns for analysis of phytolith assemblages: does count size matter? *Quat. Int.* 193, 124–140. doi: 10.1016/j.quaint.2007.11.008

Struyf, E., and Conley, D. J. (2012). Emerging understanding of the ecosystem silica filter. *Biogeochemistry* 107, 9–18. doi: 10.1007/s10533-011-9590-2

Szabo, L. Z., Kovács, S., Balogh, P., Daróczi, L., Penksza, K., and Peto, A. (2015). Quantifiable differences between phytolith assemblages detected at species level: analysis of the leaves of nine *Poa species* (Poaceae). *Acta Soc. Bot. Pol.* 84, 369–383. doi: 10.5586/asbp.2015.027

Szabo, L. Z., Kovacs, S., and Peto, A. (2014). Phytolith analysis of *Poa pratensis* (Poaceae) leaves. *Turk. J. Bot.* 38, 851–863. doi: 10.3906/bot-1311-8

Tomlinson, P. B. (1956). Studies in the systematic anatomy of the *Zingiberaceae*. *Bot. J. Linn. Soc.* 55, 547–559 doi: 10.1111/j.1095-8339.1956.tb00023.x

Tomlinson, P. B. (1961). Morphological and anatomical characteristics of the Marantaceae. *Bot. J. Linn. Soc.* 58, 55–78 doi: 10.1111/j.1095-8339.1961.tb01080.x

Tomlinson, P. B. (1969). *Anatomy of the Monocotyledons III: Commelinales-Zingiberales*. London: Oxford University Press.

Traoré, D. L., Traoré, S., and Diakité, S. (2014). Bauxite industry in guinea and value opportunities of the resulting red mud as residue for chemical and civil engineering purposes. *J. Civil Eng. Res.* 4, 14–24. doi: 10.5923/j.jce.20140401.03

Tripathi, D. K., Mishra,. S., Chauhan, D. K., Tiwari, S. P., and Kumar, C. (2013). Typological and frequency based study of opaline silica (phytolith) deposition in two common Indian *Sorghum* L. *species. Proc. Natl. Acad. Sci. India Sect. B Biol. Sci.* 83, 97–104. doi: 10.1007/s40011-012-0066-5

Tsartsidou, G., Lev-Yadun, S., Albert, R. M., Miller-Rosen, A., Efstratiou, N., and Weiner, S. (2007). The phytolith archaeological record: strengths and weaknesses evaluated based on a quantitative modern reference collection from Greece. *J. Archaeol. Sci.* 34, 1262–1275. doi: 10.1016/j.jas.2006.10.017

Twiss, P. C., Suess, E., and Smith, R. M. (1969). Morphological classification of grass phytoliths. *Proc. Soil Sci. Soci. Am. J.* 33, 109–115. doi: 10.2136/sssaj1969.03615995003300010030x

Veldkamp, J. F. (1994). Miscellaneous notes on Southeast Asian Gramineae. IX. *Blumea* 39, 373–384.

Wang, X., Jiang, H., Shang, x., Wang, T., Wu, Y., Zhang, P., et. al. (2014). Comparison of dry ashing and wet oxidation methods for recovering articulated husk phytoliths of foxtail millet and common millet from archaeological soil. *J. Archaeol. Sci.* 45, 234–239. doi: 10.1016/j.jas.2014.03.001

Wang, Y. J., and Lu, H. Y. (1993). *The Study of Phytolith and Its Application*. Beijing: China Ocean Press.

Watling, M. K., Parr, J. F., Rintoul, L., Brown, L. C., and Sullivan, A. L. (2011). Raman: infrared and XPS study of bamboo phytoliths after chemical digestion. *Spectrochimica Acta* 80, 106–111. doi: 10.1016/j.saa.2011.03.002

Watson, L., and Dallwitz, M. (1992). *The Grass Genera of the World*. Wallingford: C.A.B. International.

Webster, R. D. (1987). *The Australian Paniceae* (*Poaceae*). Stuttgart: J. Cramer.

Webster, R. D. (1993). Nomenclature of setaria (Poaceae: Paniceae). *SIDA Contrib. Bot.* 447–489.

Webster, R. D. (1995). Nomenclatural changes in Setaria and Paspalidium (Poaceae: Paniceae). *SIDA Contrib. Bot.* 439–446.

Weisskopf, A., Harvey, E., Kingwell-Banham, E., Kajale, M., Mohanty, R., and Fuller, D. Q. (2014). Archaeobotanical implications of phytolith assemblages from cultivated rice systems, wild rice stands and macro-regional patterns. *J. Archaeol. Sci.* 51, 43–53. doi: 10.1016/j.jas.2013.04.026

Weisskopf, A. R., and Lee, G. A. (2016). Phytolith identification criteria for foxtail and broom corn millets: a new approach to calculating crop ratios. *Archaeol. Anthropol. Sci.* 8, 29–42. doi: 10.1007/s12520-014-0190-7

Whang, S., Kim, S. K., and Hess, W. M. (1998). Variation of silica bodies in leaf epidermal long cells within and among seventeen species of *Oryza* (Poaceae). *Am. J. Bot.*. 85, 461–466. doi: 10.2307/2446428

Wilding, L. P., and Drees, L. R. (1973). Scanning Electron Microscopy of opaque opaline forms isolated from forest soils in ohio 1. *Soil Sci. Soc. Am. J.* 37, 647–650. doi: 10.2136/sssaj1973.03615995003700040047x

Yang, X., Song, Z., Liu, H., Van Zwieten, L., Song, A., Li, Z., et al. (2018). Phytolith accumulation in broadleaf and conifer forests of northern China: implications for phytolith carbon sequestration. *Geoderma* 312, 36–44. doi: 10.1016/j.geoderma.2017.10.005

Yeo, A. R., Flowers, S. A., Rao, G., Welfare, K., Senanayake, N., and Flowers, T. J. (1999). Silicon reduces sodium uptake in rice (*Oryza sativa* L.) in saline conditions and this is accounted for by a reduction in the transpirational by pass flow. *Plant Cell Environ.* 22, 559–565.

Zhang, J., Lu, H., Gu, W., Wu, N., Zhou, K., Hu, Y., et al. (2012). Early mixed farming of millet and rice 7800 years ago in the middle yellow river region, China. *PLoS ONE* 7:e52146. doi: 10.1371/journal.pone.0052146

Zhang, J., Lu, H., and Wu, N. (2010). Phytolith evidence for rice cultivation and spread in Mid-Late Neolithic archaeological sites in central North China. *Boreas* 39, 592–602. doi: 10.1111/j.1502-3885.2010.00145.x

Zhang, J., Lu, H., Wu, N., Yang, X., and Diao, X. (2011). Phytolith analysis for differentiating between Foxtail Millet (SetariaItalica) and Green Foxtail (*Setaria Viridis*). *PLoS ONE* 6:e19726. doi: 10.1371/journal.pone.0019726

Zhao, Z. (2011). New archaeobotanic data for the study of the origins of agriculture in China. *Curr. Anthropol.* 52, S295–S306. doi: 10.1086/659308

Conflict of Interest Statement: The authors declare that the research was conducted in the absence of any commercial or financial relationships that could be construed as a potential conflict of interest.

Annals of Plant Sciences 7.3 (2018) pp. 2096-2100

ANNALS OF PLANT SCIENCES
ISSN: 2287-688X
OPEN ACCESS
www.annalsofplantsciences.com

Research Article

Taxonomic description and annotation of *Poa albertii* Regel (Poaceae: Pooideae, Poeae, Poinae) from North Western Himalayas, India.

Mudassir Ahmad Bhat[1], Sheikh Abdul Shakoor[1,2] and Amarjit Singh Soodan[1]*

[1]Systematics and Biodiversity Laboratory, Department of Botanical and Environmental Sciences, Guru Nanak Dev University, Amritsar, Punjab-143005, India.

[2]Department of Botany, Govt. Degree College, Kulgam (J & K) - 192231, India.

Received: 1/27/2018; **Accepted:** 2/19/2018

Abstract: *Poa albertii* Regel, a native to Central Asia, has been described from North-Western Himalayan region and annotated to the latest system of grass classification. A detailed taxonomic description in the latest format, along with illustrations and Scanning Electron Micrograph of diagnostic features is provided to diagnose *P. albertii* Regel from allied species.

Keywords: Grasses, Poa, Himalayas, Taxonomy.

Introduction

Poa L. Salkimotu Cabi and Dogan, 2012) is the type genus of the grass family Poaceae Barnhart. The genus includes more than 550 species distributed worldwide (Gillespie and Soreng, 2005). A majority of species occur in temperate to alpine regions. Species identification in the genus is rendered difficult by the existence of polymorphism and high incidence of polyploidy, apomixis and hybridization (Stebbins, 1950; Clausen, 1961; Tzvelev, 1983; Hunziker and Stebbins, 1987; Kavousi et al., 2015). Clayton and Renvoize (1986) concluded that Poa was an extremely uniform genus for which infrageneric classification was difficult to achieve. The affinities of nearly half of the species are unknown while rest of the species has been put in informal groups (Soreng et al., 2009).

Despite difficulties mentioned in the preceding part, *Poa* has attracted the attention of several agrostologists including Bor (1970) who reported 13 species of the genus from Iran. Other reports include Cope (1982) from Pakistan (33), Chen *et al.*, (2006) from China (156), Press *et al.*, (2000) from Nepal (32), Noltie (2000) from Bhutan including some parts of Sikkim and Darjeeling (29) with the species number given in the parenthesis. More recently, Soreng and Peterson (2012), provided a revisionary account of the genus from Mexico with new reports resulting from latest delimitation of species within the genus.

Despite wide distribution in the Himalayas, taxonomic works in the genus have been marked by unusually long intermissions. Stapf (1896) studied the genus for Hooker's 'Flora of British India' followed by Duthie (1883, 1906), Bor (1941, 1960), Stewart (1945), Raizada *et al.,* (1983), Babu (1977) and Naithani (1985). Rajbhandari (1991) published a taxonomic monograph of the genus *Poa* from the Himalayan region. The author included fifty two species with a key for their identification. Recently, Nautiyal and Gaur (2017) reported 45 species (and 2 subspecies) of the genus *Poa* spp. from Uttarakhand (India) with a key based on morphological characters. Olonova, *et al* (2017) has scrutinized the dwarf species of *Poa* section *Stenopoa* of the Himalayan region and demarcated ten species of which *Poa attenuata* Trin., *Poa glauca* Vahl and *Poa. albertii* Regel were put in a closely related group within the section.

The present paper validates P. *albertii* Regel through detailed taxonomic description supported by illustrations of diagnostic parts and a key to taxonomic demarcation.

Materials and Methods

Occurrence and Type Location: The species is common in alpine grazing meadows (3000-5200 m asl.) of the north-western Himalayan region. The species was collected from Nyoma (district Leh) in the cold desert of Ladakh. The site of collection is located at 33°12'197"N to 78°39'243"E at an elevation of 4203m asl and experiences a cold temperate climate. The species was collected on July 4, 2014 (Fig. 1) during explorations of the north-western Himalayan region for diversity of grasses. Herbarium sheets of preserved specimens have been deposited in the Herbarium of the Department of Botanical & Environmental

***Corresponding Author:**
Mudassir Ahmad Bhat,
Department of Botanical & Environmental Sciences,
Guru Nanak Dev University,
Amritsar (Punjab)-143005, India.
E-mail: assoodan@gmail.com

Sciences, Guru Nanak Dev University, Amritsar (voucher nos 7373 to 7375).

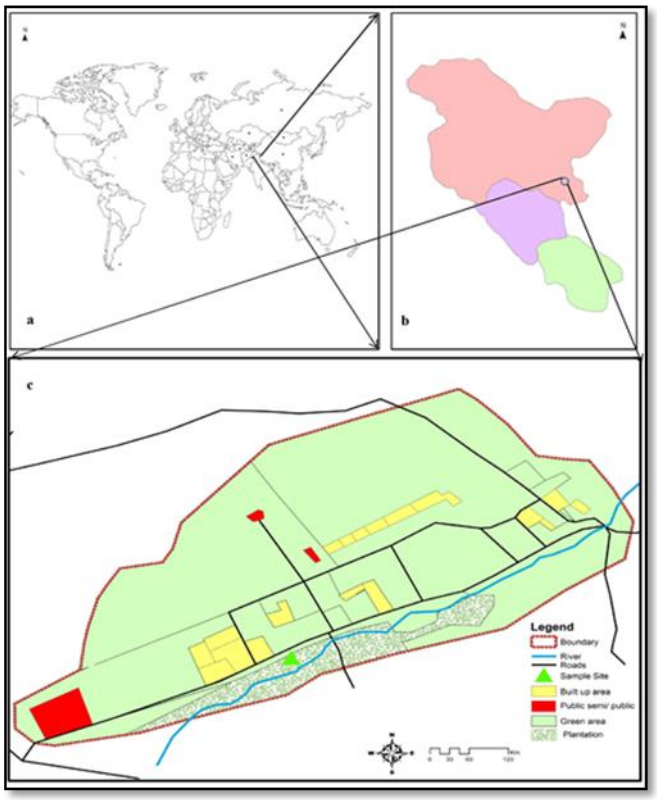

Fig. 1. a) Distribution of *Poa albertii* Regel b) North- Western Himalayan region c) Collection site of *Poa albertii* Regel.

Methodology: Stereoscopic examination of the specimens was followed by taxonomic description and identification with the help of taxonomic literature (Bor 1960) and online sources viz., e-floras of China, Pakistan, and Online Grass Flora of the world. Illustrations were prepared manually by drawing the vegetative and floral parts, tracing and inking the drawings followed by scanning with HP Scanjet G3110 scanner. Information on the distribution in temperate and tropical Asia has been included to indicate the places and areas that show a sizeable occurrence of the species (e-flora of China). Spikelet formula has been written in the format proposed by Allred and Columbus (1988) with some modifications. The spikelet diagram has been prepared in the software (Adobe Photoshop 7.0) by employing symbols improvised from time to time (Schaffner 1916, Arber 1934, Singh 1999, Subrahmanyam 2004, Craene 2010, Kumar 2014). In the diagram, lateral compression of the spikelets has been shown by drawing wedge shaped glumes followed by fertile florets indicated by horizontal solid lines and dashed lines represent reduced florets. Essential whorls have been indicated by three anthers with a unilocular ovary in the centre. A bifid style is also indicated. Surface features of caryopses were visualised and imaged through stereoscopic examination and Scanning Electron Microscopy (ZEISS-EVO LS10) operated at an accelerating voltage of 15 kv at appropriate magnifications.

Taxonomic account

Etymology: The generic name is a direct adoption of the feminine Greek noun, 'poa (πόα)= grass, fodder'. With no change of spelling, generic name ' Poa' is treated as a feminine noun even after adaption as a generic name because it has an established gender in the source language. Specific epithet is commemorative of the Swiss botanist, Albert Regel. The first name of the author has been put in the genitive case of a Latin noun employing the inflectional termination 'i' of the genitive case. As specific epithet commemorates a gentleman (not a woman), it is treated as a masculine epithet which, consequently, does not show gender accord with the feminine generic name.

Synonyms: *Poa albertii* var. *triflora* Regel Gamayunova, A. P. 1956. Poa. 1: 221–238. In Fl. Kazakstana. *Poa crymophila* Keng Tzvelev, N. N. 2001. Poa IN: Pl. Cent. Asia 4: 156–177. *Poa roshevitzii* Golosk. Filatova, N. S. 1969. Poa. 92–97. In N. S. Filatova Ill. Oprd. Rast. Kazakh. *Poa mustangensis* K.R. Rajbhandari, 1880. Act. Hort. Petrop. 7: 611. *Poa arnoldii* A. Melderis, 1978. Enum. Fl. Pl. Nepal, 1: 142. *Poa rangkulensis* Ovchinnikov &

Chukavina, lzvest. 1956. Otdel. Estestven. Nauk Akad. Nauk Tadzhik. SSR. 17: 41.

Taxonomic description: Perennial; Culm erect, 10-30 cm long. (Fig. 2a) Leaf blades 2.0-5.0 cm long, 1.0-1.5 mm wide. Ligule membranous, 1.5-2.0 mm long (Fig.2b). Inflorescence an open panicle, 4-8 cm long. Spikelets solitary, tinged with purple, 2-3 floreted, pedicelled, laterally compressed, 4.0-5.0 mm long (Fig. 2c). Disarticulation of spikelets above the glumes. Glumes unequal, (Fig.2d) lower glume lanceolate, 2.5-3.5 mm long, 1 keeled, 3 veined, apex acute (Fig. 2e). Upper glume, 3.0- 4.0 mm long, 1 keeled, 3 veined, 1.1-1.2 length of lower glume, 0.9-1.0 length of the fertile lemma (Fig.2f). Fertile lemma lanceolate, 3.0-4.5 mm long, lemma bigger than the glumes, 5 veined, keel shortly pubescent for half of its length, marginal veins for one third, other parts glabrous (Fig. 2g). Palea shorter than the lemma, keels scabrid (Fig. 2h). Lodicules 2, anthers 3, 1.2-1.5 mm long, stigmas 2. (Fig. 2i). A single fertile floret (enclosing the caryopsis) with rachilla segment and occasionally by a reduced floret as well is the dispersal unit (the diaspore). The diaspore is light yellow to purple in colour (Fig. 2 j-l). Caryopsis 1.0-1.5 mm long, reddish-brown, adherent pericarp, ovate to obovate with a slight lateral compression, hilum punctiform, stylopodium present(Fig. 2 m-n), surface reticulate with undulating striations (Fig. 2o-r). Common, in alpine grazing meadows, between 3000–5200 m elevation.

Flowering & Fruiting: June-September

Asia-Temperate: China; China North-Central, China South-Central, Inner Mongolia, Tibet, Xinjiang, Qinghai. Middle Asia; Kirgizistan, Tadzhikistan, Kazakhstan, Uzbekistan. Mongolia; Mongolia. Russia, Iran West Asia; Afghanistan.

Asia-Tropical: Indian Subcontinent; Eastern Himalaya, Nepal, Pakistan.

Spikelet formula:

R^1 : Reduced floret 1
F_5 : 2-3 fertile florets, lemma 5 veined
--- : Disarticulation above the glumes
G_3 : Lower glume 3 veined
G_3 : Upper glume 3 veined
Pan: Inflorescence, a panicle

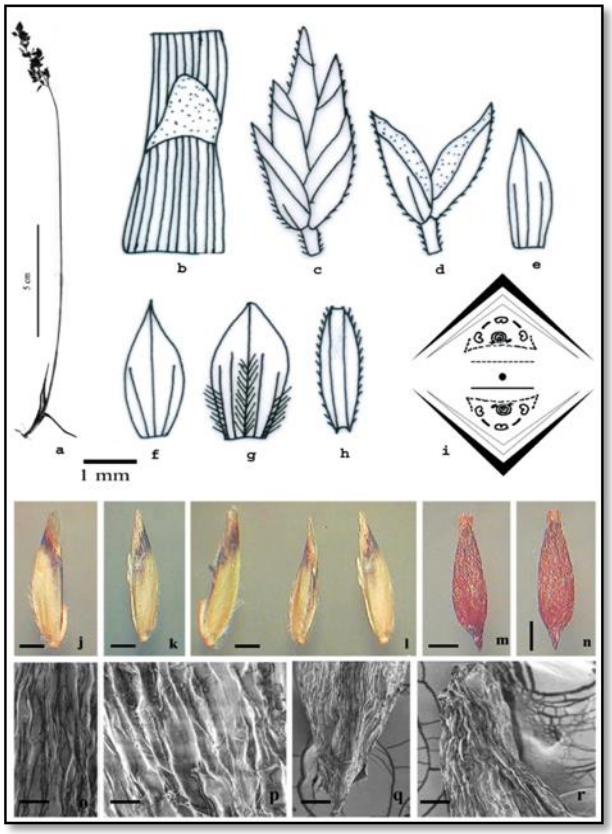

Fig. 2. ***Poa albertii***: a) habit; b) ligule; c) spikelet; d) glumes; e) lower glume, dorsal view; f) upper glume, dorsal view; g) lemma, dorsal view; h) palea; I) spikelet diagram; j-l) diaspore; m-n) caryopsis; o-r) SEM Micrographs of caryopsis [Bar: 5cm (a) 1mm (b-h) 0.7mm (j-l) 0.3mm (m-n) 50µm (o-p) 300µm (q-r)].

Table 1. Diagnosis of *Poa albertii* Regel from related species

Species	Ligule length (mm)	Spikelet length (mm)	Number of fertile florets	Callus surface	Surface between lemma veins
Poa albertii Regel	1.0-3.5	3.0-6.0	2-3	Glabrous	Glabrous
Poa attenuata Trin.	1.0-2.5	2.5-4.5	2-5	Webbed	Moderatly pubescent
Poa glauca Vahl	1.0-2.0	3.8-7.0	2-4	Glabrous or webbed	Glabrous or pubescent
Poa koelzii Bor	1.0-3.0	4.0-6.0	2-5	Glabrous	Densely pubescent
Poa lahulensis Bor	2.0-4.0	5.0-7.2	2-4	Glabrous or sometimes hairy	Sparsely pubescent

Identification key:

1. Plants densely tufted ……*Poa attenuata*
1b. Plants tufted moderately ……..2
2a. Lemma glabrous between the veins……..*Poa albertii*
2b. Lemma pubescent between the veins……3
3a. Callus glabrous or webbed…….*Poa glauca*
3b. Callus usually glabrous ……4
4a. Ligule 1-3 mm long ……..*Poa koelzii*
4b. Ligule 2-4 mm long…….....*Poa lahulensis*

Acknowledgements

The authors grateful to Professor Incharge Emerging Life Sciences Laboratory, Guru Nanak Dev University, Amritsar, Punjab (India) for Scanning Electron Microscopy (SEM) The help received from Mr. Musaib Ahmad Wani (Guru Ram Das School of Planning, GNDU, Amritsar) in designing the map of the study area is gratefully acknowledged. The first author is thankful to the University Grant Commission, New Delhi for financial assistance under Major Research Project (MRP) fellowship.

References

1. Allred, K, and Columbus, J.T. "The grass spikelet formula: an aid in teaching and identification. *Journal of Range Management* 41. (1988): 350-351. Print.

2. Arber, A. "*The gramineae: a study of cereal, bamboo and grass*". Cambridge University Press. (1934). Print.

3. Babu, C.R. "*Herbaceous Flora of Dehradun*" Council of Scientific and Industrial Reaserch (CSIR), New Delhi. (1977). Print.

4. Bor, N.L. "Some Common U.P. Grasses". *Indian For. Rec. n.s. Bot.* 2. (1941):1–220. Print.

5. Bor, N.L."*The Grasses of Burma, Ceylon, India and Pakistan (Excluding Bambuseae)"* Pergamon Press. (1960). Print.

6. Bor, N.L. "*Poa L. In: Rechinger K.H. (ed.), Flora Iranica"* Graz, Austria: Akademische Druck - u Verlagsanstalt. 70. (1970): 20–46. Print.

7. Cabi E, Doğan M "Poaceae. In Güner A, Aslan S, Ekim T, Vural M, Babaç MT, editors. Türkiye Bitkileri Listesi (Damarlı Bitkiler)". İstanbul, Turkey: Nezahat Gökyiğit Botanik Bahçesi ve Flora Araştırmaları Derneği Yayını. (2012): 690- 756. Print.

8. Chen S. *et al., Poa* L. In: www.eFloras.org Flora of China. Published on the Internet. (2006): http://www.efloras.org/flora_page.aspx?flora_id=2 /accessed on 28.07. 2017.

9. Clausen J, Introgression facilitated by apomixis in polyploidy Poas. *Euphytica* 10. (1961): 87–94. Print.

10. Clayton, W.D, and Renvoize, S.A. "Genera Graminum: Grasses of the World". London, UK. *Kew Bull.* 13. (1986): 1–389. Print.

11. Clayton, W.D., Vorontsova, M.S., Harman KT, Williamson H, "Grass Base - The Online World Grass Flora". 2006: http://www.kew.org/data/grasses-db.html/ accessed on 28.07. 2017.

12. Cope, T.A. "*Poa* L. In: www.eFloras.org Flora of Pakistan. Herbarium Royal Botanic Garden, Kew. Published on the Internet (1982): http://www.efloras.org/flora_page.aspx?flora_id=5 /accessed on 28.07. 2017.

13. Craene, L.P.R.D. *"Floral diagrams: an aid to understanding flower morphology and evolution*". The Edinburg Building, Cambridge CB2 8RU, Cambridge University Press, UK. (2010). Print.

14. Duthie, J.F. "*A list of the grasses of North-western India. Indigenous and cultivated*". Roorkee, (1883). Print.

15. Duthie, J.F. "*Catalogue of the Plants of Kumaon and of the Adjacent Portions of Garhwal and Tibet, based on the collections of Strachey and winter bottom during the years*" London, (1906): 1846-1849. Print.

16. Gillespie, L.J., and Soreng, R.A. "Phylogenetic analysis of the bluegrass genus *Poa* based on cpDNA restriction site data". *Syst. Bot.* 30. (2005): 84–105. Print.

17. Hunziker, J.H., and Stebbins, G.L. "*Chromosomal evolution in the Gramineae*". In: Soderstrom, T.R. *et al.,* (eds.), Grass Systematic and Evolution, Smithsonian Institution Press, Washington DC, USA. (1987): 179–187. Print.

18. Kavousi, M, Assadi, M, Nejadsattari, T. "Taxonomic revision of the genus *Poa* L. in Iran, new additions to Flora Iranica, and a new identification key". *Turk. J. Bot.* 39. (2015): 105–127. Print.

19. Kumar, A. "*Exploration and Systematics of the grass flora of Punjab*". Ph.D. Thesis, Guru Nanak Dev University. (2014). Print.

20. Naithani, B.D. "*Poa L. Flora of Chamoli*". Botanical Survey of India (BSI), Howrah, India. 2. (1985): 748–750. Print.

21. Noltie, H.J. "*Flora of Bhutan: The Grasses of Bhutan*". Royal Botanic Garden Edenburgh and Royal Government of Bhutan. 3. (2000): 549–572. Print.

22. Nautiyal, D.C, and Gaur, R.D. "*Poa* L. species in Uttarakhand, India and keys for their identification". *Taiwania***.** 62. (2017): 75–92. Print.

23. Olonova, M.V, Chen, Y, Miehe, S, Rajbhandri, K.R, and Barkworth, M. "Taxonomic notes on the dwarf bluegrasses (Poa L., Poaceae) of section Stenopoa in Pan-Himalayas". *Taiwania.* 62. (2017): 315-320. Print.

24. Press, J.R, Shrestha, K.K, and Sutton, D.A. "*Poa* L. In: www. Efloras. org. Annotated Checklist of the Flowering Plants of Nepal". Natural History Museum, London. Published on the Internet. 2000: http://www.efloras.org/flora_page.aspx?flora_id=110/accessed on 28.07. 2017.

25. Rajbhandari, K.R. *"A Revision of the genus Poa L. (Gramineae) in the Himalaya".* In: Ohba and Malla (eds.), The Himalayan Plants, University of Tokyo Press. 2. (1991): 169–261. Print.

26. Raizada, M.B, Jain, S.K, and Bahadur, K.N. "*Grasses of the Upper Gangetic Plain Part III (Pooideae)".* Jugal kishore and Co., Dehradun. (1983). Print.

27. Schaffner, J.H. "A general system of floral diagrams". *Ohio J.Sci.* 16.8. (1916): 360-366. Print.

28. Singh, G. "*Plant systematics Theory and practice".* Oxford and IBH Publishing Co. Pvt. Ltd., London. New Delhi. (1999). Print.

29. Soreng, R.J, Gillespie, L.J, and Jacobs, S.W.L. *Saxipoa* and *Sylvipoa*- two new genera and a new classification for Australian *Poa* (Poaceae: Poinae). *Aust. Syst. Bot.* 22.6. (2009): 401–412. Print.

30. Soreng, R.J, Peterson, P.M. "Revision of *Poa* L. (Poaceae, Pooideae, Poeae, Poinae) in Mexico: new records, re-evaluation of *P. ruprechtii*, and two new species, *P. palmeri* and *P. wendtii*. *PhytoKeys* 15. (2012): 1–104. Print.

31. Stapf, O. "*Poa. In: Hooker, J.D. (ed.) Flora of British India".* L. Reeve and Co., London. 7. (1896): 337–346. Print.

32. Stebbins, G.L. "*Variation and Evolution in Plants".* Columbia University Press, New York, USA, 1950. Print.

33. Stewart, R.R. "The Grasses of North-west India". *Brittonia* 5. (1945): 404–468. Print.

34. Subrahmanyam, N.S. "*Modern plant taxonomy".* Vikas Publishing House Pvt. Ltd. New Delhi. 2004. Print

35. Tzvelev, N.N. *Poa* L. In: Tzvelev, (ed.), "Grasses of the Soviet Union", (translated from the Russian edition of 1976). Oxonian Press Pvt. Ltd., New Delhi. 1. (1983): 649–722. Print.

Cite this article as:

Mudassir Ahmad Bhat, Sheikh Abdul Shakoor and Amarjit Singh Soodan. Taxonomic description and annotation of Poa albertii Regel (Poaceae: Pooideae, Poeae, Poinae) from North Western Himalayas, India. *Annals of Plant Sciences 7.3 (2018) pp. 2096-2100.*

http://dx.doi.org/10.21746/aps.2018.7.3.1

Source of support: University Grant Commission, New Delhi
Conflict of interest: Nil